5-2015

Hybrid Hydrogels for Tissue Engineering

Ho Joon Lee
Clemson University

HYBRID HYDROGELS FOR TISSUE ENGINEERING

A Dissertation
Presented to
the Graduate School of
Clemson University

In Partial Fulfillment
of the Requirements for the Degree
Doctor of Philosophy
Bioengineering

---

by
Ho Joon Lee
May 2015

Accepted by:
Dr. Ken Webb, Committee Chair
Dr. Martine LaBerge
Dr. Jeoung Soo Lee
Dr. Ying Mei

ABSTRACT

Hydrogels have been widely investigated for their versatility in biomedical applications such as tissue engineering scaffolds and minimally invasive vehicles for site-specific delivery of bioactive molecules. Hybrid hydrogels combine the strengths of intrinsic bioactivity from naturally derived materials and superior control over network physical and chemical properties from synthetic materials. The most prominent approach in three-dimensional (3D) hybrid matrices is the use of MMP-sensitive peptides derived from native extracellular matrix molecules to crosslink synthetic polymers. These peptide-based techniques have several limitations such as high cost, limited mechanical properties, and reduced degradation kinetics that limit the network crosslinking density and mechanical properties. This led us to develop a novel hydrid hydrogel system, *in situ* photopolymerizable, degradable, poly(ethylene glycol) (PEG) diacrylate / hyaluronic acid (HA) semi-interpenetrating networks (semi-IPNs).

In the first set of studies, we determined the effects of network composition (PEGdA and HA molecular weight and concentration) on 3D cell spreading and identified polymerization-induced phase separation as the underlying mechanism responsible for the ability of PEGdA/HA semi-IPNs to support 3D cell spreading. Semi-IPNs with optimal network composition including a blend of three different PEGdA providing improved degradation kinetics demonstrated the ability to support long-term fibroblast cell spreading, migration, and network formation. In addition, the selected semi-IPNs were also found to possess elastic moduli significantly higher than most alternative hybrid hydrogels and within the range reported as optimal for osteogenic

differentiation of mesenchymal stem cells. In second study, we investigated the ability of the semi-IPNs to support hMSC differentiation as a preliminary study towards bone tissue engineering application. Gene expression, alkaline phosphatase activity, histological analysis, and calcium quantification demonstrated the semi-IPN's ability to support osteogenic differentiation over 35 days of culture. In the final study, we incorporated poly-L-lactic acid (PLLA) nanospheres in semi-IPNs to test the hypothesis that provision of hydrophobic domains capable of supporting higher protein adsorption than the PEG network could increase extracellular matrix accumulation. Significantly increased collagen deposition was observed in histological sections and by quantitative analysis.

Overall, the results of this work suggest that PEGdA / HA semi-IPNs and their composite derivatives offer potential as a hybrid matrices for therapeutic cell transplantation. In the future, the biofunctionality of these hybrid networks can be further enhanced by inclusion of growth factors or biochemicals.

DEDICATION

This work is dedicated to Young-Ok Lee, my mother, Ansoon Kim, my wife and Jason Jung-Jae Lee, my son. I am truly and deeply grateful for their patience, support, and love.

ACKNOWLEDGMENTS

I would like to thank my advisor, Dr. Ken Webb for his patience, encouragement and guidance throughout my Ph. D. study. I could not have completed my dissertation study without his help. I would also like to thank my committee members, Dr. Martine LaBerge, Dr. Jeoung Soo Lee, and Dr. Ying Mei for their kind understanding and valuable inputs on my research. I am also thankful to my lab mates, Atanu Sen, Jeremy Zhang, and Sooneon Bae for their help, discussions on research, and being together in the lab.

I would like to acknowledge and thank the following faculty members, post-doctoral fellow, technical staffs and students for their assistance: Aesha Desai, Dr. Jorge Rodriguez, and Dr. Dalphine Dean for their help with AFM study; Cassie Gregory for her help with various assay techniques; Chad L. McMahan and Linda Jenkins for their assistance in histology; Dr. Guzeliya Korneva in Materials Synthesis, Characterization, and Testing Core for her professional assistance on MTS testing; and finally Dr. Terri Bruce and Rhonda Reigers Powell in Clemson Light and Imaging Facility for their help with confocal and wide-field microscopy imaging. I also appreciate the help from our department administrative staffs, Leigh Humpries, Michelle Kirby, Sherri Morrison, Maranda Arnold and Maria Torres.

Funding for this project was provided by grant #8P20GM103444 from the National Institute of General Medical Sciences through the SC Bioengineering Center of Regeneration and Formation of Tissues (SC BioCRAFT).

TABLE OF CONTENTS

Page

Table of Contents (Continued)

Page

Table of Contents (Continued)

Page

Table of Contents (Continued)

Page

LIST OF TABLES

LIST OF FIGURES

List of Figures (Continued)

Figure Page

CHAPTER ONE

INTRODUCTION

1.1 Cell Therapy and Tissue Engineering

The early attempts to repair defective tissues or organs in regenerative medicine were to simply transplant (inject) somatic cells into a lesion area, but typically this approach led to little success [1,2]. Transplanted cells may be perfused out or die at the early stage of transplantation [3]. Cell death occurs in the first few days post-transplantation, caused by the combination of ischemia (a restriction in blood supply to tissues) and inflammation. Also the lack of matrix can induce cell death and this is mediated by the anoikis signaling pathway [1,4]. The most widely used tissue engineering strategy to avoid initial cell death and increase cell retention is to combine cells and biologically active molecules together within the tissue engineering scaffold [5] which allows the creation of biomimetic three-dimensional (3D) microenvironments that provide biomolecular cues that direct cellular function, guiding the spatially and temporally complex multicellular processes of tissue formation and regeneration [6]. Cellular encapsulation in scaffold matrices helps successful cell transplantation by preventing the anoikis signaling pathway and prohibiting immediate cell perfusion while permitting the diffusion of gas, nutrients, wastes and bioactive molecules by fine-tuning the pore sizes [7]. Additionally, advanced 3D microenvironment systems are needed to better understand cellular activities using *in vitro* models in order to later realize their potential *in vivo* since there are significant differences in cellular activities, especially in

stem cell differentiation between two-dimensional (2D) and 3D culture conditions [8–11].

1.2 Monolayer vs. Three Dimensional (3D) Culture

Cells in monolayer culture (2D surface) develop an apical/basal polarity with one side in contact with the culture substrate and the other exposed to culture media that is non-physiological for most cell types. Additionally, cell-cell contact only occurs at the periphery of cells spread in 2D monolayers. However, in the *in vivo* (3D) environment, cells interact with neighboring cells as well as the ECM [12]. Mass transport is also different in 3D culture from 2D monolayer culture. Soluble factors are not diffusion limited in 2D culture, whereas diffusion gradients play a key role in transport of biochemical factors produced from native ECM [13].

Cell-matrix interactions in 3D environments reflect a narrowed integrin usage (more dependency on $\alpha 5$ integrin) and enhanced biological activity relative to monolayer culture such as cell adhesion (by a factor of 6) [10]. These differences in morphology have significant impacts on cell function. Breast epithelial cells exhibited a tumoral trend when assayed in 2D culture, while regressed to normal state upon transferal to 3D models which resembled their natural niche [14]. In the same way, increased chondrogenesis has been reported in ESCs cultured as 3D embryoid bodies when compared to the monolayer culture [15]. Morphogenesis, migration, and proliferation of cells in 3D culture are restricted by matrix, whereas 2D surface offer no restriction to cell migration as shown in Figure 1.1 [11]. Cell interaction with microenvironment (ECM) is more important factor

in directing cell phenotype than its genotype [14,16]. Thus, cells should be evaluated in the context of the ECM [11].

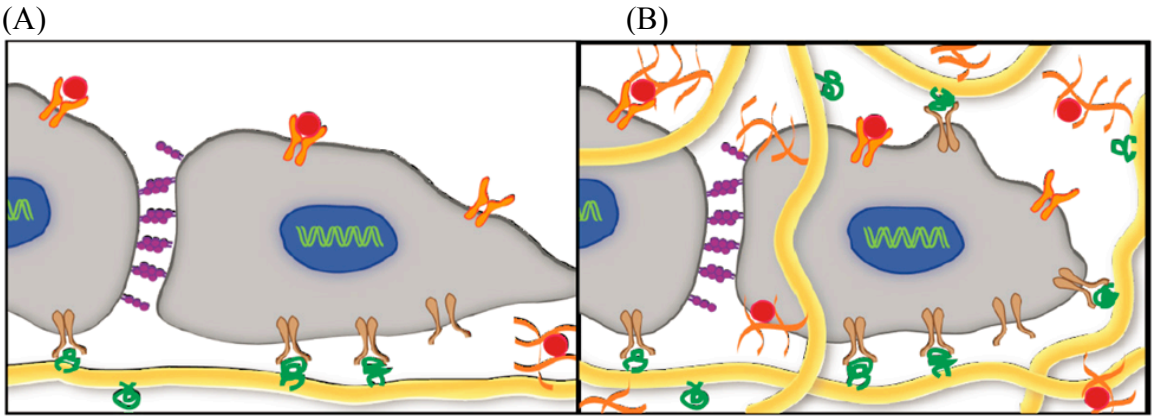

Figure 1.1 Comparison between monolayer (2D) and 3D interactions. Cells placed in 2D culture (**A**) become polarized and orient in a specific direction that confines their interactions with adsorbed proteins (yellow fiber) through integrin binding (brown) receptors to specific ligands (green) located on specific regions of the cell. This polarization also limits their interactions with media components and soluble factors (orange receptors and red ligands) on the opposite side of the cell, while confining cell-cell interactions and migration to a plane. In contrast, 3-D culture (**B**) conditions enable isotropic interactions with extracellular biomolecules and chemical factors through receptor-ligand binding on all surfaces of the cell as well as isotropic cell-cell interactions and migration [17].

1.3 Native Extracellular Matrix (ECM)

In order to achieve successful tissue regeneration, 3D cell transplantation scaffolds must mimic natural niches closely. This requires a comprehensive insight into the complex and dynamic nature of the extracellular matrix (ECM) and cells within the matrix [11]. It is a hierarchically organized structure composed of a three-dimensional array of protein fibers and filaments embedded in a hydrated gelatinous network of polysaccharide chains of glycosaminoglycans (GAGs).

GAGs are hydrophilic, unbranched, negatively charged polysaccharide chains that form stiff and highly extended conformations. Their negative charges attract counter ions inducing an osmotic effect that enables the matrix to occupy large volumes of water. Most GAGs are sulfated, covalently linked to protein via linker proteins and are synthesized intra-cellularly and released via exocytosis. The four main groups of GAGs are hyaluronic acid, chondroitin sulfate, keratin sulfate, and heparin sulfate. The exception among the GAGs is hyaluronic acid which is the simplest GAG molecule and is released directly from the cell surface by an enzyme complex embedded in the plasma membrane, not sulfated, and not covalently linked to proteins. HA is found in most mammalian tissue and fluid, especially prevalent during embryogenesis and wound healing where its presence modulates cell migration in the extracellular space by controlling the level of hydration in tissues. Proteins with covalently attached GAGs constitute proteoglycans (PGs) which fill the majority of the ECM interstitial space within the tissue in the form of hydrated gel with varying porosity and charge density, allowing them to regulate the molecular diffusion of molecules and cell migration [18–

22]. From this unique nature (hydrated state and glycosylated protein filaments), PGs associated with collagen fibers provide the ECM with mechanical buffering which resists compressive stresses. Additionally, PGs bind a variety of growth factors, acting as a storage reservoir from which they can be enzymatically released by cellular proteolytic activity [20,23,24].

The fibrous proteins of the ECM can be categorized as structural (i.e., collagen and elastin) and adhesive (i.e., fibronectin and laminin) types and their fibrous forms provide mechanical integrity of ECM. Collagen is the most abundant protein in the ECM (up to 30% total protein mass) which is secreted locally by cells, for instance, fibroblasts in most connective tissues, osteoblasts in bone, and chondrocytes in cartilage [19,20]. Various chemically distinct forms of collagen (28 types in vertebrates identified to date) exist and they assemble into different supramolecular structures, mostly fibrils and network type, to have functional diversity [25,26]. Fibrous collagens (type I, II, and III) form the backbone of the collagen fibril bundles within the interstitial tissue stroma. Collagen type IV is a network-forming collagen resulting in a mesh-like lattice which constitutes a major portion of the basal lamina. Cells bind to this basal lamina via indirect binding to laminin adhesive proteins [19,26,27]. Another major fibrous protein is elastin and its fiber form provides recoil to tissues that undergoes repeated stretch. Elastin precursor (tropoelastin) molecules assemble to form fibers via covalent bonding of lysine residues between individual tropoelastin molecules, which renders the ECM elastic. Collagen associates with elastin and forms interwoven fibrous protein structures. These

structures provide the ECM with tensile strength and limit elastin stretch by tight association with collagen fibrils [20,28].

Fibronectin (FN) is adhesive protein in the ECM consisting of two subunits and plays crucial role in cell attachment and ECM organization with several binding sites to other FN dimers, to collagen, to heparin and to integrin receptors. It can be stretched several times over its resting length by neighboring cellular traction force [29]. This traction force-dependent nfolding of FN exposes cryptic integrin-binding sites recognized by integrins on cell surface, resulting in integrin-ECM ligand ($\alpha 5\beta 1$) adhesion binding and also promoting FN-fibril assembly. Integrin receptors on the cell surface bind to a fibronectin domain containing the well-known tripeptide adhesion sequence arginine-glycine-aspartic acid (RGD) and the neighboring synergy site while other distinct protein domains bind to collagen and heparin [30]. Additional binding sites (IIICS) within FN contains peptide sequence REDV and LDV which mediate specific cell type binding such as neural cells and lymphocytes. FN is also a regulating factor for cell migration timing during development [21,31]. As mentioned above, another adhesive protein, laminin is associated with basement membranes. Multiple peptide sequences such as RGD, YIGSR, IKVAV, heparin and collagen IV binding regions have been identified in laminin. These insoluble, adhesive type proteins are deposited on this backbone of fibrous proteins [18,30]. Integrin-ECM ligand binding interactions provide communication between the intracellular and extracellular environments which have been shown to play critical roles in cell shape, migration, proliferation and differentiation [28,32].

The ECM is a dynamic cellular microenvironment that undergoes constant remodeling (i.e. assembly and degradation of its constituents) by cells particularly during the normal physiological process of development, differentiation, and wound healing. Also, the mechanical properties and biochemical composition of ECM varies considerably from tissue to tissue (e.g. lungs versus skin versus bone), locally within one tissue (e.g. renal cortex versus renal medulla), as well as from one physiological state to another (normal versus cancerous) [18,20,30]. Cells embedded within ECM have to change from an adhesive phenotype to a migratory phenotype prior to their migration within its three-dimensional structure [33]. During cell migration, cells secrete proteolytic enzymes (proteases) that cleave a variety of ECM substrates to break down physical barriers that inhibit cell locomotion. The most prominent example of this protease is matrix metalloproteinase (MMP) family which consists of 23 structurally related endopeptidases in humans. There are four different classes of MMPs and they degrade different types of ECM molecules or activate other types of MMPs [34]. Most MMPs are secreted in latent form as pro-enzymes and later activated by the displacement of the pro-domain by conformational change or proteolysis induced by the protease plasmin or by other MMPs [35]. This MMP activity is counterbalanced by tissue inhibitors of metalloproteinases (TIMPs) and the collagen crosslinking activity of lysyl oxidase (LOX) and transglutaminases, which result in locally stiffened ECM [18,20,36,37]. During the process of tissue remodeling, cells degrade the ECM with matrix metalloproteinase (MMPs) as they deposit their own ECM components simultaneously. Both processes are regulated by spatiotemporal integrin-mediated signaling pathways [30,38]. The ECM also

contains growth factors (or cells producing growth factors) and other bioactive molecules, as well as binding sites for cell-surface molecules exposed upon MMP proteolysis [34,39]. Growth factors modulate cell growth and migration in the form of controlled (release) feedback process for tissue homeostasis [40]. Cell-derived growth factors may either be directly released for immediate signaling or embedded within the matrix by binding proteins and later released by proteolytic degradation [32,39].

Cells in ECM sense and convert mechanical stimuli into biochemical signals via cell-surface receptors [6]. Upon injury, recruited neighboring fibroblasts synthesize and deposit large amounts of ECM proteins, resulting in stiffened matrix. The elevated elasticity and deposited ECM induce trans-differentiation of fibroblasts or other tissue residing cells into other cell types, for instance, epithelial cells to mesenchymal cell transition or bone marrow derived mesenchymal stem cells into myofibroblast [41,42]. Also, remodeled ECM attracts the directional migration toward wound site [43]. Once wound site is populated with healthy cells, feedback mechanisms are initiated to restore tissue homeostasis and resolve fibrosis [20,41,42].

1.4 Hydrogel as Synthetic ECM

In tissue engineering, hydrogels are applied as space filling agents (bulking, adhesion barrier, and biological glue), delivery vehicles for bioactive molecules, and three-dimensional cell transplant scaffold as they can provide highly swollen 3D environment enabling diffusive transport. Among these applications, hydrogels are appealing scaffold materials as they are structurally similar to the ECM of many tissues,

capable of being processed under cytocompatible conditions and delivered in a minimally invasive manner [6,11,44,45].

Hydrogels can be categorized by the origin of macromere materials, naturally-derived hydrogels and synthetic hydrogels. Representative naturally-derived hydrogels may be protein-based (collagen, gelatin, and fibrin) or polysaccharide-based (e.g., alginate, chitosan, hyaluronic acid, and dextran) [45]. Naturally-derived hydrogels possess intrinsic bioactivities such as cell adhesion and biodgradability, which are advantageous over synthetic hydrogels. For example, collagen and fibrin are clinically well-established, FDA-approved materials for the healing of burns and chronic wounds, and used as tissue sealants, respectively [6]. Especially, collagen is an attractive material as it is the most abundant protein in mammalian tissues and can self-aggregate to form stable fibers [46]. Also collagens can form fibers and scaffolds by introducing various chemical linkers (i.e. glutaraldehyde, formaldehyde, carbodiimide) [47,48], by crosslinking with physical treatments (i.e. UV irradiation, freeze-drying, heating) [47,49], and by blending it with other polymers (i.e. HA, PLA, poly(glycolic acid) (PGA), poly(lactic-coglycolic acid) (PLGA), chitosan, PEO) [47,48,50,51]. However, the use of naturally derived hydrogels is often restricted due to concerns of potential immunogenicity, pathogen transmission, difficulties in purification process as well as poor mechanical properties [45,52]. In addition, their mechanical properties cannot be readily manipulated, especially due to batch-batch variability and complexity. Alternatively, synthetic hydrogels have advantages over naturally derived hydrogels, such as greater and systematic control of material compositions and properties for the

design of scaffolds for multiple tissue types [53,54]. Various non-immunogenic synthetic materials have been tested as 3D hydrogel scaffolds for cell transplant application, including poly(ethylene glycol) (PEG), poly(vinyl alcohol) (PVA), poly(acrylic acid) (PAA), and various polypeptides. These hydrogels can be polymerized *in situ* under mild physiological conditions [6,45,55].

The concept of hybrid hydrogel is to integrate the advantages of both naturally derived and synthetic hydrogel. As synthetic hydrogels exhibit minimal or no intrinsic bioactivities by themselves, they require the incorporation of biofunctional oligopeptide sequences (e.g. RGD and MMP sensitive peptides), proteins (e.g. collagen), and other biological molecules (e.g. heparin) from the native ECM to mimic natural ECM as hybrid hydrogel concept [6,11,56–58]. With these biologically inert characteristics, synthetic hydrogel can be a useful tool for 3D *in vitro* tissue culture scaffold to investigate cellular response to ECM as it allows independent control of biomolecular and structural cues from native ECM [6,59]. Among these synthetic components in hybrid hydrogel, PEG-based hydrogels have been widely investigated in tissue engineering as they have critical properties such as easy structural modification and proven history of successful application in many clinically-approved products [6,45]. In this dissertation research, we will focus on the modification of PEG based hydrogel to mimic the native ECM and improve its bioactivities over other PEG based hydrogel scaffolds.

1.5 Design Strategy – Engineering ECM Cues

Successful 3D cell transplant scaffolds need to mimic critical aspects of the natural ECM and must meet critical design criteria; biocompatibility, geling (crosslinking) mechanism, mechanical properties (stiffness), degradation, and mass transport. These properties or design variables are specified by the intended scaffold application and environment into which the scaffold will be placed (target microenvironment) as shown in Figure 1.2 [60]. Additionally, selection of the most appropriate scaffolding material is crucial in a tissue-engineered construct. Synthesis of the appropriate hydrogel scaffold materials is governed by the physical properties (gel formation mechanism, mechanical characteristics, and degradation), the mass transport properties, and the biological interaction requirements (biocompatibility and target microenvironment) of each specific application [44].

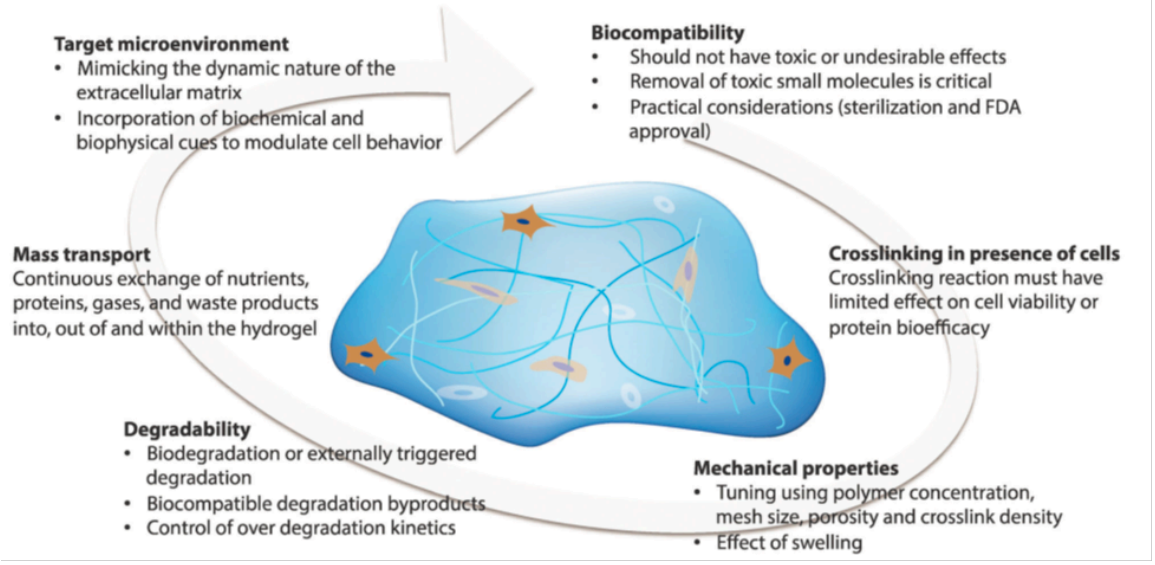

Figure 1.2 Design considerations, factors dictating 3D tissue engineering scaffold [60]

1.5.1 Biocompatibility

Biocompatibility is the first and most critical factor to consider prior to cell encapsulation. The ideal way to encapsulate cells is *in situ* polymerization while the hydrogel is forming for homogeneous distribution of cells and in the case of *in vivo* applications, avoiding invasive surgical procedures. Scaffolds designed to encapsulate cells must be capable of being gelled without damaging the cells and must be nontoxic to the cells and the surrounding tissue after gelling. When naturally-derived materials such as collagen are used, there should be no cross-species immunological response. Along with naturally-derived polymers such as collagen, alginate, and fibrin; PEO and PEG are currently used in many FDA-approved medical applications such as spinal sealant. However, additional care should be taken post gelation as there are small toxic molecules during hydrogel fabrication [44,60]. For example, unreacted maleimides in Michael-type addition reactions are highly potent neurotoxins [61]. Photoinitiators, such as 2,2-dimethoxy-2-phenyl-acetophenone used frequently in free-radical polymerization, can be cytotoxic [62].

1.5.2 Mass transport

Most chemically crosslinked polymer hydrogels are dense network acting similar to a porous structure [54], with a mesh sizes ranging nanometer to the order of tens of nanometers allowing appropriate diffusion of nutrients and metabolites to and from the encapsulated cells and surrounding tissue. *In vivo*, most cells exists within 100 μm of capillary (one of exception is chondrocytes where no blood vessel exists in cartilage tissue), and diffusion is the primary method of mass transport over this range [63].

Additionally, diffusion governs mass transport within hydrogel networks due to their nanoporous structure [44]. Crosslinking density and molecular weight of macromer determines its nanoporous structure (mesh size) and resulting molecular weight cut-off of solutes. Its porosity changes with matrix stiffness. The diffusion of small molecules is more hindered in stiffer matrices [64–67].

1.5.3 Mechanism for hydrogel formation

Common polymer scaffold fabrication techniques use harsh conditions for live cells such as high temperature, pH changes, and various organic solvents that can denature proteins, which makes many fabrication techniques incompatible with live cell encapsulation [60]. However many hydrogel formulations have been shown as injectable, *in vivo, in situ* polymerizable 3D cell transplant scaffolds [68–71]. The success of this approach depends on the ability to control both pre- and post-gelation properties including gelation rates and liquid flow properties [44].

PEGs has linear and branched (multiarm or star) structures. The basic PEG structure is PEG diol with two hydroxyl end groups, which converted into other functional groups, such as methyloxyl, carboxyl, amine, thiol, azide, vinyl sulfone, acetylene, and acrylate as listed in Figure 1.3 [45,68,72–74]. This functionalized PEG can be further modified as thermally reversible hydrogel from block copolymer of PEG and poly-L-lactic acid (PLLA) [75]. Degradable PEG based hydrogels can be formed by incorporating either hydrolytically degradable poly(lactic acid) or enzyme specific cleavage sequences of oligopeptides [73,74].

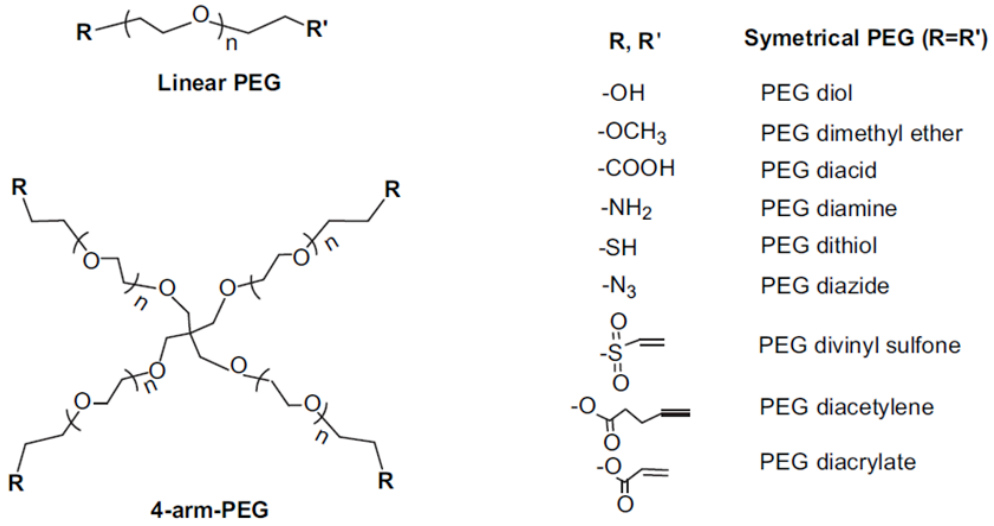

Figure 1.3 Structures of linear PEG and four arm PEG with various functional end groups [45]

The two or more functional end groups can be used for crosslinking the network and also for crosslinking bioactive peptides such as MMP sensitive and cell adhesion peptides. They are also used for conjugating with biomolecules such as growth factors [45]. The most commonly used polymerization methods for cell encapsulation applications (in presence of cells under physiological conditions) are free radical polymerization (Figure 1.4) [68,76–79], Michael-type addition (Figure 1.5) [80,81], and thiol-ene reaction [82,83].

Free radical polymerization involves the formation of free radicals via decomposition of an initiator by light, temperature, or redox reaction to yield primary radical species [84]. These free radicals propagate through unsaturated functional groups (carbon-carbon double bond) such as acrylate bonds on the PEG macromers and chain polymerization occurs, resulting in covalently crosslinked polymer networks (Figure 1.4) [85]. In these systems, complete gelation is achieved in relatively short times (seconds to a few minutes). Photopolymerization of PEG diacrylate (PEGdA) hydrogels has been extensively investigated in tissue engineering and regenerative medicine applications since it offers advantages such as well-characterized reaction kinetics and facile *in situ* polymerization in presence of cells with spatiotemporal control [86]. However, free radicals can be transferred to proteins, affecting their bioactivity, or transferred to biomolecules present in the cell membrane, affecting cell viability [60,87].

(A) (B)

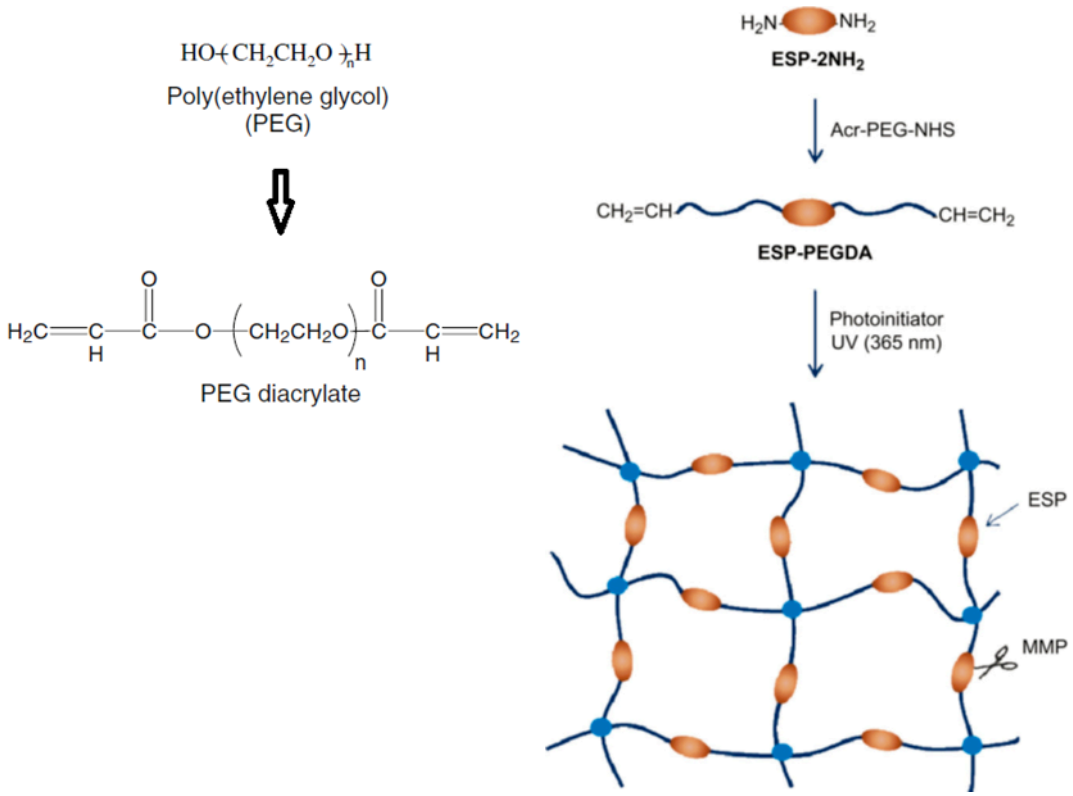

Figure 1.4 Chemical structures of PEG macromer and its diacrylate derivatives (A) [85] and synthesis of enzyme sensitive peptide (ESP) containing PEGdA by conjugating acrylate-PEG-NHS with ESP diamine (ESP-2NH_2) (B) [45]

Michael addition is a step-growth approach to crosslink PEG hydrogel network under mild physiological condition in direct contact with tissues, cells and biological molecules [45,85] using PEG or multiarm PEG macromers functionalized with acrylate, maleimide, or vinyl sulfone group with dithiol monomers [88]. Michael-type addition reactions occur between acrylates and thiols, and between maleimide and thiol groups [28]. This reaction takes longer (hours) relative to the time of completion in free-radical polymerization. This mechanism was extended to include cell adhesion motif and enzymatic (MMP) degradation peptides as ECM mimics. For example, vinyl sulfone functionalized four-arm PEG underwent two-step Michael addition reaction presented on mono-cysteine adhesion peptides (RGD) and bis-cysteine MMP sensitive peptides for 3D cell culture application (Figure 1.5) [89].

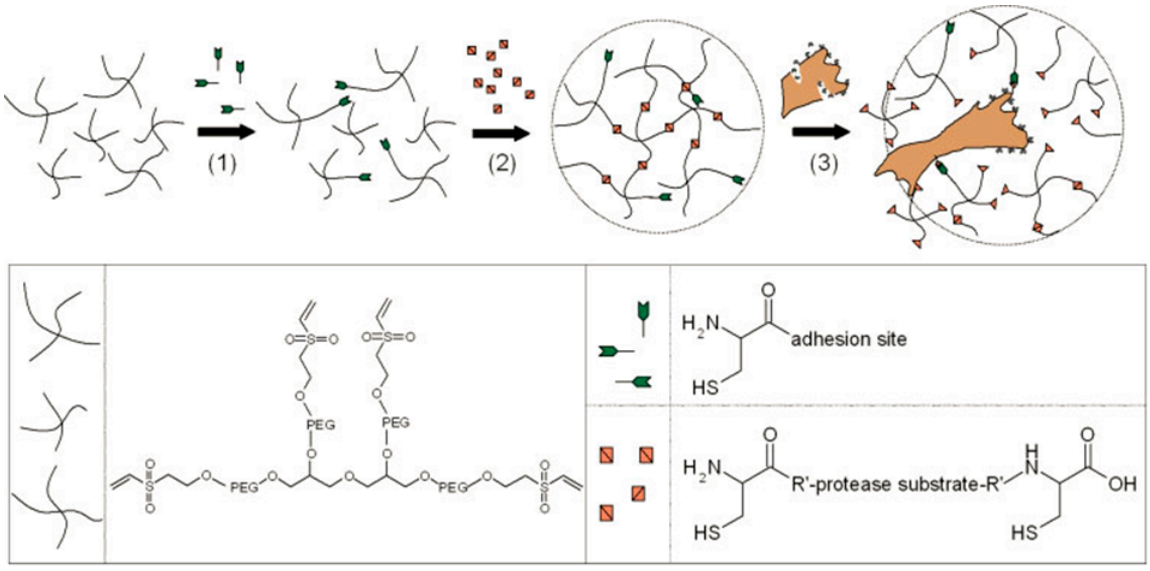

Figure 1.5 A Michael type addition reaction between vinyl sulfone functionalized multi-arm PEGs and mono-cysteine adhesion peptides (step 1, stoichiometric deficit) or bis-cysteine MMP sensitive peptides (step 2, stoichiometric balance) was used to form gels from aqueous solutions in the presence of cells and cells locally interact with networks by adhesion and protease secretion (step 3) [89].

1.5.4 Engineering ECM cue – adhesion

Although many hydrogels are nontoxic and do not stimulate an immune response, they are also biologically inert and do not facilitate cell adhesion. Additionally, ECM proteins such as laminin, fibronectin, and vitronectin typically do not readily absorb to the hydrogel due to their hydrophilic nature [90]. Therefore, the minimum requirement for anchorage-dependent cells to survive on and within synthetic PEG-based scaffolds is to render them cell-adhesive. In order to design highly specific adhesive surface, many groups have covalently incorporated cell adhesion peptide sequences capable of binding to cell receptors [73,90,91]. The most common peptide sequence is the arginine-glycine-aspartic acid (Arg-Gly-Asp or RGD) sequence, derived from ECM proteins such as fibronectin, laminin, vitronectin and collagen. While most cell types bind to the RGD sequence, an additional region (IIICS) within fibronectin has been identified to contain the peptide sequences, arginine–glutamic acid–aspartic acid–valine (REDV) that permit the adhesion of specific cell types such as neural cells and lymphocytes. Other common peptides from laminin include tyrosine–isoleucine–glycine–serine–arginine (YIGSR), and isoleucine–lysine–valine–alanine–valine (IKVAV). The IKVAV peptide motif involved in neurite growth, and a heparin and collagen IV binding region [90]. There are two forms of RGD peptides, linear RGD and cyclic RGD (cRGD). cRGD peptide sequence shows increased the affinity to integrin avβ3 and can enhance biological activity up to 240 times in comparison with linear RGD analogues [92–94]. The incorporation of cRGD peptides into the PEGDA hydrogels can better mimic the native RGD loop structure and benefits the cell adhesion [45,95].

1.5.5 Engineering ECM cue – degradation

The native ECM is dynamic matrix continuously remodeled for homeostasis and tissue regeneration [19]. Therefore, the temporal and spatial variability of ECM properties must be introduced into 3D culture models in order to simulate realistic microenvironments. The incorporation of cell adhesion peptide sequences in PEG hydrogels does not guarantee prolonged cell survival when cells are encapsulated within 3D scaffolds due to the nanometer mesh size of the crosslinked PEG network being less than the average diameter of a cell. This small mesh size acts as a physical barrier to cell migration and cell morphogenesis, resulting in a spherical cell morphology that is non-physiological for many cell types [54,96]. Therefore, the successful design of scaffolds for cell transplantation requires rendering the scaffolds degradable. Degradation allows cell spreading and migration and can regulate the release of matrix-tethered biomolecules that induce different cellular functions. Ideally, the rate of scaffold degradation should mirror the rate of new tissue formation [97,98].

Degradation in hybrid hydrogel matrix can be achieved via ester bond hydrolysis, enzymatic hydrolysis, or a combination of these mechanisms [60]. Synthetic hydrogels can be designed to include degradable polymers within their network such as poly(lactic acid) [99] or poly(caprolactone) [100] blocks in combination with PEG backbone for hydrolytic degradation. Similarly, the scaffolds can be built by co-polymerization of different ratios of degradable and non-degradable macromers [101]. The degradation rate can be controlled by the number of incorporated hydrolytically labile bonds in the hydrogel. The ratio between the number of two bonds offers predictable degradation

profiles independent of cellular interactions as hydrolysis is an autocatalytic process [102]. The degradation rate of hydrolytically labile gels (e.g. PEG-PLA copolymer) can be manipulated by the composition of the material but not the environment [103]. However, hydrolytic degradation is not representative of the cell-mediated and dynamic process of proteolysis that takes place within the native ECM. Instead, native ECM derived molecules (i.e. collagen and fibrinogen) or protease sensitive peptide sequences for degradation within synthetic hydrogel may present the site for enzymatic degradation and constitutes hybrid hydrogel susceptible to cellular enzymatic degration [11].

Degradation of polymer is mediated by surface or bulk processes, or sometimes a combination of the two. Hydrophilic polymers often exhibit bulk degradation process as the rate of uptake of water is faster than the rate of conversion of polymer into water soluble materials [104]. Enzymatic degradation site is usually localized to where cells/enzymes are present while hydrolysis occurs throughout the bulk of the network [11,60,85].

The rate of enzymatic degradation will depend both on the number of cleavage sites in the polymer and the amount of available enzymes in the scaffold environment [73,74]. Incorporation of peptide sequences susceptible to cleavage by cell-secreted proteases (i.e., plasmin-sensitive or MMP sensitive sequences) into PEG hydrogels manipulate gel degradation dynamically in response to cell-mediated events [28,74,97,105–108]. However, these substrates do not degrade particularly fast which may limit cellular infiltration within the scaffold [Chung S J Biomed Mater Res 2006] and these peptides can also be cleaved by a variety of MMPs. Additionally, local pH and

ionic strength, enzyme concentration, and temperature may affect enzyme-substrate formation, resulting in degradation profile change [60]. Thus, recent strategies have focused on enhancing proteolytic degradation of PEG hydrogels by using combinatorial methods of peptide libraries consisting of MMP substrate sequences with increased catalytic activity [28,109,110], by increasing the spatial presentation of these signaling molecules within the hydrogel network [111], or by increasing the number of MMP-sensitive peptides [112]. These hydrogel systems allow accelerated proteolysis, giving a broader *in vivo* application.

1.5.6 Engineering ECM cue – matrix stiffness

Once the scaffold is produced and implanted, formation of tissues with desirable properties relies on scaffold mechanical properties on both the macroscopic and the microscopic level. Macroscopically, the scaffold must bear loads to provide structural stability to the wound site until cells have produced their own functional ECM. Microscopically, the scaffold must transmit mechanical loads to encapsulated cells and maintain certain stiffness as cell growth and differentiation are dependent on these mechanical inputs [113–116]. In the *in vivo* microenvironment, cellular level mechanical forces consist of endogenous (generated by cells) and exogenous (applied to cells) forces. Most of endogenous forces occur from cytoskeletal contractility [117,118]. Gravity and tissue specific interactions such as endothelial cells exposed to pulsatile shear forces from blood flow are examples of exogenous forces [119]. Additionally, it is well known that cellular function is modulated by local matrix stiffness. *In vivo*, tissue modulus ranges from Pa (liver tissue and adipose tissue) to GPa (bone) [59]. And this stiffness range is

not static as it changes during physiological processes such as embryonic development, tissue remodeling during wound healing, and in pathological responses like tumorigenesis [120]. Individual cells can sense the stiffness change of surrounding ECM to which they adhere and interact [121]. Various mechanotransducers in the cell convert mechanical stimuli into chemical signals that regulate cell responses such as adhesion, spreading, migration and proliferation [122]. Mechanochemical conversion is mediated by ion channels [123], primary cilia [124], integrins [125], G-protein receptors [126], cell–cell adhesions [127], and the cytoskeleton [128]. In particular, the integrin protein family is a widely studied force transducer that serves as a mechanical linkage between ECM and the cytoskeleton [129]. On the exterior of the cell, integrins bind ECM protein ligands including collagen, laminin, and fibronectin, suggesting integrin receptors serves as integrators of extracelluar signals [130]. Cells sense matrix stiffness by cellular contractility and traction forces. Actin stress fibers are tensed by mysosin motors and cytoskeletal contractility is transmitted to ECM as traction forces [131–133]. In response to variation in substrate stiffness, cells alter cytoskeletal organization, cell-substrate (focal) adhesions, and other processes important for regulating cell behaviors [134–137]. An increasing substrate stiffness results in increased cell-matrix (substrate) adhesion, demonstrated by elongated adhesions (changes in cell shape) and increased tyrosine phosphorylation of focal adhesion kinase (FAK) [138]. Califano showed that endothelial cells on compliant substrates adopt an elongated spindle-shaped morphology, while those on stiffer substrates exhibit more isotropic spreading, demonstrating that both cell area and substrate stiffness are significant predictors of traction force generation [139].

Matrix stiffness also modulates cell-cell assembly, migration, and proliferation. Cells on compliant substrates (< 1kPa) prefer cell-cell interactions rather than migration and self –assemble into network. When placed on stiffer substrates, cells prefer cell-substrate interactions [139,140]. Cellular responses to gradients of different stimuli are referred as durotaxis, the process by which cells respond to changes in matrix rigidity. Fibroblasts migrate toward substrates of increasing stiffness [141]. The sensitivity of cell migration to stiffness gradients may have important implications for disease states such as fibrosis or tumorigenesis that are accompanied in increases in ECM stiffness.

Stem cell differentiation is also controlled either by matrix stiffness or actomyosin contractility. Engler and co-workers showed that mesenchymal stem cell differentiation is controlled by matrix stiffness where neuronal differentiation occurred on soft surface (two dimensional – monolayer culture condition) substrates and osteogic differentiation occurred on stiffer 2D substrates [142]. Chondrocytes in stiffer matrices (up to 500 kPa) tend toward preliferative states rather than differentiated phenotype, resulting in decreased collgen II synthesis [47,143]. A recent study by Mooney and co-workers demonstrated that matrix stiffness also governed stem cell commitment in 3D culture. They encapsulated mesenchymal stem cells in non-biodegradable alginate matrix with different stiffness under 50:50 mixture of adipogenic and osteogenic medium. At low elastic modulus, stem cells differentiated toward adipogenic lineage, whereas, at higher elastic modulus values, stem cells differentiated toward osteogenic lineage even though cells remains restricted to a spherical morphology during osteogenic differentation [8]. Polymer concentration, the stoichiometry of reactive groups, and crosslinking density are

all commonly used to tune the mechanical properties of cell-compatible hydrogels and accordingly to control the cellular microenvironment [60,144,145].

1.5.7 Engineering ECM cues - incorporated biofunctionality

In addition to cell adhesion motif and MMP sensitive peptide sequences (for degradation), hybrid hydrogel scaffold may require growth factors and morphogens incorporated to the scaffold backbone for sequestering and controlled release in order to mimic the native ECM [146,147]. Cell signaling molecule have been covalently attached to hydrogel polymers to enhance either ECM production (TGFβ tethered to PEG network) [148] or ectopic bone formation process (oligopeptide derived from BMP-2) [149]. Multiple factors may also be incorporated into hydrogels to manipulate tissue formation [150].

1.6 State of the Art Approaches

There are several state of the art researches ongoing to enhance bioactivities of 3D hybrid hydrogel scaffolds and to better understand cellular activities in 3D culture conditions.

Additional feedback mechanism, other than stiffness of the matrix, is required for matrix remodeling. Kubow and coworkers compared native ECM scaffolds with fibronectin based scaffolds stiffened by chemical crosslinking and showed differential scaffold remodeling by fibroblasts. Native scaffolds from decellularized ECM were progressively remodeled over stiffer, manually deposited (crosslinked) fibronectin fiber (on silicon sheet) based scaffold [151]. Legant and co-workers also pointed out the importance of spatio-temporal interplay between collagen and FN on matrix remodeling [152]. The hydrogel networks often lack the fibrillar network structure of the ECM protein backbone. To address this issue, the scaffolds need to couple self-assembly mechanism within the network [11,153,154].

In addition to engineering cellular biochemical cues in hydrogel matrix, directed migration is required for maintenance and development of numerous physiological processes [19,155]. Cell migration is proportional to adhesion ligand density up to a critical value [156].

1.7 Concluding Remarks

Scaffold design is the most important factor for successful *in vivo* cell transplantation and *in vitro* 3D cell culture. The design depends on the target tissue and microenvironments where transplanted cells reside. The design requirements for successful cell delivery are biocompatibility, mass transport, mechanical properties (stiffness), and degradability. These design criteria need to be considered for the continued enhancement of these scaffolds for regenerative medicine applications. For the development of a functional tissue construct, it is important to understand the natural microenvironment of the source cell and the innate mechanisms of cell differentiation and tissue regeneration. This knowledge forms the backbone of the biomimetic approach for cell differentiation and tissue regeneration. Significant progress has been made using PEG hydrogel scaffolds as ECM mimics to support and direct cell behavior and tissue regeneration. Numerous efforts have focused on investigating the effects of biological signal identity, gel degradation rate, and mechanical properties on cell behavior, but little work has been done to independently tune these properties in order to isolate and quantify the individual effects of these factors on cell behavior. Finally, this dissertation study is aimed to develop a novel cell transplant scaffold for tissue engineering application with these design criteria.

CHAPTER TWO

RESEARCH OBJECTIVES

2.1 Project Rationale

In general, tissue engineering uses the combination of living cells, biocompatible materials (scaffolds), and suitable biochemical and physical factors to restore, improve or replace biological functions of a failing tissue or organ [157,158]. Tissue engineering scaffolds should provide biophysical and biochemical milieus that direct cellular behavior and function. As a scaffolding material, hydrogels have been widely investigated because of their biochemical similarity with highly hydrated GAG components of the extracellular matrix (ECM) and *in situ* polymerization capability under mild physiological conditions with highly defined spatio-temporal control. Hydrogels can be used as carriers for transplanted cells, biochemical factors, or both simultaneously and matrices that induce morphogenesis *ex vivo* and *in vivo*. Hydrogels are made either from naturally-derived or synthetic polymers, or combinations thereof, referred to as hybrid hydrogels. This hybrid concept takes advantage of inherent bioactivities of naturally derived materials and the well-defined, reproducible, and tunable nature of synthetic polymer networks [6]. During the course of tissue regeneration, the degradation rates of scaffolds must be matched with the rate of regeneration of newly formed tissues [159,160]. The native ECM is degraded by various protease activities, mainly by plasmin and matrix metalloproteinases (MMP) family. The incorporation of protease sensitive peptides identified from native ECM within the synthetic hydrogel networks renders

hybrid hydrogels biodegradable and has been used to create 3D matrices for the culture of a variety of cell types. However, these peptide sequences only possess primary structure, resulting in reduced degradation rate and require high cost for production for clinical use [28,110,161]. In addition, these hybrid hydrogel networks often have limited mechanical properties (less than 1 kPa elastic modulus value) to support cell migration within the networks. Along with native ECM-inspired peptides or other naturally derived materials for bioactivity, polyethylene glycol (PEG) has been extensively used as synthetic backbone of hybrid hydrogels due to its excellent biocompatibility and easy control of scaffold architecture [45,85]. PEG has been also used as surface coating material for implants due to its resistance to protein adsorption [162]. So matrix deposition and assembly on PEG based hydrogel scaffold may be limited [163–165].

Our novel hybrid hydrogel system developed in this dissertation research represents an opportunity to overcome the limitations of peptide-based hybrid hydrogel scaffolds. In tissue engineering applications, this system may serve as a cost effective 3D *in vivo* cell transplant vehicle that will eventually bring about regeneration of native tissue ECM composition as well as a substrate for host cell infiltration and colonization.

2.2 Overall Objective

The overall objective of this project was to develop polyethylene glycol diacrylate (PEGdA) / hyaluronic acid (HA) semi-interpenetrating polymer networks (semi-IPNs) capable of supporting 3D cell spreading, migration, differentiation, and extracellular matrix (ECM) deposition for cell therapy applications. In Specific Aim 1 (Chapter 3), the mechanism that allows semi-IPNs to support encapsulated cell spreading was identified. Then semi-IPNs were further optimized by investigating the effect of network compositions on spreading and migration of encapsulated cells and a selected semi-IPN composition was tested for long term cellular remodeling. In Specific Aim 2 (Chapter 4), human mesenchymal stem cells were encapsulated within the optimized semi-IPNs and cultured under osteogenic conditions to test the ability of semi-IPNs to support long-term stem cell differentiation. In Specific Aim 3 (Chapter 5), hydrophobic poly-L-lactic acid (PLLA) nanospheres were incorporated in semi-IPNs to enhance ECM deposition inside the network.

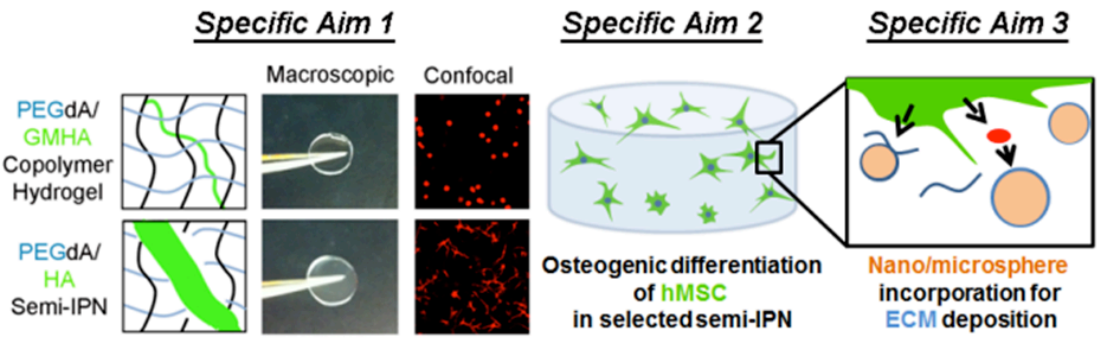

Figure 2.1 Outline of research objectives.

2.3 Specific Aims

2.3.1 Specific aim 1

To investigate the mechanism of semi-IPNs to create a space for cell activities and the effect of network composition on spreading and migration of encapsulated cells in hydrogel network in order to select the optimal combination for long term cellular remodeling inside hydrogel scaffold. We hypothesized that the incorporation of native HA supports initial and long-term survival, spreading, and migration of encapsulated cells by Hase activity combined with hydrolysis of PEGdA backbone. Hence we aimed to 1) investigate the changes in physicochemical properties during photopolymerization of semi-IPN hydrogels consisting of PEGdA and unmodified HA, 2) evaluate the effects of network composition (HA concentration, HA molecular weight, PEGdA concentration, PEGdA chemistry) on encapsulated human fibroblast spreading, and 3) prepare semi-IPNs with various PEGdA blends to obtain improved control over degradation kinetics, and 4) test the ability of the optimal formulation to support long term cell survival and sustained migration.

2.3.2 Specific aim 2

To test the ability of the optimized semi-IPN to support long term stem cell differentiation for hard tissue application. We hypothesized that the semi-IPN with optimal mechanical properties for osteogenic differentiation can support prolonged osteogenic differentiation of mesenchymal stem cells. Hence we aimed to 1) evaluate optimized semi-IPNs as 3D microenviroments for osteogenic differentiation of

encapsulated human mesenchymal stem cells during long-term culture by expression of osteogenic markers, collagen deposition, and mineralization.

2.3.3 Specific aim 3

To incorporate nano/microspheres in semi-IPNs as hydrophobic domains to increase ECM deposition. We hypothesized that PEG-based hydrogels support limited ECM molecule deposition due to its hydrophilic nature and that hydrophobic surfaces of polylactic acid (PLA) nano/microspheres incorporated in semi-IPN can support ECM binding and serve as nucleation sites for ECM deposition and assembly. Hence we aimed to 1) develop preparation and recovery methods for PLA nano/microspheres of varying size, 2) incorporate nano/microspheres into hybrid semi-IPNs and evaluate cellular remodeling using human dermal fibroblasts by assessing ECM molecule (collagen) accumulation both quantitatively and qualitatively by comparison to negative control group (semi-IPN without nano/microspheres).

CHAPTER THREE

PEG DIACRYLATE/HYALURONIC ACID SEMI-INTERPENETRATING NETWORK COMPOSITIONS FOR 3D CELL SPREADING AND MIGRATION

3.1 Introduction

Hydrogels have been widely investigated as matrices for therapeutic cell transplantation based upon their ability to be delivered using minimally invasive methods, crosslinked in situ under mild conditions, and provide viscoelastic mechanical properties similar to many soft tissues [166,167]. Conventionally, hydrogels for tissue engineering applications have been prepared from either naturally-derived or synthetic macromolecules. Many naturally-derived materials such as collagen, fibrin, and hyaluronic acid (HA) form hydrogels that intrinsically support cell adhesion and cell-mediated enzymatic degradation. However, these networks possess relatively limited mechanical properties and can be vulnerable to rapid degradation and contraction unless stabilized with additional crosslinking agents. Hydrogels formed from synthetic materials such as polyethylene glycol (PEG) offer superior control over the network physical and chemical properties, but lack intrinsic bioactivity to support cell adhesion and cell-mediated degradation. Many recent efforts in the field have sought to create hybrid or biosynthetic hydrogels composed of both naturally-derived and synthetic materials that combine the strengths and minimize the limitations of each type of material when used alone [11,58,168].

One of the most prominent strategies for the creation of hybrid hydrogels has been the modification of synthetic networks with oligopeptides derived from natural extracellular matrix (ECM) molecules, including the RGD sequence to support cell adhesion and matrix metalloproteinase (MMP)-substrate sequences to support proteolytic degradation [74,169]. Recent work in this field has shown that hybrid networks containing RGD and MMP-sensitive peptides are effective 3D matrices for the culture of a variety of cell types and support cell proliferation, migration, and ECM deposition [89,112,170]. When combined with growth factors, various types of PEG-peptide hydrogels have been shown to support bone regeneration and angiogenesis *in vivo* [89,108,171–174]. Despite their success, there are several limitations to peptide-based hybrid hydrogels. First, oligopeptides are difficult to synthesize in large quantities and expensive while most tissue defects requiring cell-based therapy are relatively large [175]. In addition, most oligopeptides are linear sequences of amino acids only possessing primary structure, resulting in reduced degradation kinetics relative to the native macromolecules from which they are derived [161]. Consequently, gel formulations that support cellular activity are frequently prepared at low polymer concentrations and crosslinking densities, severely limiting their mechanical properties [89,176–178]. This has led several groups to explore screening alternative peptide sequences and strategies for increasing the number of degradable sites [28,110,112,179].

Alternatively, the use of intact or modified naturally-derived macromolecules to form hybrid hydrogels offers several benefits including substantially lower cost and preservation of native structure potentially supporting higher rates of enzymatic

degradation and greater diversity of bioactivity [180]. For example, PEGylated fibrinogen derivatives have been used to prepare hybrid hydrogels with improved control over mechanical properties and degradation rate compared to native fibrin that have been used for orthopaedic, neural, and cardiovascular applications [181–185]. Hybrid hydrogels based on chemically-modified HA crosslinked with reactive PEG derivatives have been investigated as degradable adhesion barriers and vocal fold augmentation materials [163,164,186]. While the above studies have used co-polymer networks, our group has recently investigated the possibilities of semi-interpenetrating polymer networks (semi-IPNs) composed of hydrolytically degradable PEG-diacrylates (PEGdA) and native HA [187–189]. The previous studies have shown that these hydrogels support increased cell spreading and proliferation relative to fully synthetic networks that is dependent on cellular hyaluronidase activity. The objective of the present study was to systematically examine the effects of PEGdA/HA semi-IPN network composition on cell spreading. 3D spreading of encapsulated fibroblasts exhibited a biphasic response to HA concentration, required a minimum HA molecular weight, decreased with increasing PEGdA concentration, and was independent of hydrolytic degradation at early time points. Incorporation of native HA increased gel turbidity, suggesting a potential mechanism of microphase separation resulting in HA-enriched defects in the network structure. Finally, semi-IPNs with optimized PEGdA degradation rate and HA formulation supported sustained 3D cell migration in a gel-within-gel encapsulation model.

3.2 Materials and Methods

3.2.1 Synthesis of PEGdA macromers with ester linkages containing variable alkyl spacers

Three different types of PEGdA macromers with varying susceptibility to hydrolytic degradation were synthesized by a two-step process as previously reported [188]. Briefly, PEG (4000 MW, Fluka, Buchs, Switzerland) was reacted with either chloroacetyl chloride, 2-chloropropionyl chloride, or 4-chlorobutuyrl chloride (Sigma-Aldrich, St. Louis, MO) in the presence of triethylamine (TEA, Sigma) at a 1:4:1.8 molar ratio in dry dichloromethane (Sigma). After 24 hours reaction at room temperature, the reactants were filtered, washed with sodium bicarbonate and water, dried with anhydrous sodium sulfate, and then precipitated in ethyl ether. After recovery, each resulting intermediate product was reacted with sodium acrylate (5X molar ratio) in dry dimethylformamide (Acros, Morris Plains, NJ) for 30 hours at 50, 85, and 100 ^{0}C to yield PEG-bis-(acryloyloxy acetate) [PEG-bis-AA], PEG-bis-(acryloyloxy propanoate) [PEG-bis-AP], and PEG-bis-(acryloyloxy butyrate) [PEG-bis-AB], respectively. The products were purified by filtration, rotary evaporation, and precipitation in ethyl ether and dried under vacuum. The structures of each PEGdA and the degree of acrylation were determined from the ^{1}H-NMR (Brucker 300 MHz, $CDCl_3$) spectra. All samples achieved acrylation efficiencies greater than 90%.

3.2.2 Synthesis of methacrylated HA (GMHA)

GMHA was synthesized as previously described [189]. Briefly, HA (1g, MW:1.5 MDa, LifeCore Biomedical, Chaska, MN) was dissolved at 1% (w/v) concentration in

deionized water and then TEA (7.33 mL), glycidyl methacrylate (7.33 ml, Acros), and tetrabutyl ammonium bromide (7.33 g, Acros) were added with 3 hours mixing between addition of each reagent. The reaction was allowed to proceed for 12 hours at room temperature followed by 1 hour at 60 °C. The GMHA product was precipitated in acetone, re-dissolved in deionized water, dialyzed, and recovered by lyophilization.

3.2.3 Cell culture

Adult normal human dermal fibroblasts (NHDF, Lonza, Walkersville, MD) were cultured in 75 cm^2 tissue culture flasks with DMEM/F-12 50:50 1X media (Mediateach, Herdon, VA) with L-glutamine supplemented with 10% (v/v) bovine growth serum (Hyclone, Logan UT), and 50 U/mL penicillin and 50 μg/mL streptomycin (Mediatech). Medium was changed every 2 days and cells were passaged at a 1:3 ratio for expansion. All encapsulation studies were done with cells between passages 4 and 5.

3.2.4 Effect of semi-IPN network composition on fibroblast morphology

HA and GMHA (1.75% w/v) and PEGdA (30% w/v) stock solutions were prepared in 1X-PBS (0.1 M, pH 7.4). Acryl-PEG-GRGDS was synthesized by conjugating GRGDS peptide (Bachem, Torrance, CA) to acryl-PEG-NHS (Jenkem, Beijing, China) as previously described [169]. Based upon pilot studies, 6% w/v PEG-bis-AP containing 0.36% w/v 1.5 MDa HA was selected as an initial baseline gel composition. In order to systematically investigate the effect of semi-IPN network composition on the morphology of encapsulated fibroblasts, a series of studies was performed in which one parameter of the gel composition (HA concentration, HA molecular weight, PEGdA concentration, PEGdA chemistry) was varied while the others

were held constant. 250 μl gel precursor solutions were prepared containing PEGdA and HA at varying concentrations, acryl-PEG-GRGDS (1 μmol/mL), 2-hydroxy-1-[4-(hydroxyethoxy) phenyl]-2-methyl-1-propanone (I-2959, BASF, Florham Park, NJ, 0.1% w/v), and NHDF (5×10^6 cells/mL). Sample volumes (50 μl) were pipetted in between glass coverslips separated by 1 mm Teflon spacers and exposed to low intensity UV light (365nm, 10mW/cm^2, Blak-Ray B100-AP, Upland, CA) for 5 minutes on each side of the disc as previously described [Kutty JK J Biomater Sci Polym Ed 2009]. Hydrogels with encapsulated cells were cultured in Petri dishes (BD, San Jose, CA) with 3mL culture medium. For studies examining the effect of HA concentration, homogeneous synthetic PEGdA hydrogels (no HA) and co-polymer networks in which native HA was replaced with the same concentrations of GMHA were also prepared. For the study examining the effect of PEGdA concentration, the HA concentration was also varied in order to maintain the 6% w/w ratio of HA:PEGdA present in the baseline gel composition with 6% w/v PEGdA and 0.36% w/v HA. Gels containing encapsulated cells (n=4 samples / group) were cultured for 7 days, fixed with 4% paraformaldehyde (Sigma-Aldrich) in 1X-PBS for 1 hour, permeabilized with 0.1% Triton X-100 (Sigma-Aldrich) in 1X-PBS for 5 minutes and, stained with Alexa Fluor 647-phalloidin (Life Technologies, Grand Island, NY). Samples were imaged using Nikon Ti-Eclipse confocal microscope. Cell morphology at 200μm depth inside hydrogel was visualized and compared to assess cell spreading and network connectivity. Average cell circularity (dimensionless parameter defined as circularity = $(4\pi\times\text{area})/\text{perimeter}^2$, ranging from 0 to 1, with 1 being a perfect

circle) was calculated from confocal images using the NIH Image J Software Analyze Particles feature.

3.2.5 Hydrogel turbidity and mechanical properties

To assess gel turbidity, PEG-bis-AP semi-IPNs (6% w/v, 100 μL volume) with varying HA concentration/molecular weight and copolymerized hydrogels with GMHA without NHDF cells (n=4 per group) were photopolymerized as described above. As an additional control, semi-IPNs were also prepared with 0.36% w/v dextran (80 and 1100 kDa, Sigma). The sample discs were placed in 24 well plates and absorbance was measured at 570 nm using μQuant UV-VIS spectrophotometry (BIO-TEK Instruments). The final absorbance values were normalized by subtracting the average value of blank wells. Turbidity was calculated as Turbidity = $-\ln(10^{-A})$, where A=absorbance.

To measure hydrogel mechanical properties, semi-IPNs composed of 1) PEG-bis-AP (6% w/v) with varying concentrations of HA and 2) varying concentrations of PEG-bis-AP with HA maintained at 6% w/w HA:PEGdA were photopolymerized as described above. Hydrogels were cut into custom made dumbbell shaped samples with 30 mm gauge length, 5 mm width, and 1 mm thickness. The samples (n=3/group) were subjected to 35% strain at 5 mm/min using an MTS Synergy 100 (MTS Systems Corporation) at room temperature. Each sample was tested three times to ensure that slippage did not occur.

3.2.6 Hydrogel degradation study

To evaluate the effect of PEGdA macromer chemistry on hydrogel degradation, semi-IPNs were crosslinked as 1) homogeneous networks containing each of the 3

different PEGdAs and 2) blended networks composed of all 3 PEGdAs mixed in varying ratios. All samples were prepared at 6% w/v total PEGdA concentration with 0.36% HA w/v (1.5 MDa). After photopolymerization, samples were equilibrated with NHDF culture medium with 0.1% w/v sodium azide (Sigma-Aldrich), washed with deionized water, lyophilized, and weighed (Wd_0). Samples were incubated in 4mL of cell culture media with sodium azide in scintillation vials in a cell culture incubator with 5% CO_2 supply at 37 °C. Medium was changed once every 2 days. At each time point, samples (n=3/group) were collected, washed with deionized water, lyophilized, and weighed (Wd_t). Percent mass loss was calculated as $[(Wd_0–Wd_t)/Wd_0]\times100$.

3.2.7 NHDF morphology and migration in PEGdA blend / HA semi-IPNs

PEGdA macromer blend (12.5% PEG-bis-AA; 37.5% PEG-bis-AP; 50.0% PEG-bis-AB) at 6% w/v final concentration was prepared with 0.36% w/v HA (MW: 1.5 MDa) and acrylate-PEG-GRGDS (1 μmol/mL) and I-2959 (0.1%). In order to evaluate fibroblast morphology during long-term culture, NHDF (10×10^6 cells/mL final concentration) were uniformly dispersed within the gel precursor solution and photopolymerized as described above. Hydrogel samples (n=4/time point) were cultured in 35 mm Petri dishes for 3, 7, 14, 21, 28, and 35 days, then fixed and stained with Alexa 647-phalloidin and imaged by confocal microscopy. To assess the gel's capacity to support cellular invasion and migration, a gel-within-gel encapsulation system was used. NHDF were first entrapped within small fibrin clots (120,000 cells / 4 μl) prepared from 1% human fibrinogen (Enzyme Research Laboratories) with 2.5 mM calcium chloride (Sigma) and 0.001 U/mL thrombin (Enzyme Research Laboratories). After gelation for

15 minutes at 37°C, NHDF-loaded fibrin clots were gently placed within 50 μl solutions of the semi-IPN formulation described above (without additional cells) and gels formed by photopolymerization. As controls, NHDF-loaded fibrin clots were also polymerized within hydrogels of the same composition without native HA and co-polymerized networks with comparable concentrations of GMHA. Hydrogel samples were imaged at day 0, 3, 7, 10, 14, 18, and 21 using phase contrast microscopy (Zeiss). For 3D images, NHDF-loaded fibrin clots were harvested at day 14 and prepared for confocal microscopy as described above. Samples were three dimensionally scanned with 20 μm z-interval.

3.2.8 Statistical analysis

Quantitative data for hydrogel turbidity and elastic modulus were compared by ANOVA using Tukey's method for post-hoc comparisons (one-way ANOVA followed by Bonferroni's multiple comparison test). p values < 0.05 were considered to be statistically significant. All quantitative data are presented as mean ± standard deviation.

3.3 Results

3.3.1 Effect of HA concentration on 3-D fibroblast morphology

NHDF were encapsulated in photopolymerized PEG-bis-AP hydrogels, PEG-bis-AP / HA semi-IPNs containing varying concentrations of HA, and PEG-bis-AP / GMHA copolymer hydrogels. After 7 days in culture, cells in PEG-bis-AP hydrogels without HA were unable to spread and retained a spherical morphology (Figure 3.1A, circularity =0.65±0.08). In contrast, PEG-bis-AP/HA semi-IPNs supported extensive cell spreading that qualitatively appeared to be greatest at 0.36 and 0.54% HA and moderately decrease

at 0.72% HA and higher (Figure 3.1B-E), although all samples had circularity values ranging between 0.11-0.14 with no significant differences among these groups. Cells within copolymer hydrogels formed with comparable amounts of GMHA were unable to spread (Figure 1F, circularity=0.68±0.09), demonstrating that the ability of PEG-bis-AP/HA semi-IPNs to support cell spreading is a unique property of the semi-IPN network structure.

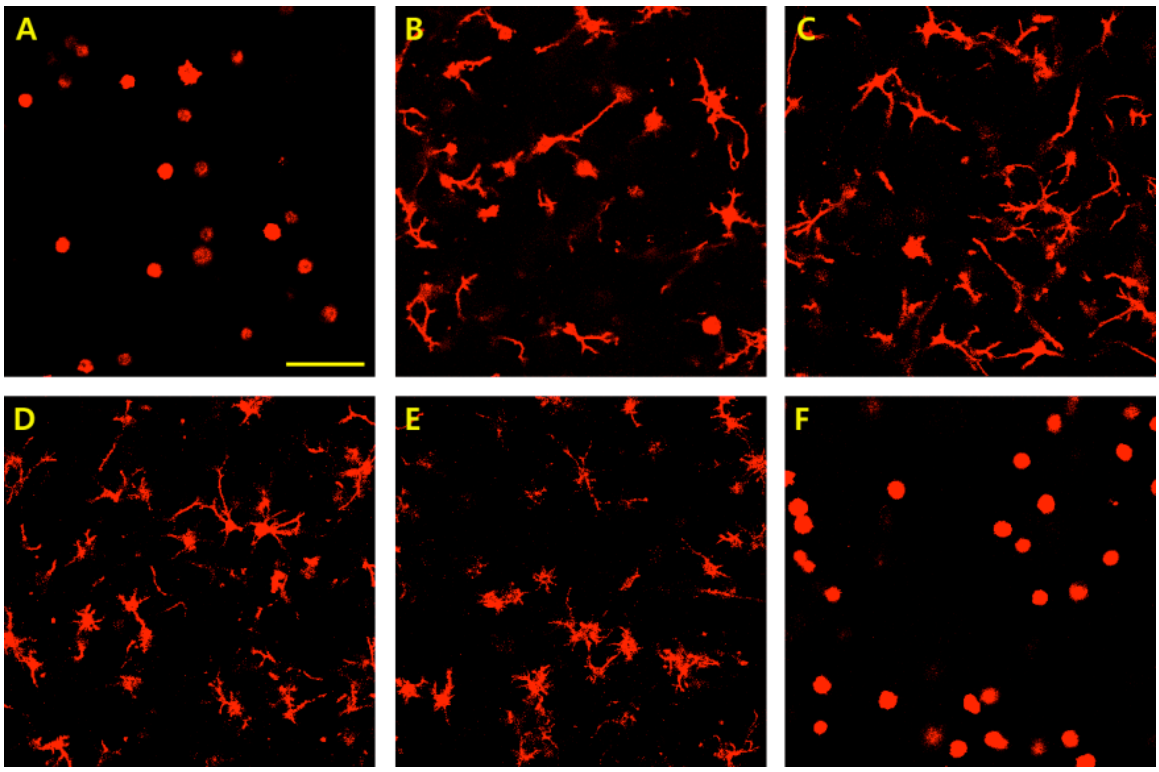

Figure 3.1 Confocal microscopy images of actin-stained human dermal fibroblasts encapsulated within 6% w/v PEG-bis-AP hydrogel (A), PEG-bis-AP/HA semi-IPNs containing 0.18% w/v HA (B), 0.36% w/v HA (C), 0.54% w/v HA (D), 0.72% w/v HA (E), and PEG-bis-AP/GMHA co-polymer hydrogel containing 0.36% w/v GMHA (F) at 200 μm depth after 7 days culture, scale bar = 100 μm.

3.3.2 Physico-chemical characterization of PEG—bis-AP/HA semi-IPNs and hydrogels

The effect of HA incorporation on hydrogel physico-chemical properties was analyzed by measuring turbidity and tensile properties. Figure 3.2 shows the turbidity of both PEG-bis-AP/HA semi-IPNs and PEG-bis-AP/GMHA copolymer hydrogels measured by spectrophotometry. Relative to PEG-bis-AP hydrogels, incorporation of native HA to form semi-IPNs significantly increased sample turbidity in a dose-dependent manner. The turbidity of copolymer hydrogels containing comparable amounts of GMHA was not significantly different than the PEG-bis-AP control at any concentration tested.

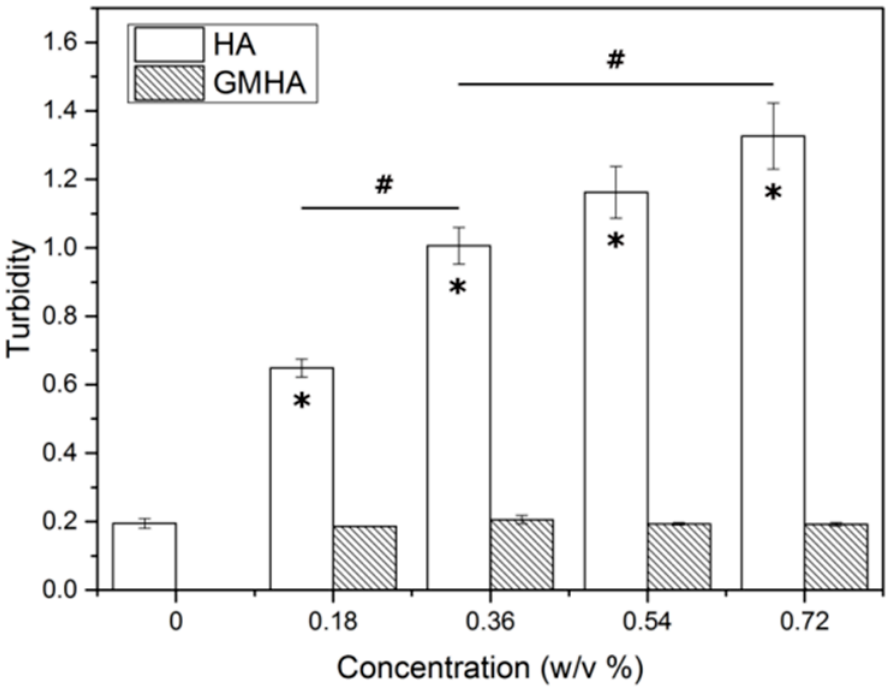

Figure 3.2 Turbidity of 6% w/v PEG-bis-AP hydrogels, PEG-bis-AP/HA semi-IPNs containing varying amounts of HA, and PEG-bis-AP/GMHA copolymer hydrogels containing varying amounts of GMHA. *=$p<0.05$ relative to PEG-bis-AP hydrogel and #=$p<0.05$ between groups.

The mechanical properties of PEG-bis-AP/HA semi-IPNs were measured by tensile testing. The elastic modulus of semi-IPNs containing 0.18% w/v HA was modestly higher than the PEG-bis-AP hydrogel without HA and then elastic moduli values decreased with increasing HA content with the differences being statically significant at the two highest concentrations (Figure 3.3).

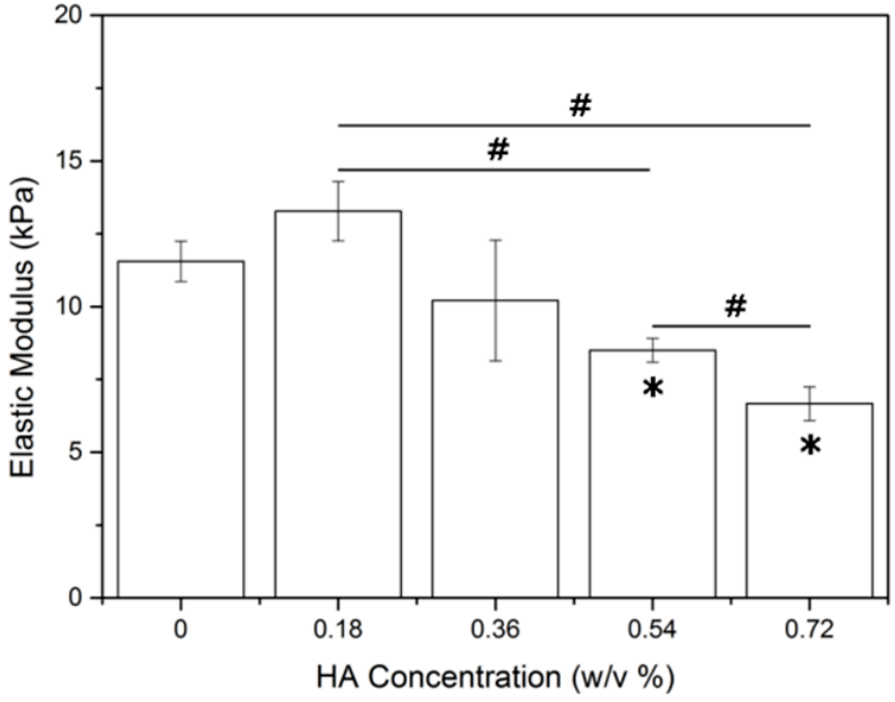

Figure 3.3 Elastic modulus of 6% w/v PEG-bis-AP hydrogels and PEG-bis-AP/HA semi-IPNs containing varying amounts of HA. *=$p<0.05$ relative to PEG-bis-AP hydrogel and #=$p<0.05$ between groups.

3.3.3 Effect of HA molecular weight on 3-D fibroblast morphology and gel turbidity

NHDF were encapsulated in semi-IPNs containing 6% w/v PEG-bis-AP and 0.36% w/v HA of varying molecular weight (MW). Semi-IPNs containing low MW (100 kDa) HA did not support the spreading of fibroblasts, which retained a spherical morphology (circularity = 0.69±0.03) after 7 days in culture (Figure 3.4). At 700 kDa HA MW and higher, all samples exhibited comparable cell spreading and circularity values ranging between 0.17-0.21. These results demonstrate that a minimum threshold for HA MW exists that is required to support cell spreading. Semi-IPNs prepared with high MW HA (700-1500 kDa) that supported cell spreading exhibited significant increases in gel turbidity, while the 100 kDa HA group was not significantly different from the PEGdA only control (Figure 3.5). Semi-IPNs prepared with dextran at both low (80 kDa) and high (1100 kDa) MW did not exhibit significant changes in turbidity relative to the PEGdA control.

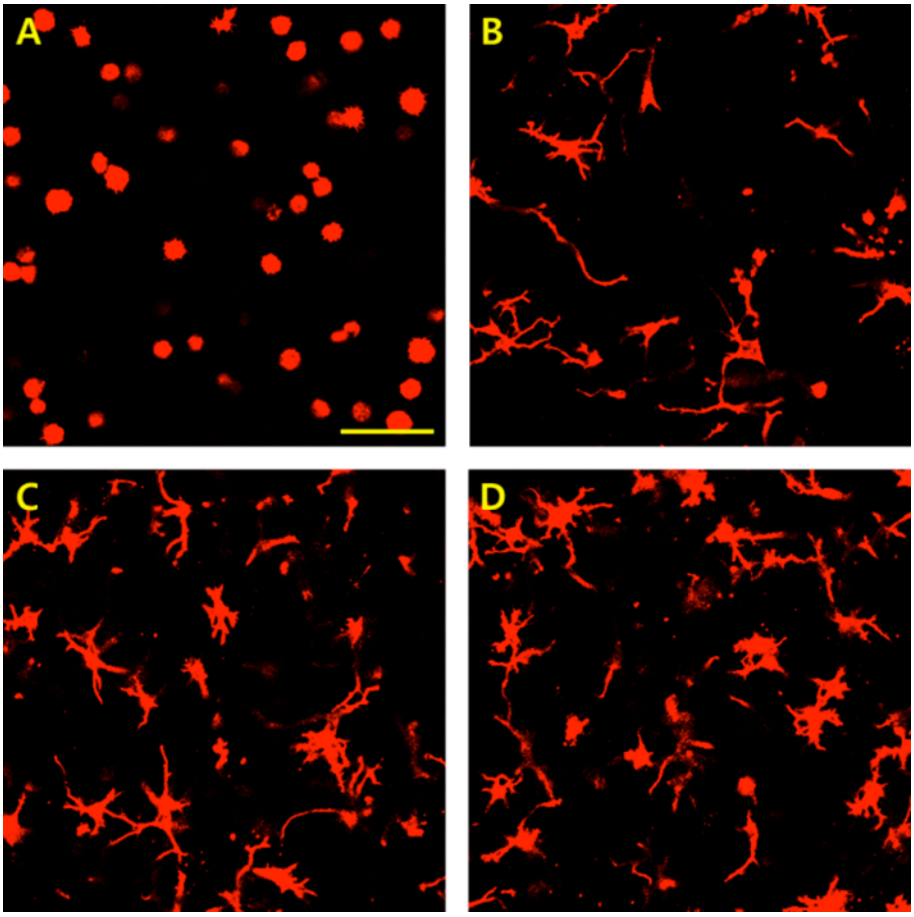

Figure 3.4 Confocal microscopy images of actin-stained human dermal fibroblasts encapsulated within 6% w/v PEG-bis-AP / 0.36% w/v HA semi-IPNs prepared using HA with molecular weights of 100 kDa (A), 700 kDa (B), 1.0 MDa (C) and 1.5 MDa (D) at 200 μm depth after 7 days culture, scale bar = 100 μm.

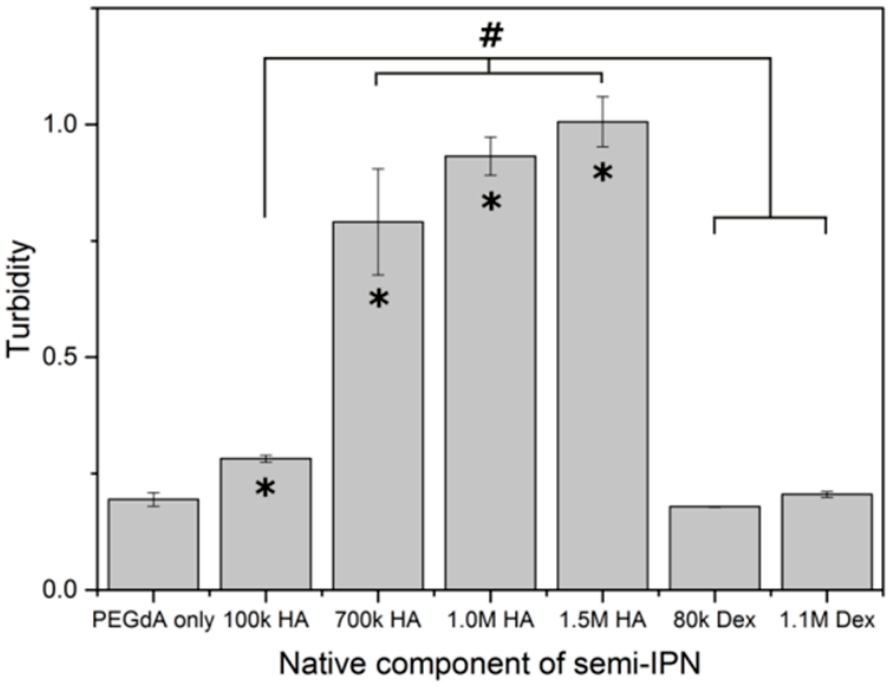

Figure 3.5 Turbidity of 6% w/v PEG-bis-AP hydrogel and PEG-bis-AP/HA and PEG-bis-AP/dextran semi-IPNs containing 0.36% w/v HA or dextran of varying molecular weight. *=$p<0.05$ relative to PEG-bis-AP hydrogel and #=$p<0.05$ between groups.

3.3.4 Effect of PEG diacrylate macromer concentration and chemical structure on 3-D fibroblast morphology

NHDF were encapsulated in semi-IPNs containing various concentrations of PEG-bis-AP and HA, maintaining constant 6% w/w PEG/HA ratio. Semi-IPNs containing 4-6% PEG-bis-AP effectively supported cell spreading at 7 days with the most robust response observed at the 4% concentration (Figure 3.6). Cell spreading was substantially reduced as the PEG-bis-AP concentration was increased to 8% and minimally present at 10%. Circularity values steadily increased with increasing PEGdA concentration, although the maximum value reached was 0.32±0.02 at 10% PEGdA, which was significantly lower that PEGdA hydrogel controls without HA. Tensile testing showed that semi-IPN elastic modulus increased from 10.2 +/- 2.07 kPa at 6% to 28.0 w/v +/-2.65 kPa and 76.0 +/- 3.61 kPa at 8 and 10% concentration, respectively. Samples prepared at 4% were visibly weaker and could not be evaluated by tensile testing.

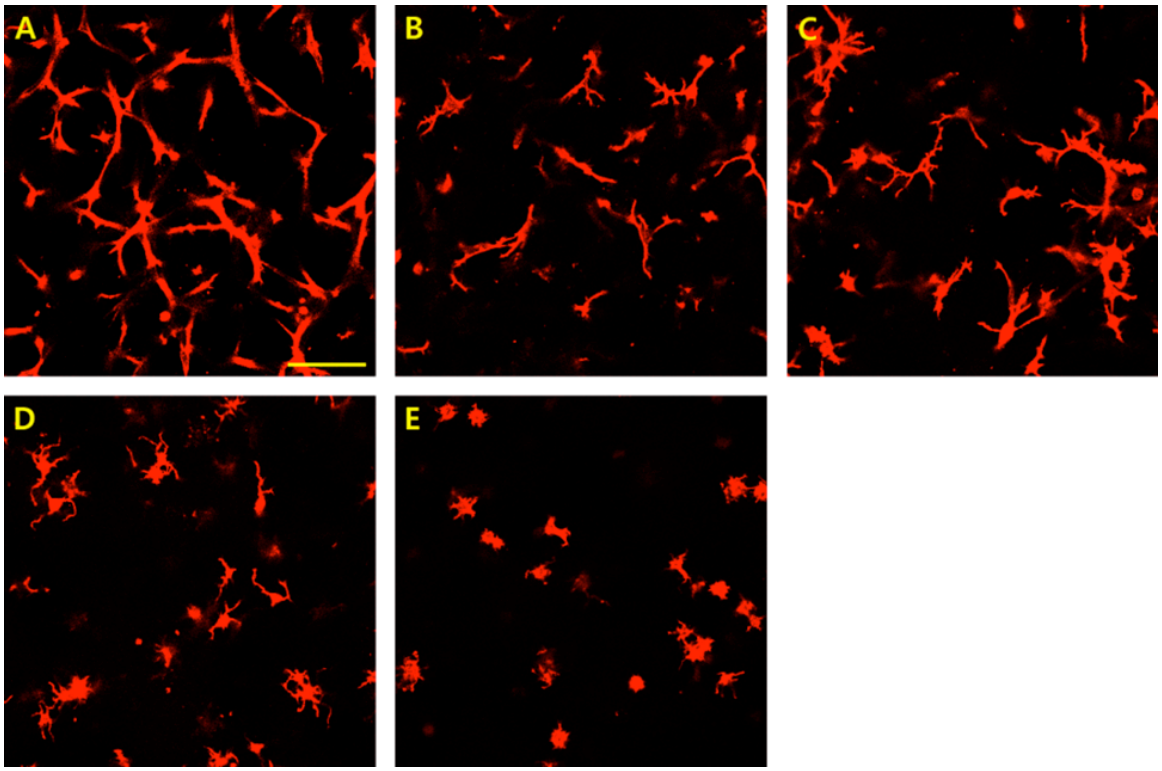

Figure 3.6 Confocal microscopy images of actin-stained human dermal fibroblasts encapsulated within PEG-bis-AP / HA semi-IPNs containing varying concentrations of PEG-bis-AP and HA; 4% w/v PEG-bis-AP with 0.24% w/v HA (A), 5% w/v PEG-bis-AP with 0.30% w/v HA (B), 6% w/v PEG-bis-AP with 0.36% w/v HA (C), 8% w/v PEG-bis-AP with 0.48% w/v HA (D) and 10% w/v PEG-bis-AP with 0.60% w/v HA (E) at 200 μm depth after 7 days culture, scale bar = 100 μm.

NHDF were also encapsulated in semi-IPNs prepared from various PEGdA macromers with varying chemical structures (PEG-bis-AA, PEG-bis-AP, or PEG-bis-AB) previously shown to provide different susceptibility to hydrolytic degradation [188]. As early as 3 days post-encapsulation, fibroblast spreading was observed in all semi-IPN compositions (Figure 3.7). Circularity values for all three groups ranged from 0.17-0.21 without significant differences. Cells encapsulated within homopolymer hydrogels of even the most rapidly hydrolytically degrading macromer (PEG-bis-AA) without HA did not exhibit any spreading (data not shown). These results confirm that the initiation of cell spreading within these gels is attributable to the HA component and independent of PEG macromer chemistry and hydrolytic degradation.

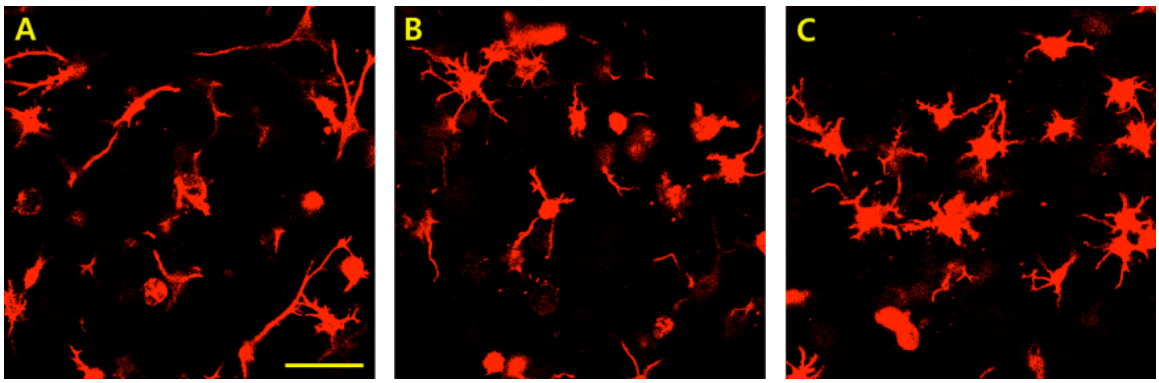

Figure 3.7 Confocal microscopy images of actin-stained human dermal fibroblasts encapsulated within 6% w/v PEGdA / 0.36% w/v HA semi-IPNs formed from PEG-bis-AA (A), PEG-bis-AP (B), and PEG-bis-AB (C) macromers at 200 μm depth after 3 days culture, scale bar = 100 μm.

3.3.5 Degradation kinetics of various semi-IPNs

In preparation for longer-term studies, the hydrolytic degradation kinetics of semi-IPNs prepared from PEGdA macromers with varying chemical structure were studied during incubation in serum-containing medium. For semi-IPNs prepared from each of the three different PEGdA macromers individually, PEG-bis-AA semi-IPNs showed the fastest degradation rate (complete degradation at day 7), PEG-bis-AP showed intermediate degradation rate (complete degradation at day 18), and PEG-bis-AB based semi-IPNs showed the slowest degradation rate (ca. 34% mass loss at day 42) (Figure 3.8A). In order to achieve a broader range of degradation profiles, blended PEGdA compositions (C1-C7, Figure 3.8B) containing the 3 different PEGdA macromers in various ratios were evaluated. A gel composition consisting of 12.5 % PEG-bis-AA, 37.5% PEG-bis-AP, and 50% PEG-bis-AB ('C1') was found to exhibit relatively linear mass loss over 5 weeks and was used for all further studies.

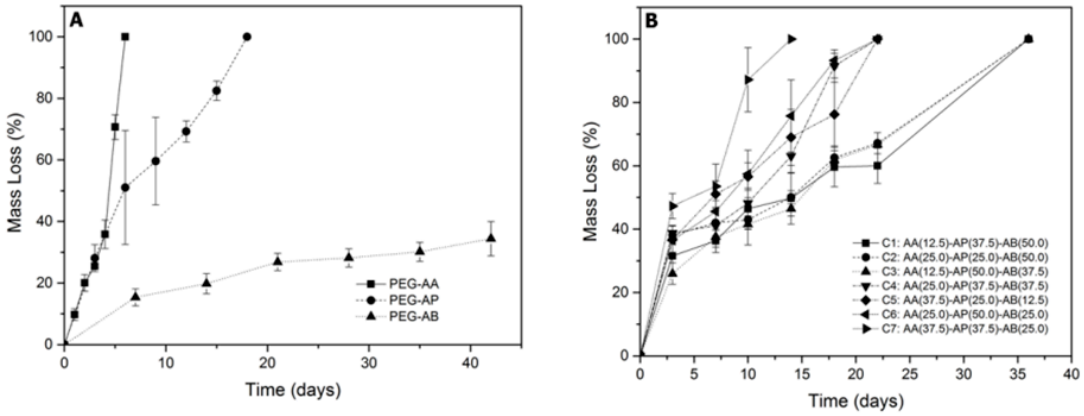

Figure 3.8 Mass loss of 6% w/v PEGdA / 0.36 % w/v semi-IPNs prepared with homogeneous (A) and blended (B) PEGdA composition in routine culture medium containing 0.1% w/v sodium azide.

3.3.6 Long-term 3-D fibroblast culture in blended PEGdA/HA semi-IPNs

In the first long-term culture study, NHDF were homogeneously encapsulated within semi-IPNs (6% w/v 'C1' PEGdA blend / 0.36% w/v HA) and cultured for 35 days. As shown in Figure 3.9, NHDF spreading progressively increased over the culture period and the cell number exhibited little change, suggesting limited cell proliferation. This is in contrast to blended PEGdA only (no HA) or blended PEGdA/GMHA hydrogel controls, where cells remained restricted to a spherical morphology and cell number visibly decreased by approximately 50% within 14 days (data not shown).

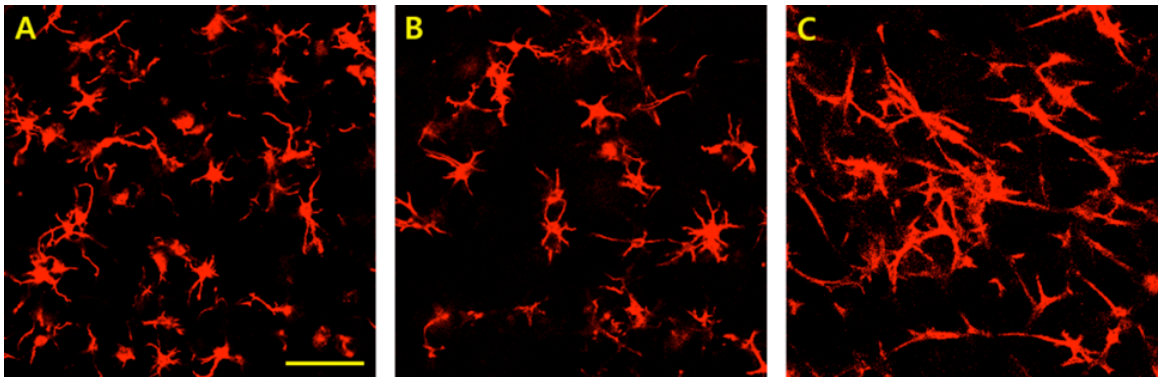

Figure 3.9 Confocal microscopy images of actin-stained human dermal fibroblasts encapsulated within 6% w/v blended PEGdA (C1-12.5% PEG-bis-AA, 37.5% PEG-bis-AP, 50.0% PEG-bis-AB) / 0.36% HA semi-IPNs at 200 μm depth after 7 days (A), 21 days (B), and 35 days (C) culture, scale bar = 100 μm.

In order to assess the ability of NHDF to migrate through blended PEGdA/HA semi-IPNs, NHDF were pre-encapsulated within fibrin clots that were subsequently entrapped within semi-IPNs during photopolymerization. Within 3 days, NHDF began to migrate out of the fibrin clots into the surrounding semi-IPNs (Figure 3.10A). NHDF migration progressively increased over time, reaching 1.5 mm depth within 21 days (Figure 3.10B/C). NHDF-loaded fibrin clots encapsulated within blended PEGdA/GMHA copolymer hydrogels as a control exhibited limited migration into the surrounding gel after 21 days in culture (Figure 3.10D). 3D confocal reconstruction confirmed that NHDF-loaded clots and cellular outgrowth was occurring within the 3D network volume rather than on the gel surface (Figure 3.9E).

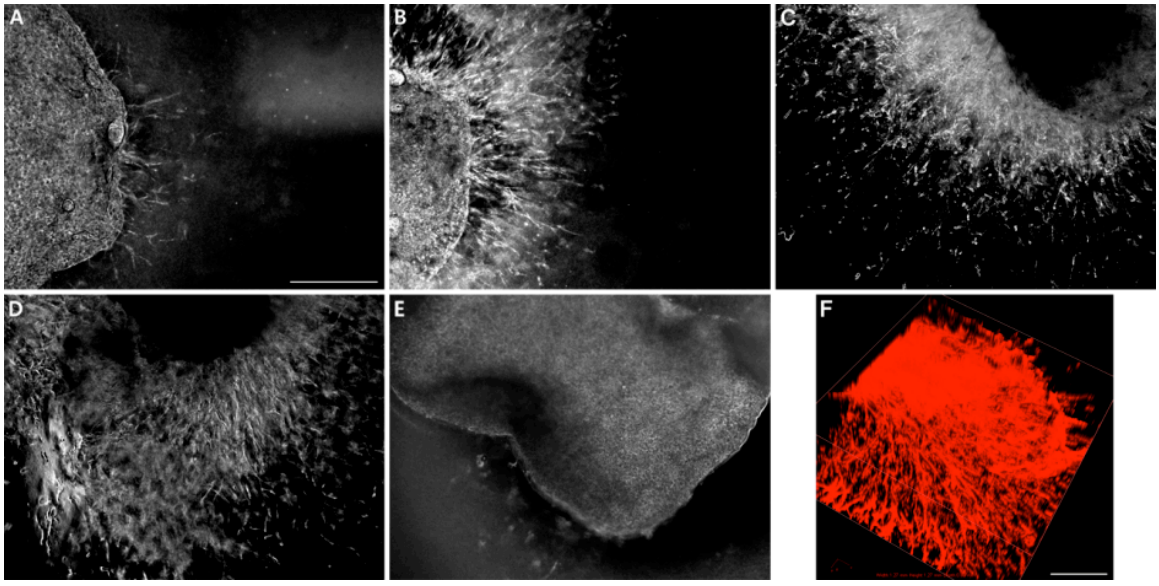

Figure 3.10 Migration of human dermal fibroblasts pre-encapsulated within 1% w/v fibrin clots into surrounding 6% w/v blended PEGdA (C1-12.5% PEG-bis-AA, 37.5% PEG-bis-AP, 50.0% PEG-bis-AB) / 0.36% w/v HA semi-IPNs after 3 days (A), 7 days (B), 14 days (C) 21 days (D) and 6% w/v blended PEGdA (C1) / 0.36% w/v GMHA copolymer hydrogels after 21 days (E) culture. 3D confocal reconstruction of fibroblasts migrating from fibrin clots into surrounding 6% w/v blended PEGdA (C1) / 0.36% w/v HA semi-IPN after 14 days in culture (F). Scale bars = 500 μm.

3.4 Discussion

The efficacy of cell-based therapy can be substantially improved by the use of scaffolds that serve as a provisional matrix for cell adhesion, migration, and proliferation. Synthetic hydrogels offer injectable matrices with defined structure and composition; however, such networks generally possess nanometer-scale mesh sizes that restrict encapsulated cells to a spherical morphology. For most anchorage-dependent cell types, the ability to adopt a spread morphology is essential for survival, migration, proliferation, and differentiation [190–192]. Therefore, there is a critical need for the development of hybrid networks incorporating naturally-derived components that support localized, cell-mediated remodeling.

As an alternative to the prevailing approach of crosslinking synthetic macromolecules with protease-sensitive oligopeptides, our group has previously shown that semi-IPNs composed of hydrolytically degradable PEG diacrylates and native HA support rapid 3D cell spreading in a hyaluronidase-dependent manner [187]. These materials are attractive candidates because other PEG and HA derivatives have been successfully translated for clinical applications [193,194]. In this study, the effect of semi-IPN network composition on 3D cell spreading was systematically examined, beginning with a baseline gel formulation composed of 6% w/v PEG-bis-AP macromer that provides an intermediate rate of hydrolytic degradation and 0.36% w/v HA (1.5 MDa). Fibroblast spreading in 3D exhibited a biphasic response to varying the concentration of HA, initially increasing at levels higher that those originally tested by Kutty et al. (0.18% w/v), then subsequently declining at 0.72% or higher. We

hypothesized that the activity of PEGdA/HA semi-IPNs originates from polymerization-induced phase separation as previously suggested by Ouasti and co-workers. [195]. In support of this hypothesis, fibroblast spreading was completely eliminated when native HA was replaced with a methacrylated HA derivative (GMHA) that could be covalently incorporated into the network, thereby limiting its potential to undergo phase separation. Gel turbidity was also evaluated as a quantitative measure of phase separation and found to increase with increasing HA concentration in semi-IPNs, but not copolymerized hydrogels containing GMHA. Finally, when the HA molecular weight was varied, it was observed that cell spreading required relatively high HA molecular weight, consistent with the increased tendency for phase separation as solute molecular weight increases. Interestingly, semi-IPNs prepared with dextran, even at high molecular weight, did not result in increased gel turbidity. This result suggests that HA is unique among various materials tested for the non-crosslinked component of these semi-IPNs, including collagen and gelatin in previous studies [187], in its ability to induce phase separation, at least to a degree sufficient to create microdomains that allow cell spreading. This is likely attributable to the unique properties of HA in terms of water-binding capacity; H-bonding and self-association; and solution rheology [196].

The ability of cells to spread and migrate in 3D has also been found to be dependent on the hydrogel's mechanical properties [112,176,178]. Tensile testing showed that the elastic modulus of semi-IPNs decreased with increasing HA concentration, likely due to the increasing level of phase separation creating defects within the network structure. However, it is particularly important to note that the elastic moduli values for

6% PEG-bis-AP with 0.36% and 0.54% HA that most effectively supported cell spreading ranged between 8-10 kPa. In contrast, most peptide-crosslinked hydrogels that support cell spreading/migration are characterized by elastic shear moduli values generally around and below 1 kPa, approximately an order of magnitude lower [96,175,179,197]. The higher mechanical properties of PEGdA/HA semi-IPNs offer several advantages including increased mechanical stability and resistance to cell-mediated contraction. In addition, recent studies have shown that substrate mechanics influence stem cell differentiation in both 2D and 3D culture systems and the elastic modulus of PEGdA/HA semi-IPNs is in close approximation to values shown to most efficiently promote osteogenic differentiation of human mesenchymal stem cells [8,142].

We also investigated the effect of variation in PEGdA concentration and chemical composition on 3D fibroblast spreading. Higher polymer concentrations resulted in increased mechanical properties and strongly inhibited cell spreading at PEGdA concentrations of 8% w/v and greater, despite corresponding increases in HA concentration to maintain a constant PEGdA:HA w/w ratio. This observation is consistent with many previous reports in the literature, although as noted above, the range of mechanical properties was much higher in PEGdA/HA semi-IPNs [112,176,178,181,197]. At 6% w/v, all three PEGdA chemical compositions supported the initiation of cell spreading within three days. In combination with previous work showing that the most slowly degrading PEG-bis-AB exhibits negligible mass loss at 3 days [189], this result demonstrates that the initiation of cell spreading in these semi-IPNs is independent of hydrolytic degradation and based solely upon cell-mediated degradation

of HA. The ability of cells to begin spreading rapidly is another important advantage of these PEGdA/HA semi-IPNs relative to peptide-crosslinked networks in which a lag period of 7-14 days is often observed between the time of encapsulation and the initiation of cell spreading, particularly when encapsulation is performed with dissociated individual cells [28,96,110,170,198]. Collectively, these results suggest that photopolyermization-induced phase separation creates HA-enriched defects within the network structure that facilitate rapid hyaluronidase-mediated localized degradation that supports cell spreading.

One challenge to the application of these semi-IPNs for long-term culture and translational applications was that none of the PEGdA macromers when used alone provided an ideal degradation profile. PEG-bis-AA and PEG-bis-AP degraded too rapidly resulting in loss of mechanical integrity and contraction, while PEG-bis-AB degraded too slowly, with little further cell spreading observed beyond that at 3-7 days and subsequent reduction in cellularity at later time points, presumably as a result of cell death. Previously, Quick and co-workers showed that blending acrylated PLA-b-PEG-b-PLA macromers with different PLA block lengths and therefore hydrolytic degradation rate could produce gels with more finely controlled and linear rates of degradation [199]. We adapted this approach by creating blends of the three different PEGdAs used in this study to obtain a formulation displaying relative linear mass loss over 5 weeks. These degradation studies were performed in serum-containing medium to reflect culture conditions because gel degradation was originally noticed to be much more rapid than previously observed during degradation in PBS, likely due to the contribution of serum

esterase enzymes. Using the selected blend formulation of PEGdA, sustained cell spreading and viability was observed for up to 35 days. Finally, a gel-within-gel encapsulation model was used to test the ability of blended PEGdA/HA semi-IPNs to support cell invasion and sustained migration. Fibroblasts pre-encapsulated within fibrin clots began sprouting into the surrounding semi-IPN and progressively migrated radially outward for over 21 days. As in our dispersed cell encapsulation model, copolymer hydrogels prepared with GMHA were unable to support this behavior. These results suggest that the HA-enriched zones created by phase separation are sufficiently inter-connected, in combination with gradual hydrolytic degradation, to support sustained cell migration.

3.5 Conclusions

These studies demonstrate that through systematic optimization of network composition, PEGdA/HA semi-IPNs can be formulated to provide dynamic microenvironments that support cell survival, spreading, and sustained migration. The bioactivity of these networks is a unique feature of the semi-IPN structure derived from polymerization-induced phase separation that creates HA-enriched micro-domains susceptible to cell-mediated enzymatic degradation in combination with prolonged hydrolytic degradation. Specific advantages of these semi-IPNs relative to existing hybrid hydrogels are the ability to support the rapid initiation of cell spreading within three days post-encapsulation and the provision of improved mechanical properties.

CHAPTER FOUR

OSTEOGENIC DIFFERENTIATION OF HUMAN MESENCHYMAL STEM CELLS IN SEMI-INTERPENETRATING NETWORK

4.1 Introduction

The rationale for bone tissue engineering originated from the limitations of traditional bone graft techniques. Bone defects resulting from trauma and tumor resection are common clinical problems. Bone tissue has the ability to regenerate, but when a defect of critical size needs to be bridged, the repair attempt fails in most cases. Replacing missing bone with material from the patient's own bone (autograft) is still considered as an ideal standard. However, the limited supply from the patient and possible donor site morbidity are problematic. Allograft is another bone graft technique, replacing missing bone with material from a donor (bone bank). In this technique, there is the potential risk of disease transmission and demand still outstrips supply. Healing can also be inconsistent due to its heterogeneity [200]. As a new practice, bone tissue engineering is an alternative strategy to regenerate bone using osteogenic progenitor or mature cells on osteoconductive scaffold material with or without appropriate osteoinductive growth factors [201–204]. Regarding bone graft substitutes, they should be osteoconductive which refers to the ability to provide an interconnected structure for new bone formation on its surface (or within the entire volume of construct) by mature bone forming cells. The objective of bone graft substitutes is to reliably replicate healthy

autograft. The research focus is to develop the matrix material with better biological compatibility and functionality, cell adhesion surface, bioresorbable capability, and drug delivery potential to release growth factors (stimulating bone repair) [202,205]. The most successfully commercialized osteoconductive three dimensional scaffold materials are bioceramics which undergo *ex vivo* fabrication prior to cell seeding due to harsh condition of fabrication [206–208]. This material by itself sometimes exhibits poor osteoconductive capability, shown as limited bone formation only at the boundary of the defects [209] and may require additional fabrication processes when the defect site geometry is complicated [208]. Alternatively, hydrogel scaffolds are widely studied as non-load bearing scaffold materials for bone tissue engineering due their ability to be delivered in a minimally invasive manner and polymerized *in situ* in the presence of cells under mild conditions [44,210,211].

For osteogenic cells, the fundamental studies have focused on mesenchymal stromal cells obtained from bone marrow because these cells have shown high osteogenic activity and can be cultivated *ex vivo* in quantities appropriate for clinical applications. They also show the advantage of low morbidity and cost over autograft. However, this has little clinical impact due to the limited number of clinical studies [212]. The ability of mesenchymal stem cells to differentiate has been found to be dependent on scaffold/substrate mechanical properties in both monolayer (2D) and three-dimensional (3D) culture systems [8,142]. Specifically, substrates with elastic moduli ranging from 5 kPa to 40 kPa favor osteogenic differentiation of mesenchymal stem cells in 3D culture [8,213–215]. As an *in situ* forming or minimally invasive cell transplant scaffold

candidate, hybrid hydrogels are designed to integrate the precise control of composition/properties provided by synthetic networks with the bioactivity of naturally-derived materials. PEG derivatives crosslinked with MMP-sensitive peptides are a prominent example and have been widely used for *in vitro* culture models and *in vivo* tissue engineering [11,58,168]. However, most peptide-crosslinked hydrogels that support cell spreading/migration are characterized by elastic shear moduli values generally around and below 1 kPa, approximately an order of magnitude lower than the optimal range for osteogenic differentiation [96,175,179,197,216]. Attempts to increase the elastic modulus of hydrogel scaffolds often requires higher cross-linking density of the network, resulting in a spherical morphology of encapsulated stem cells, which is not favorable to cell viability and also for osteogenic differentiation of encapsulated stem cells [170,217,218]. To achieve high elastic modulus and proper rate of degradation simultaneously, several groups explored alternative strategies such as increasing the number of degradable sites [112,179]. However, this approach has a practical limitation for cell based therapy due to its production cost and requirement of large quantity for application [175].

In previous research, the incorporation of native hyaluronic acid (HA) into photocrosslinked networks of hydrolytically degradable PEG diacrylates (PEGdA) creates semi-interpenetrating networks (semi-IPNs) that support increased cell spreading and proliferation relative to fully synthetic networks that is dependent on cellular hyaluronidase activity [187,188]. In Chapter 3, the network composition of semi-IPNs (6% w/v PEG diacrylate with 0.36% hyaluronic acid at 1.5 MDa molecular weight) was

identified to best support cell spreading and network formation. Selected semi-IPNs with PEGdA blends and HA supported prolonged 3D fibroblast culture for 35 days and sustained 3D cell migration. It is particularly important to note that the elastic moduli values of semi-IPNs for 6% PEG-bis-AP with 0.36% and 0.54% HA that most effectively supported cell spreading ranged between 8-10 kPa, which is in close approximation to values shown to most efficiently promote osteogenic differentiation of hMSCs in 3D culture condition [8]. In this study, semi-IPN application will be expanded toward stem cell therapy, especially osteogenic differentiation of mesenchymal stem cells (MSCs) for possible hard tissue applications. *In situ* photopolymerization of autologous cell encapsulated, mechano-mimetic, degradable hydrogels can be used as bone void-filler in non-load bearing site and act as 3D cell niche [219]. Human mesenchymal stem cells (hMSCs) have encapsulated within selected semi-IPNs and cultured under osteogenic differentiation conditions for up to 35 days. Encapsulated hMSCs exhibited alkaline phosphatase expression, osteogenic gene expression, and the progressive accumulation of collagen and mineralization. Histology and quantified calcium contents showed calcified tissue formation at the end of 3D culture. Osteogenic differentiation of encapsulated hMSCs followed similar mineralization process and relatively early osteoblast maturation process compared to its gene expression profile in monolayer (2D) culture from other study [220].

4.2 Materials and Methods

4.2.1 Synthesis of PEGdA macromers with ester linkages containing variable alkyl spacers

Three PEGdAs with varying susceptibility to hydrolytic degradation were synthesized by a two-step process. First, PEG (Fluka, MW 4000) was reacted with chloroacetyl chloride, 2-chloropropionyl chloride, or 4-chlorobutyryl chloride and then the resulting intermediate products were reacted with sodium acrylate to obtain PEG-bis-AA, PEG-bis-AP, or PEG-bis-AB, as previously described in Chapter 3. All samples achieved acrylation efficiencies greater than 92.5%, determined from ^{1}H-NMR (Bruker 300 MHz, $CDCl_3$) spectra.

4.2.2 In vitro cell culture

For cell growth and expansion, human mesenchymal stem cells (hMSCs, Lonza, Walkersville, MD) were cultured in 75cm^2 tissue culture flasks at 37°C with 5% CO_2 supply. Cells were cultured with low glucose DMEM with L-glutamine media (Life Technologies, Grand Island, NY) supplemented with 10% (v/v) MSC qualified fetal bovine serum (Life Technologies), 50U/mL penicillin and 50μg/mL streptomycin (Mediatech) and 10 ng/mL basic FGF (PeproTech, Rocky Hill, NJ). Medium was changed every 2 days and cells were passaged at a 1:3 ratio for expansion after reaching 85 to 90% confluence. All encapsulation studies were done with cells between passages 5 and 6.

4.2.3 hMSC encapsulation in semi-IPNs

Hyaluronic acid with 1.5 MDa molecular weight (Lifecore Biomedical, Chaska, MN) stock solution (1.75% w/v) and PEGdA (30% w/v) stock solutions were prepared in 1X-PBS (0.1M, pH 7.4). Acryl-PEG-GRGDS was synthesized by conjugating GRGDS peptide (Bachem, Torrance, CA) to acryl-PEG-NHS (Jenkem, Beijing, China) as previously described [169]. Gel precursor solutions (250 μL in 1X PBS) were prepared containing 6% w/v PEGdA blend (12.5% PEG-bis-AA, 37.5% PEG-bis-AP, and 50.0% PEG-bis-AB) and 0.36% w/v HA, acryl-PEG-GRGDS (1μmol/mL), 2-hydroxy-1-[4-(hydroxyethoxy) phenyl]-2-methyl-1-propanone (I-2959, BASF, Florham Park, NJ, 0.05% w/v), and hMSCs (final concentration at 12.5×10^6 cells/mL). hMSCs were uniformly dispersed within the gel precursor solution by pipetting. Sample volumes (55 μl) were pipetted in between glass separated by 1 mm Teflon spacers and exposed to low intensity UV light (365nm, 10mW/cm^2, Black-Ray B100-AO, Upland, CA) for 5 minutes on each side of the disc. Hydrogels with encapsulated cells were cultured in 35 mm diameter Petri dishes (BD, San Jose, CA) with 3mL culture medium. For osteogenic differentiation studies, encapsulated hMSCs were cultured with low glucose DMEM media with L-glutamine (Life Technologies) supplemented with 10% (v/v) MSC qualified fetal bovine serum (Life Technologies), 50U/mL penicillin and 50μg/mL streptomycin (Mediatech) in the presence of osteogenic differentiation supplements (50 μM ascorbic acid-2-phosphate (right?), 10 mM β-glycerophosphate, and 100 nM dexamethasone, all from Sigma-Aldrich).

4.2.4 Monitoring of encapsulated hMSC morphology under osteogenic differentiation condition

hMSCs were encapsulated as described above in semi-IPNs. Hydrogel samples (n=3/time point) were cultured in 35mm Petri dishes for 21 and 28 days, then fixed with 4% paraformaldehyde (Alfa Aesar, Ward Hill, MA), permeabilized with 0.1% Triton X-100 (Sigma-Aldrich), and stained with Alexa Fluor 647-phalloidin (Life Technologies). The morphologies of encapsulated cells were imaged using a Nikon Eclipse Ti confocal microscopy at 200 μm z-depth.

4.2.5 Alkaline phosphatase (Al-P) activity

hMSCs encapsulated in semi-IPNs were prepared and cultured in full osteogenic media for 7, 14, 21, and 28 days. At each time point, four hydrogel samples were harvested (n=4), washed twice with 1X PBS for 3 minutes each, and stored at -80°C freezer. For analysis, hydrogel samples were thawed and lysed with 0.1% Triton X-100 (Sigma) solution by manual homogenization. Residual hydrogel debris and cells were removed by centrifugation at 10,000 rpm for 5 minutes and supernatant was recovered for analysis. Prior to alkaline phosphatase activity measurement, total protein concentration was measured for normalization of alkaline phosphatase activity using BSA Total Protein Assay kit (Thermo Scientific, Waltham, MA). Alkaline phosphatase activity of encapsulated hMSCs was measured using alkaline phosphatase activity kit according to manufacturer's protocol (Sigma-Aldrich).

4.2.6 Quantitative RT-PCR

hMSCs encapsulated in semi-IPNs were prepared and cultured in growth (expansion) media for 1 day (24 hours). After 1 day, 4 hydrogel samples were harvested as reference condition (calibrator) samples for gene expression. For the rest of samples, culture media was switched to osteogenic differentiation media and cultured for 7, 14, 21, and 28 days. At each time point, four hydrogel samples were harvested (n=4), manually homogenized, lysed with 500 μL of RLT buffer (Qiagen, Valencia, CA) at room temperature, and stored at -80°C freezer. After thawing and centrifugation at 13,000 g for 15 minutes at 4°C, supernatant was collected for analysis. Total RNA was isolated using the Qiagen RNeasy mini kit (Qiagen) and treated with Turbo DNA-free DNase I Kit (Life Technologies) to remove trace amounts of genomic or plasmid DNA. cDNA was synthesized using 1 μg of total RNA from each sample as template using Retroscript Kit (Life Technologies) and Rotorgene 3000 light thermal cycler (Corbett Research, Mortlake, NSW, Australia). Real-time RT-PCR was performed with Quantitect SYBR green PCR Kit (Qiagen) using custom-designed primers (Table 4.1). Relative gene expression levels were calculated using ΔΔCt method with using β-2-microglobulin (β2MG) as an internal control and the day 1 static samples as reference condition (calibrator) [221]. The following PCR parameters were utilized: 95°C for 90 second followed by 45 cycles of 95°C for 30 seconds and 55°C for 60 seconds.

Target gene	Sense primer	Antisense primer
RUNX2	5'-CGAATGGACTATCCAGCCAC-3'	5'-TCCACTCTGGCTTTGGGAAG-3'
Collagen I	5'-TGCTGGTGCTCCTGGTACTC-3'	5'-TCCAGAGGGACCTTGTTTGC-3'
SP7	5'-TTCACTATGGCTCCAGTCCC-3'	5'-GAGTACGGCTTCTTTGTGCC-3'
Al-P	5'-ACCGAGATACAAGCACTCCC-3'	5'-TCACGTTGTTCCTGTTCAGC-3'
IBSP	5'-GGGAGTACGAATACACGGGC-3'	5'-TAGCCATCGTAGCCTTGTCC-3'
BGLAP	5'-GCGCTACCTGTATCAATGGC-3'	5'-TCCTGAAAGCCGATGTGGTC-3'
β2MG	5'-TGTGCTCGCGCTACTCTCTC-3'	5'-CGGATGGATGAAACCCAGAC-3'

Table 4.1 Target genes and primers for real time RT-PCR analysis.

4.2.7 Calcium and collagen staining

Encapsulated hMSCs were cultured with osteogenic supplements for 7, 14, 21, 28, and 35 days as described above, then fixed with 4% paraformaldehyde. Fixed hydrogels were gradually infiltrated by OCT (Optimal Cutting Temperature) compound (Sakura Finetechnical, Torrance, CA) by varying concentration of OCT in 1X PBS solution (increasing concentration from 25 to 100% OCT). Samples in OCT were snap-frozen using liquid N_2, then sectioned using Leica CM 1950 cryostat for desired thickness. Calcium on 6 μm sections was visualized using von Kossa (Poly Scientific, Bay Shore, NY) with Safranin O counter stain (Acros Organics) and Alizarin red S (Acros Organics) staining. 15 μm sections were stained for collagen using aniline blue (Poly Scientific). Stained sections were imaged using Nikon UZ-100 widefield microscopy.

4.2.8 Calcium quantification

Both acellular and hMSC encapsulated hydrogels were cultured with osteogenic supplements for 7, 14, 21, 28, and 35 days as described above. 4 samples from each group were harvested, then washed twice with 1X PBS, frozen at -80°C overnight, and lyophilized using Labconco Freezone 4.5 freeze dryer. Dry weights of samples were measured. Then samples were acid hydrolyzed at 90°C in 1 mL of 6 N Ultrex HCl (Fisher Scientific, Pittsburgh, PA) overnight, dried under continuous stream of nitrogen gas (Airgas National Welders, Atlanta, GA), re-dissolved with diluted 0.01 N Ultrex HCl solution (Fisher Scientific) and centrifuged at 12,500 rpm to remove undissolved impurities. Sample supernatants were diluted either 100 or 200 times volume with 0.5% w/v lanthanum oxide (Alfa Aesar) in 0.3 N Ultrex HCl solution (Fisher Scientific). Calcium concentrations of samples were measured using Perkin Elmer AAnalyst 200 atomic absorption spectrometer and normalized by dry weight of each sample previously measured. Absorbance reading was converted to calcium concentration based on calcium standard curve.

4.2.9 Statistical analysis

Quantitative data for calcium quantification, Al-P activities and osteogenic gene expression by RT-PCR were compared by ANOVA using Tukey's method for post-hoc comparisons (one-way ANOVA followed by Bonferroni's multiple comparison test). p values < 0.05 were considered to be statistically significant. All quantitative data are presented as mean ± standard deviation.

4.3 Results

4.3.1 Alkaline phosphatase activity

hMSCs were encapsulated within semi-IPNs and cultured in the presence of osteogenic supplements for 28 days. Total protein assay results indicated there was no significant increase in protein level after day 7 in culture (data not shown here). Alkaline phosphatase (Al-P) activity increased over time in culture, with levels measured at days 21 and 28 significantly higher than day 7 (Figure 4.1). However, the normalized Al-P level of day 14 was not significantly different from day 21 and 28 ($p<0.05$).

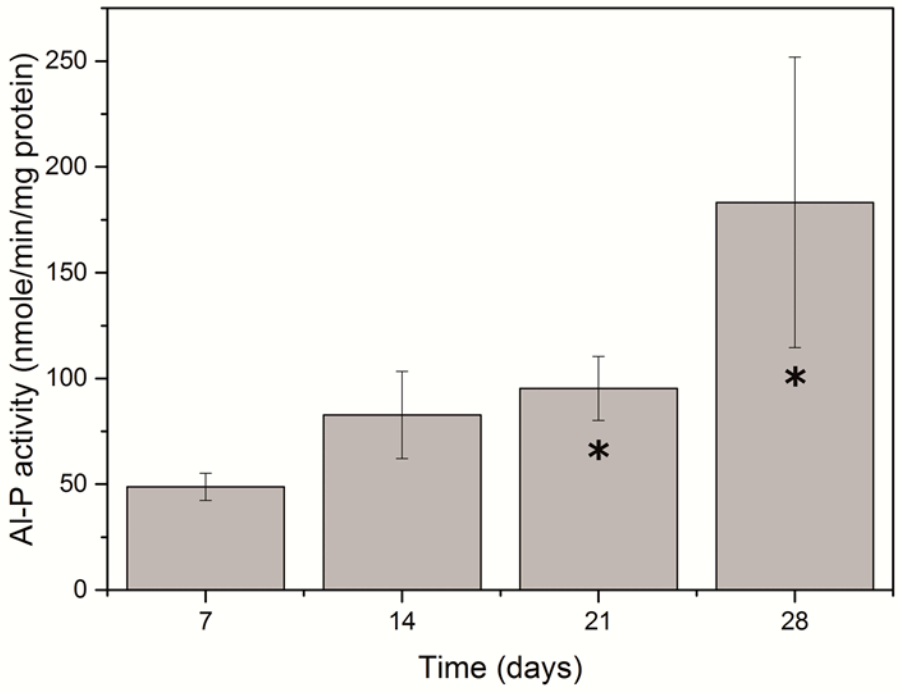

Figure 4.1 Alkaline phosphatase activity normalized by total protein concentration of hMSCs encapsulated in semi-IPNs at different time points during culture in the presence of full osteogenic supplements, *=$p<0.05$ relative to day 7.

4.3.2 Osteogenic gene expression

hMSC mRNA expression levels of several genes related to osteogenic differentiation were examined after 7, 14, 21, and 28 days of culture with osteogenic supplements. In general, hMSCs exhibited significantly increased expression of all genes examined at day 7 relative to control at day 0 (Figure 4.2). Expression levels of osterix (SP7, Figure 4.2B), integrin-binding sialoprotein (IBSP, Figure 4.2D), and collagen type I (Figure 4.2E) significantly decreased at later time points beyond day 7. In case of runt-related transcription factor 2 (RUNX2, Figure 4.2A) and osteocalcin (BGLAP, Figure 4.2F), increased gene expression levels relative to the day 0 control were maintained throughout the differentiation period. Interestingly, expression levels of alkaline phosphatase (Al-P) were significantly increased over time up to day 21 and later decreased at day 28. However, it still maintained higher level of gene expression compared to day 0 (Figure 4.2C).

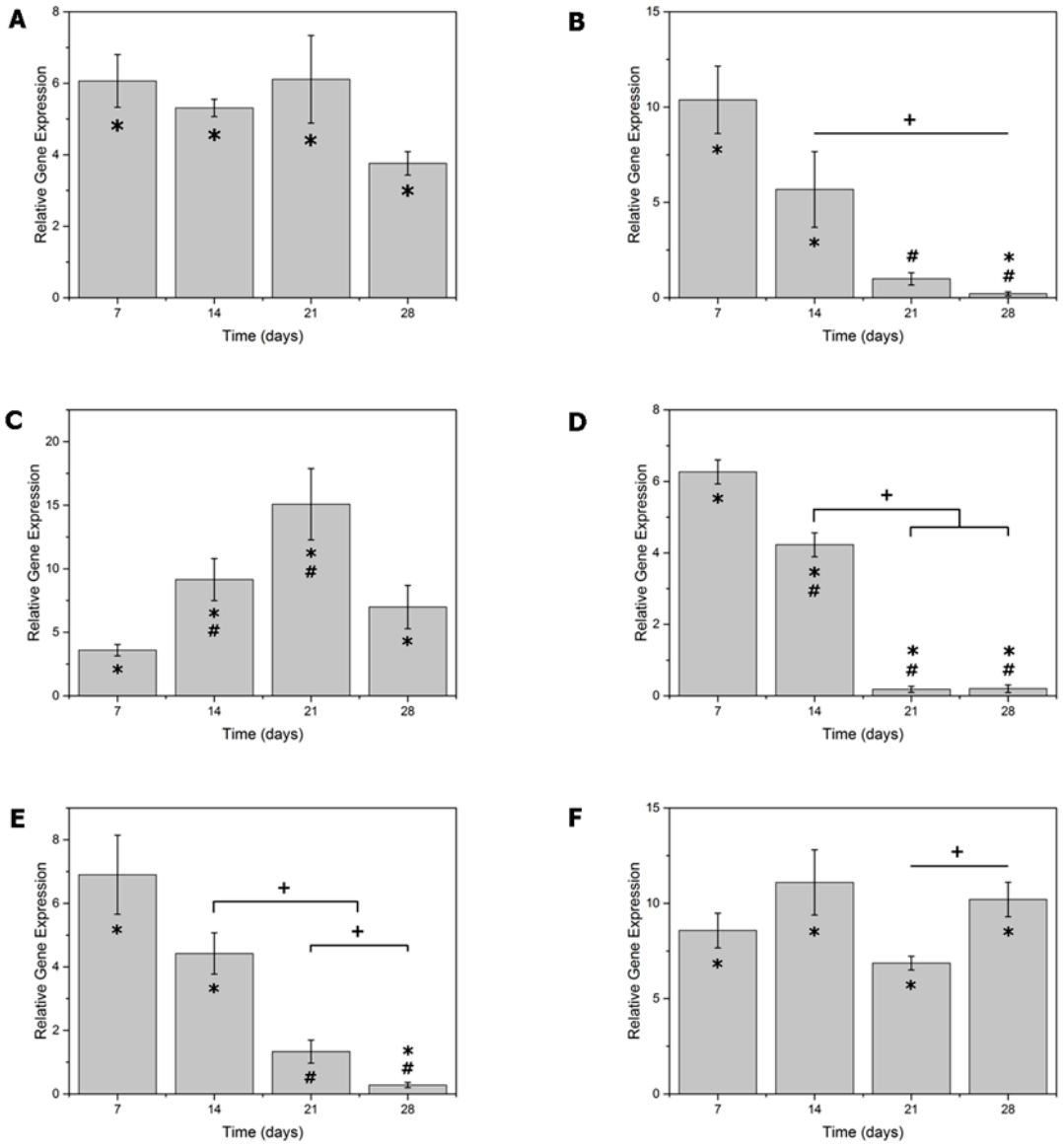

Figure 4.2 mRNA expression levels of RUNX2 (A), osterix (SP7) (B), alkaline phosphatase (C), bone sialoprotein (IBSP) (D), collagen type I (E), and osteocalcin (OCN) (F) at different time points during culture in the presence of full osteogenic supplements. *=$p<0.05$ relative to day 0 control, #=$p<0.05$ and +=$p<0.05$ between groups.

4.3.3 hMSC morphology encapsulated in semi-IPN under osteogenic differentiation condition

hMSCs were homogeneously encapsulated in photopolymerized 6% w/v PEGdAs (12.5% PEG-bis-AA, 37.5% PEG-bis-AP, 50.0% PEG-bis-AB) / 0.36% w/v HA semi-IPNs and cultured in full osteogenic media for 35 days. The selected semi-IPNs supported the survival and spreading of hMSCs. After 21 days in culture, the semi-IPNs showed increasing macroscopic opacity and encapsulated cells had spread and begun to form a connected network (Figure 4.3A and B). The extensive mineralization in semi-IPNs after 28 days of culture (Figure 4.3C) limited the ability of the confocal laser to penetrate into the 3D structure, resulting in imaging only a limited number of cells (Figure 4.3D).

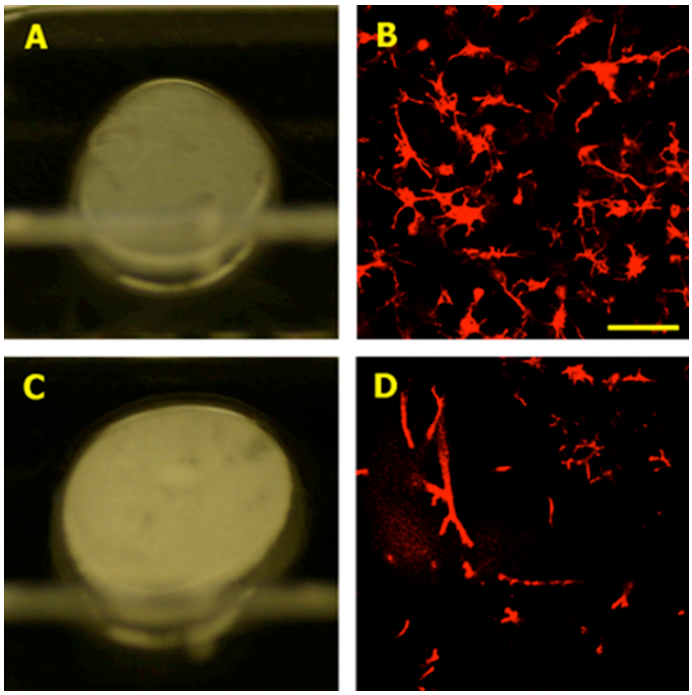

Figure 4.3 Macroscopic images of hMSC encapsulated 6% w/v PEGdAs / 0.36% w/v HA semi-IPNs after 21 days in culture (A), and 28 days in culture (C), confocal microscopy images of actin-stained hMSC encapsulated in semi-IPNs at 200 mm z-depth after 21 days in culture (B), and 28 days in culture (D), scale bar = 100 μm.

4.3.4 Collagen deposition and calcification in hMSC encapsulated semi-IPNs

Collagen deposition was modest at day 7 and then increased substantially after 21 days in culture (Figure 4.4A-C). Both calcium staining images (Figure 4.4G-I) showed that mineralization increased with the time in culture, similar to observations of collagen staining. Both collagen and calcium were homogeneously deposited throughout the entire volume of hydrogels.

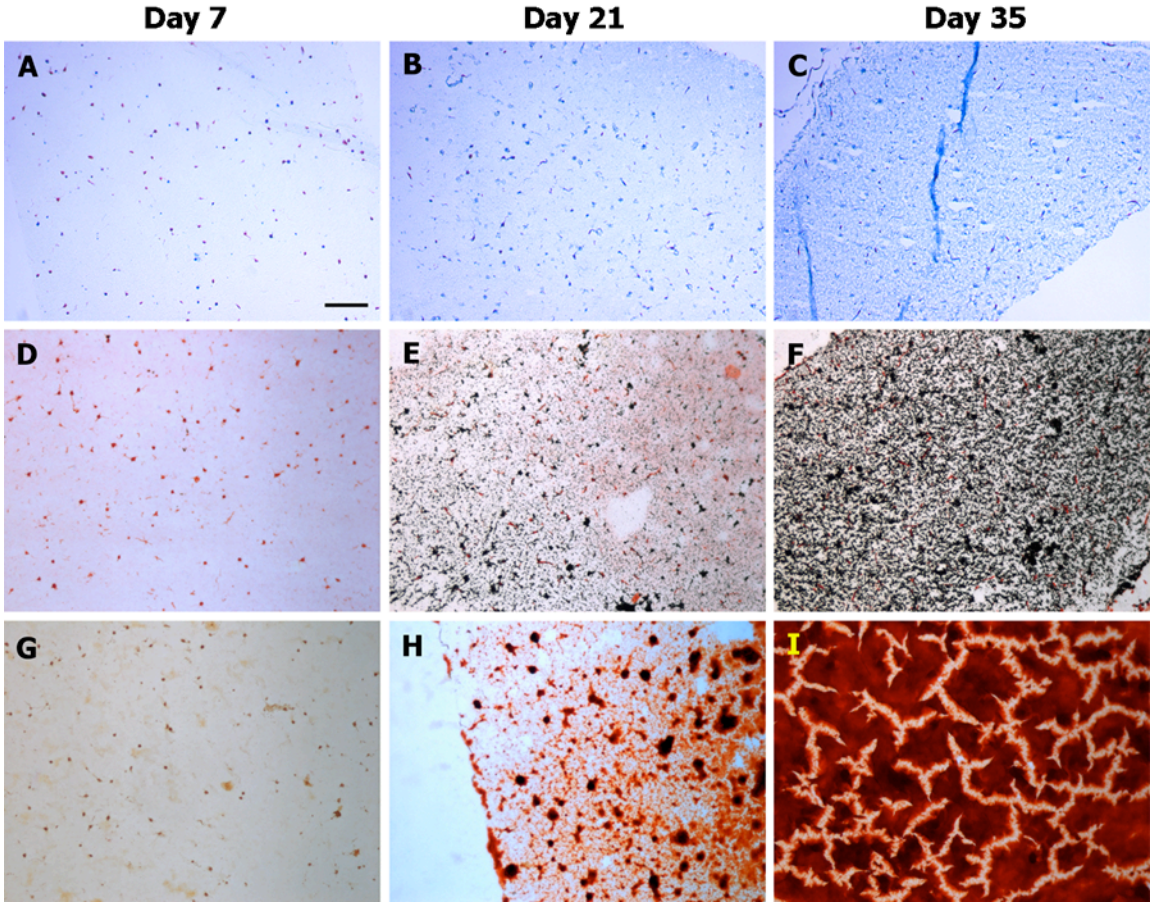

Figure 4.4 Histological sections of semi-IPNs with encapsulated hMSCs stained with aniline blue for collagen (A-C), von Kossa for calcium (D-F), and Alizarin red S for calcium (G-I) after 7, 21, and 35 days in culture, scale bar = 100 μm.

4.3.5 Quantitative calcification

In order to determine the contribution of non-physiological calcification, acellular semi-IPNs were included in the study as a negative control. As an additional control, semi-IPNs with encapsulated hMSCs were cultured without dexamethasone to investigate spontaneous osteogenic differentiation in the absence of a specific osteoinductive stimulus. Encapsulated hMSCs in full osteogenic media (OB) showed significantly increased calcification over time (Figure 4.5). Calcification in the experimental group was also significantly higher than both control groups at all (time) points. The acellular control group showed only a modest level of non-specific calcification. The control group without dexamethasone also exhibited minimal calcification through day 21, but significantly higher levels of calcium at days 28 and 35 relative to the acellular group.

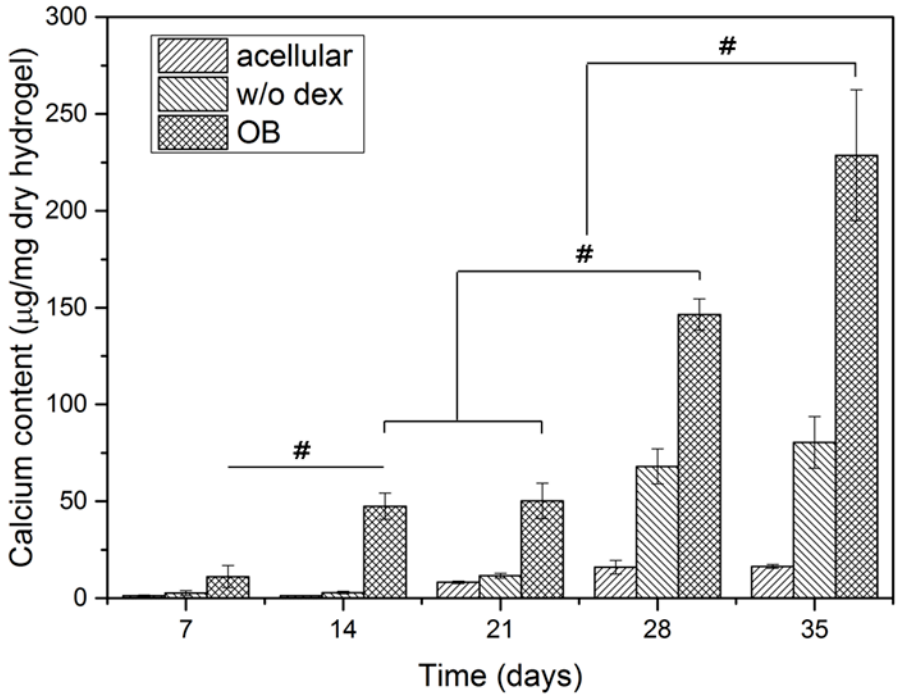

Figure 4.5 Calcium content measured in semi-IPN hydrogels normalized to sample dry weight. All samples were cultured in full medium with osteogeneic supplements (ascorbic acid-2-phosphate, betaglycerophosphate, and dexamethasone) except w/o dex where dexamenthasone was omitted. Only statistical analyses for OB group shown here for graphical clarity, #=$p<0.05$ between groups.

4.4 Discussion

This study was designed to both qualitatively and quantitatively asses the ability of selected semi-IPNs to support osteogenic differentiation of encapsulated hMSCs. It was previously shown that, by the formation of HA-enriched zones from polymerization-induced phase separation, semi-IPNs composed of hydrolytically degradable PEG diacrylates, acrylate-PEG-GRGDS and native HA support rapid 3D cell spreading and migration in a hyaluronidase-dependent manner. PEGdA/HA semi-IPNs were also able to support cell spreading at relatively high levels of mechanical properties (~10 kPa elastic modulus) compared to alternative hybrid hydrogels as shown in Chapter 3. This elastic modulus value was previously reported as optimal for osteogenic differentiation in three-dimensional (3D) culture [8]. In addition, the initial matrix stiffness is important as hMSCs are no longer reprogrammable once they have committed to the lineage specified by matrix elasticity after the initial week in culture [142]. As shown in Chapter 3, selected semi-IPNs maintained about 70% of initial mass after 1 week of culture while it provided the space for cell spreading.

To test of its feasibility as a scaffold for cell transplantation and 3D *in vitro* culture platform, hMSCs were photo-encapsulated within 6% w/v PEGdA/ 0.36% HA semi-IPNs with previously selected compositions (12.5% PEG-bis-AA, 37.5% PEG-bis-AP, and 50.0% PEG-bis-AB) and cultured under osteogenic differentiation conditions for up to 35 days. Confocal microscopy images showed spindle- shaped morphology of hMSCs encapsulated within semi-IPNs. Initial cell spreading occurred within the space filled with HA where HAse degrades first [187]. Cell spreading was supported in selected

semi-IPNs and could be observed till day 28. At later stage of culture (day 35), confocal scanning was hindered by deposited calcium (image not shown). Since hMSC viability and spreading are dependent on 3D network degradability, this enzymatic degradation positively affected long-term survival of transplanted stem cells and enhanced osteogenic differentiation and mineralization [9,170,217,218].

Alkaline phosphatase (Al-P) activity increased over time in 3D culture. Other research groups have also reported similar trends in Al-P activities for encapsulated hMSCs and dependency of differentiation on matrix degradability. Anderson and co-workers observed increased Al-P activity over time and over increasing MMP sensitive peptide concentration in thiol-ene hydrogels over 21 days of culture, suggesting osteogenic differentiation was influenced by network degradability [170]. Benoit and co-workers also reported the increasing trend of Al-P activity in 3D culture and its dependency on copolymer network composition (i.e. degradation rate). The Al-P activity increased over time and with increased degradability along with increased osteopontin and type I collagen expression [218]. Temenoff and co-workers reported different biphasic behavior (lowest Al-P activity at day 14 for all conditions) of Al-P activities in 3D MSC culture using oligo(poly-(ethylene glycol) fumarate) hydrogel [222].

When gene expression related to osteogenic differentiation of MSCs in 3D hydrogel culture was investigated and compared to other 3D culture studies, the temporal patterns and gene expression levels are not consistent with one another due to the fact that gene expression of encapsulated hMSCs depends on the surface characteristics (topography, chemistry, surface energy, and interplay of stiffness and adhesion ligand

presentation) of materials and changed accordingly [215,218,223–225]. Protein related to ECM maturation and bone cell phenotype, alkaline phosphatase (Al-P) gene expression of hMSCs encapsulated within semi-IPNs followed similar trend to 2D monolayer culture, with a peak around day 12 to 18 and subsequent decrease [220,226]. Early marker genes associated with extracellular matrix (ECM, type I collagen) and master gene controlling MSC differentiation into pre-osteoblast (runt-related transcription factor, RUNX2) exhibit different patterns of expression from each other. Collagen type I reached its peak expression level at day 7 and gradually decreased during subsequent stages of differentiation, which followed general profile of monolayer culture reported by Stein et al. and Born et al., but different from increasing trend in 3D culture reported by Benoit and co-workers [218,220,226]. However, RUNX2 maintained relatively similar gene expression level (no significant difference after day 7) throughout the entire differentiation period, exhibiting similar pattern to hMSCs cultured within soft (100 Pa) PEG-silica hydrogel (control to 2D monolayer culture) reported by Pek and co-workers, but different from the profile reported by Jha and co-workers. (up-regulated at day 21 compared to day 7 gene expression level) [216,227]. Osterix (SP7), which is transactivated by Runx2, regulates bone formation and plays a role in terminal maturation for osteoblast differentiation. hMSCs encapsulated within semi-IPNs showed early up-regulation of osterix at day 7, suggesting early differentiation of pre-osteoblasts to osteoblasts [228,229]. Osteocalcin (OCN), a major non-collagenous protein related to ECM mineralization, maintained high expression level after day 7 for hMSCs encapsulated within semi-IPNs, different from 2D monolayer pattern (up regulation

around days 16-20), but similar to one in 3D culture reported by Pek and co-workers [220,226,227]. Bone sialoprotein (IBSP), a major component of ECM, has been known to be a potent nucleator for hydroxyapatite formation and important for the initiation of bone mineralization. Early up-regulation of IBSP suggested early initiation of bone mineralization and the adhesion of (pre)osteoblasts to mineralized matrix [230]. Overall, hMSCs encapsulated within semi-IPNs showed similar ECM production process (collagen type I, alkaline phosphatase, osteocalcin, and IBSP) and relatively up-regulated and rapid osteoblast differentiation process (RUNX2 and SP7) compared to 2D monolayer culture reported by Stein and co-workers [220].

After 21 days of culture, calcification could be observed macroscopically and rapidly progressed over time. Although there were varying degrees of decrease in total volume of hydrogels (images not shown), hydrogels remained mechanically intact until the end of culture (day 35). Over a comparable timeframe, acellular semi-IPNs completely degrade in normal culture conditions as shown in Chapter 3, suggesting that the hybrid hydrogel network was replaced by newly formed mineralized tissue. As for acellular semi-IPNs, although they swelled more (i.e. weaker and increased volume of hydrogels) compared to semi-IPNs with hMSC, they maintained the structural integrity till day 35 by non-physiological calcium deposition. This observed calcification also coincided with histology and calcium quantification results (rapid increase in calcification after 21 days). The degree of mineralization increased for all control and experimental groups over time. However the degree and the rate of calcification was different from one another. Two control groups reached calcification plateau at day 21

(acellular hydrogel) and 28 (hydrogels in osteogenic media without dexamethasone) while experimental group showed substantial increase after day 21 as also shown in histology. Compared to other studies, the degree of mineralization (deposited calcium level) in semi-IPNs is relatively higher than those reported elsewhere [170,222]. Calcium ion transport would not be diffusion limited as IgG has been shown to be readily released from PEGdA hydrogels [188]. Additionally, it was hypothesized that Hase-mediated degradation at the early stage of cell culture could expand pore size in semi-IPNs and promote ion diffusion inside hydrogel network. Acellular control hydrogels showed little, but obvious calcium deposition, suggesting that non-physiological calcium deposition was still possible with full osteogenic media. Although it has been known that biomineralization in (acelluar) organic matrix is slow and difficult to control due to pore size and dense network structure, the process works relatively better in soft polymer with very large equilibrium water contents [231–233]. Comparably, encapsulated hMSCs and deposited collagen (produced from cells) acted as nucleation site for calcium ion and resulting in increased calcification / biomineralization [233,234]. Cell encapsulated hydrogels in osteogenic media without dexamethasone showed higher calcium deposition than acellular hydrogels, but significantly less calcium contents compared to hydrogels in full osteogenic media, indicating that semi-IPN mineralization was primarily attributable to dexamethasone-induced hMSC differentiation and spontaneous osteogenic differentiation could be achieved even in the absence of a specific osteoinductive stimulus (i.e. absence of dexamethasone supply).

4.5 Conclusions

This study demonstrated that PEGdA blend/HA semi-IPNs supported initial hMSC survival, spreading, and long term osteogenic differentiation. HA enriched zone from phase separation between the two components occurring during photocrosslinking provided the space for initial cell spreading via enzymatic degradation. Osteogenic differentiation of hMSCs encapsulated within semi-IPNs provided detailed gene expression profile in 3D culture, which followed relatively faster osteoblast maturation process and similar gene expression profile of mineralization process compared to 2D monolayer culture reported in the literature. The orchestrated prolonged degradation resulted in physiological collagen and calcium deposition during hMSC differentiation and network remodeling over 35 days in culture. These experiments suggest that PEGdA/HA based semi-IPNs are promising cell carrier materials for stem cell therapy applications. Ongoing studies are examining covalent conjugation of bioactive molecules to the HA component of these networks for sequestration and cell-mediated release during network remodeling and applications in bone tissue engineering.

CHAPTER FIVE

HYBRID HYDROGEL / HYDROPHOBIC NANOPARTICLE COMPOSITES FOR ENHANCED EXTRACELLULAR MATRIXS DEPOSITION

5.1 Introduction

Following tissue injury, the coagulation cascade produces a blood clot consisting predominantly of fibrin with smaller amounts of other plasma proteins such as fibronectin and growth factors released from damaged platelets. The fibrin clot serves as a hemostatic plug and a provisional matrix for tissue repair. During the proliferative phase, fibroblasts in healthy tissue adjacent to the wound site divide and migrate into the fibrin clot, remodeling it through a combination of cell-mediated proteolytic degradation and synthesis and organization of new extracellular matrix [235,236]. Briefly, ECM assembly *in vivo* is initiated by ECM glycoproteins binding to cell surface receptors, such as fibronectin (FN) dimers binding to α5β1 integrin receptors. Receptor binding stimulates FN self-association mediated by the N-terminal assembly domain and organizes the actin cytoskeleton to promote cell contractility [237]. FN conformational changes (compact to extended) induced by cellular traction expose additional cryptic integrin binding domains [29]. Cells use collagen V and XI to nucleate collagen fibrils, and FN and integrins to specify the assembly site at the cell surface [238–240].

Most tissue engineering and regenerative medicine strategies involve the use of a

polymeric scaffold as a transient structure to support cell adhesion, migration, proliferation, and differentiation that gradually degrades and is replaced by newly synthesized matrix. Much recent attention has focused on the use of hydrogel scaffolds due to their ability to be delivered to the injury site by minimally invasive procedures and crosslinked *in situ* using mild chemistries compatible with the encapsulation of living cells and bioactive molecules. With the exception of protein-based hydrogels (collagen, fibrin, etc.), the vast majority of hydrogels are based on hydrophilic polysaccharides and synthetic polymers [6,11,44,45]. One shared characteristic of these materials is a very low capacity for protein binding, rendering them 'blank slates' that do not interact with cells without the incorporation of exogenous cues such as RGD peptides to promote cell adhesion [45]. In fact, the most widely studied of these polymers, polyethylene glycol (PEG), has been extensively applied as a surface coating specifically intended to block protein adsorption and cell adhesion [162,241,242]. Although the most abundant ECM proteins, collagen type I and II spontaneously form fibrils *in vitro* by entropy-driven self-assembly [243], the hydrophilic nature of hydrogel network hinders cell derived matrix-protein binding, resulting in diffusional loss to the liquid phase [164,244]. This diffusional loss of ECM proteins can to some degree be compensated by increased ECM production through sequestration of proteins by specific hydrogel chemistries [101,245,246], increasing encapsulated cell density [247], and controlled release or covalent immobilization of growth factors [148,248]. As an alternative approach to this strategy of promoting increased ECM production within the hydrogel scaffolds, incorporation of collagen mimetic peptide sequence into PEG based hydrogel showed

increased collagen deposition inside scaffold [249]. However, this approach would not be cost effective because relatively large scale production is required for practical clinical applications.

Previously, the inclusion of biodegradable polymer spheres or fibers with hydrophobic surfaces showed increased volume of cell-derived matrix accumulation compared to tissues formed from cells alone when used as cell transplant scaffolds [250–252]. Based on these findings, it was hypothesized that the incorporation of biodegradable hydrophobic nanospheres within hybrid hydrogel networks could provide binding sites for secreted ECM and serve as nucleation sites for matrix assembly. In this study, submicron size (500 to 900 nm diameter) poly-L-lactic acid (PLLA) spheres were fabricated and incorporated into PEGdA/hyaluronic acid (HA) semi-IPNs described in Chapters 3 and 4. Normal human dermal fibroblasts (NHDF) were encapsulated within semi-IPNs with PLLA nanospheres (semi-IPN composites) and cultured under ascorbate-supplemented growth condition for 35 days to evaluate the effect of incorporation of PLLA nanospheres on matrix protein (collagen) deposition. Experimental groups with PLLA nanospheres exhibited higher accumulation of collagen than control (semi-IPNs without PLLA nanospheres) qualitatively (histology) and quantitatively (hydroxyproline assay). Mechanical properties obtained from tensile testing and swelling revealed the effect of inclusion of nanospheres on structural integrity of semi-IPNs. Confocal imaging and AFM force indentation showed the changes in elastic modulus profile on surface of semi-IPNs.

5.2 Materials and Methods

5.2.1 Synthesis of PEGdA macromers with ester linkage containing variable alkyl spacers

Three PEGdAs with varying susceptibility to hydrolytic degradation were synthesized by a two-step process. First, PEG (Fluka, MW 4000) was reacted with chloroacetyl chloride, 2-chloropropionyl chloride, or 4-chlorobutyryl chloride and then the resulting intermediate products were reacted with sodium acrylate to obtain PEG-bis-AA, PEG-bis-AP, or PEG-bis-AB, as previously described in Chapter 3. All samples achieved acrylation efficiencies greater than 92.5%, determined from ^{1}H-NMR (Bruker 300 MHz, $CDCl_3$) spectra.

5.2.2 Preparation of poly-L-lactic acid nanospheres

Poly-L-lactic acid (PLLA, NatureWorks, Minetonka, MN) spheres with nanometer size range (500 to 950 nm diameter) were prepared by the modified single emulsion technique [253]. Briefly, PLLA particles were dissolved (50 mg/mL) in dimethylformamide (DMF, Sigma-Aldrich, St. Louis, MO) solution and mixed with deionized water at 2:1 (PLLA solution:H_2O) ratio. Then PLLA solution was quickly sonicated for 30 seconds at 10 watt intensity using Sonic Ruptor 400 Ultrasonic Homogenizer (Omni International, Kennesaw, GA) to produce PLLA nanospheres. Solutions were continuously stirred for 4 hours to remove excessive DMF. Large size PLLA particles were removed using cell strainer with 40 micron size mesh (Fisher Scientific, Pittsburgh, PA). Filtered solution containing small size PLLA nanospheres was centrifuged at 4500 g for 10 minutes and the supernatant discarded. Nanospheres

were re-suspended in deionized water and mean particle size distribution was measured using 90 Plus particle size analyzer (Brookhaven Instruments Corporation, Holtsville, NY). PLLA spheres with target size distribution (ca. 500 nm to 1 μm diameter) were recovered and exposed to two additional washing steps (re-suspension with deionized water and recovery by centrifugation at 4500 g for 10 minutes). PLLA nanospheres were later freeze-dried using Labconco Freezone 4.5 lyophilizer and dry weight was measured. Dried spheres were re-suspended with deionized water, centrifuged at 4500 g, re-suspended with 70% ethanol for sterilization for 30 minutes, and washed with 1X PBS solution three times prior to encapsulation.

5.2.3 Semi-IPNs and semi-IPN composites photopolymerization

Hyaluronic acid (Lifecore Biomedical, Chaska, MN) with 1.5 MDa molecular weight stock solution (1.75% w/v), PLLA nanosphere stock solution (100 mg/mL) and PEGdA (30% w/v) stock solutions were prepared in 1X-PBS (0.1M, pH 7.4). Gel precursor solutions (total 250 μL in 1X PBS) were prepared containing 6% w/v PEGdA blend (12.5% PEG-bis-AA, 37.5% PEG-bis-AP, and 50.0% PEG-bis-AB) and 0.36% w/v HA, and 2-hydroxy-1-[4-(hydroxyethoxy) phenyl]-2-methyl-1-propanone (I-2959, BASF, Florham Park, NJ, 0.1% w/v), and varying amounts of PLLA nanospheres (0, 10, 20, 25, 50 mg/mL). Sample volumes (55 μl) were pipetted in between glass separated by 1 mm Teflon spacers and exposed to low intensity UV illumination (365 nm, 10 mW/cm$_2$, Black-Ray B100-AP, Upland, CA) for 5 minutes on each side of the disc.

5.2.4 Hydrogel characterization; swelling test, mechanical properties and hydrophobic domain visualization

Semi-IPNs and semi-IPN composites (6% w/v PEGdAs with 0.36% HA containing PLLA nanospheres with 10 mg/mL and 20 mg/mL concentration respectively) were photopolymerized as described above (n=6/group). Circular hydrogel samples (1mm thick, 8mm diameter) were punched out using General Hollow Steel Punches (General Tools MFG., New York, NY) and equilibrated in distilled water for 24 hours to remove any unpolymerized macromer. Samples were lyophilized and dry weights (Dw1) were measured. The gels were immersed in 1X PBS and allowed to swell for 24 hours in order to record the wet weights (Ww). Samples were lyophilized again and second dry weights (Dw2) were measured. The gel content (Dw1 / Dw2), equilibrium water content ((Ww-Dw2) / Ww2), and mass swelling ratio (Ww / Dw2) were calculated as previously described [Martens PJ Biomacromolecules 2003, Lin CC Adv Drug Deliv Rev 2006]. The weights of PLLA nanospheres in semi-IPN composite samples were subtracted in all swelling calculation based on the volume of semi-IPNs and concentration of PLLA nanospheres.

Semi-IPNs and semi-IPN composites with same composition as in swelling tests were prepared and cut into custom made dumbbell shaped samples with 30 mm gauge length, 5 mm width, and 1 mm thickness. The samples (n=3/group) were subjected to 75% strain at 30 mm/min using an MTS Synergy 100 (MTS Systems Corporation) at room temperature.

Hydrophobic surfaces within semi-IPNs and semi-IPN composites with 10 or 20 mg/ml PLLA nanosphere concentrations were visualized using histological staining. Semi-IPNs and semi-IPN composites were gradually infiltrated by OCT (Optimal Cutting Temperature) compound (Sakura Finetechnical, Torrance, CA) by varying concentration of OCT in 1X PBS solution (increasing concentration from 25 to 100% OCT). Samples in OCT were snap-frozen using liquid N_2, then sectioned using Leica CM 1950 cryostat at desired thickness. Hydrophobic domains on 10 μm sections were stained using Sudan black B (Acros Organics with other supplies from Poly Scientific, Bay Shore, NY). Stained sections were imaged using Nikon UZ-100 widefield microscopy.

5.2.5 In vitro cell culture

Normal human dermal fibroblasts (NHDF, Lonza, Walkersville, MD) were cultured in 75cm^2 tissue culture flasks at 37°C with 5% CO_2 supply. Cells were cultured in DMEM/F-12 (50/50 mix) with L-glutamine media (Mediatech, Manassas, VA) supplemented with 10% (v/v) bovine growth serum (Thermo Scientific) and 50U/mL penicillin and 50μg/mL streptomycin (Mediatech). Medium was changed every 2 days and cells were passaged at a 1:3 ratio for cell expansion after reaching 85 to 90% confluence. All encapsulation studies were done with cells between passages 5 and 6.

5.2.6 NHDF encapsulation in semi-IPNs and semi-IPN composites

Hyaluronic acid with 1.5 MDa molecular weight stock solution (1.75% w/v), PLLA nanosphere (100 mg/mL) stock solution, and PEGdA (30% w/v) stock solutions were prepared in 1X-PBS (0.1M, pH 7.4). Acryl-PEG-GRGDS was synthesized by conjugating GRGDS peptide (Bachem, Torrance, CA) to acryl-PEG-NHS (Jenkem,

Beijing, China) as previously described [169]. Gel precursor solutions (250 μL in 1X PBS) were prepared containing 6% w/v PEGdA blend (12.5% PEG-bis-AA, 37.5% PEG-bis-AP, and 50.0% PEG-bis-AB), 0.36% w/v HA, acryl-PEG-GRGDS (1μmol/mL), 0.1% w/v I-2959 initiator (BASF in 70% ethanol solution), PLLA nanosphere (0, 10, 20 mg/mL as final concentration each) and NHDF (final concentration at 10.0×10^6 cells/mL). Prior to cell addition, all other components were mixed and vortexed to uniformly disperse PLLA nanospheres. NHDF were then added and uniformly dispersed within the gel precursor solution by manual pipetting. Sample volumes (55 μl) were pipetted in between glass coverslips separated by 1 mm Teflon spacers and exposed to low intensity UV light for 5 minutes on each side of the disc. Semi-IPNs and semi-IPN composites with encapsulated cells were cultured in growth media with addition of 1mM ascorbic acid-2-phosphate (Sigma-Aldrich) in 35 mm diameter Petri dishes (BD, San Jose, CA) with 3mL culture medium.

5.2.7 Monitoring of encapsulated NHDF morphology

Semi-IPNs and semi-IPN composites (10 and 20 mg/mL PLLA nanosphehere concentrations) with encapsulated NHDF (n=2/time point in each group) were cultured in 35mm Petri dishes for 7, 21 and 35 days, then fixed with 4% paraformaldehyde (Alfa Aesar, Ward Hill, MA), permeabilized with 0.1% Triton X-100 (Sigma-Aldrich), and stained with Alexa Fluor 594-phalloidin (Life Technologies). The morphologies of encapsulated cells were imaged using a Nikon Eclipse Ti confocal microscopy at various z-depths.

5.2.8 Surface characterization by AFM

Semi-IPNs and semi-IPN composites (10 and 20 mg/mL PLLA nanosphehere concentrations) with encapsulated NHDF (n=3/time point) were cultured in 35mm Petri dishes for 7, 21 and 35 days. Acellular semi-IPNs and semi-IPN composites with 10 and 20 mg/mL PLLA nanosphere concentrations were also prepared as day 0 samples. At each time point, gels were washed with 1X PBS and tested for nano-indentation in 1X PBS immersion using a Molecular Force Probe 3D AFM (MFP-3D, Asylum Research, Santa Barbara, CA, USA) using silicon nitride cantilevers (NanoAndMore USA, Lady's Island, SC, 0.08 N/m spring constant, 5.0 μm tip radius, and 37.7 kHz resonance frequency) at room temperature. The elastic moduli of the semi-IPNs and semi-IPN composite surfaces were calculated by fitting the nano-indentation data with Hertz model [254,255]. Five indentation curves were collected at random positions of each sample.

5.2.9 Collagen histological staining

Deposited collagen within semi-IPNs and semi-IPN composites (10 and 20 mg/ml PLLA nanospheres) with encapsulated NHDF was visualized by histological staining. Semi-IPNs with encapsulated NHDF were cultured in 1mM ascorbic acid-2-phosphate supplemented growth media for 7, 21 and 35 days as described above, then fixed with 4% paraformaldehyde, gradually infiltrated by OCT, snap frozen with liquid N_2, and then cryosectioned as previously described in detail (5.2.4). 15 μm sections were stained for collagen using aniline blue (Poly Scientific). Stained sections were imaged using Nikon UZ-100 widefield microscopy.

5.2.10 Scanning electron microscopy imaging

Extracellular matrix deposition on semi-IPNs and semi-IPN composites surface was studied using scanning electron microscopy (SEM; Hitachi S-4800, Japan). 15 μm thick cryosections from each semi-IPNs and semi-IPN composites (10 and 20 mg/mL PLLA nanospheres) group with encapsulated NHDF at day 35 were dehydrated through grade series of ethanol solutions and hexamethyldisilazane (United Chemical Technologies, Bristol, PA), sputtered with gold for 2 minutes in prior to imaging.

5.2.11 Collagen quantification

Semi-IPNs and semi-IPN composites (10 and 20 mg/mL PLLA nanospheres) with encapsulated NHDF were cultured in growth media supplemented with ascorbic acid-2-phosphate (Sigma-Aldrich) for 7, 21, and 35 days. 12 samples from each group at each time point were harvested, washed twice with 1X-PBS, collected in three 1.7 mL centrifuge tubes (n=4 in each tube), and stored in -80°C in deep freezer. Samples were thawed, manually homogenized, lysed with 0.1% w/v Triton X-100 (Sigma-Aldrich), sonicated for 10 minutes in ice bath, and centrifuged at 10,000 g at 4°C for 10 minutes. Supernatants were recovered and the amount of total DNA measured using Pico-green assay (Life Technologies) according to manufacturer's instruction. The remaining sample volumes were mixed with equal volumes of 12N hydrocholoric acid (Fisher Scientific) to have 6N as final HCl concentration and acid-hydrolyzed overnight at 120°C. The digested products were centrifuged at 10,000 g for 10 minutes at room temperature and supernatants were used for hydroxyproline assay. Briefly, hydroxyproline in acid hydrolyzed samples was reacted with p-dimethylamino benzaldehyde and chloramine-T

hydrate (both from Sigma-Aldrich). Absorbance was measured at 558 nm and hydroxyproline concentration was calculated from a standard curve prepared with trans-4-hydroxy-L-proline (Sigma-Aldrich). Total collagen content of the semi-IPNs was estimated from hydroxyproline assay result based on the estimation that hydroxyproline made up about 13.2% of the total collagen [256,257]. Total collagen amounts were normalized by total DNA contents from Pico-green assay results.

5.2.12 Statistical analysis

Quantitative data were analyzed by ANOVA using Tukey's method for post-hoc comparisons (one-way ANOVA followed by Bonferroni's multiple comparison test). p values < 0.05 were considered to be statistically significant. All quantitative data are presented as mean ± standard deviation.

5.3 Results

5.3.1 PLLA nanosphere production

Various intensities and exposure times of sonication were tested to increase the product yield of PLLA nanospheres with mean size distribution ranging from 500 to 900 nm diameter. Sonication intensity at 10 Watts for 30 seconds was identified as the optimal condition for production of PLLA nanospheres in this size range. PLLA nanosphere yield was 16.2% w/w (dry weight of product/dry weight of raw PLLA particulate). Most of yield loss occurred through the removal of large size spheres (larger than 50 μm size microspheres) using the cell strainer.

5.3.2 Hydrogel characterization; swelling and mechanical properties of semi-IPNs containing various amounts of PLLA nanospheres and hydrophobic domain visualization

The effect of PLLA nanosphere incorporation on semi-IPNs physical properties was analyzed by measuring swelling and elastic modulus. Semi-IPNs containing 10 mg/mL PLLA nanospheres did not exhibit any significant differences in gelation efficiency and swelling relative to controls without PLLA nanospheres (Figure 5.1). When the PLLA nanosphere concentration was raised to 20 mg/ml, gelation efficiency significantly increased and swelling significantly decreased relative to both composites containing 10 mg/ml and the control gels without PLLA nanospheres. Figure 5.2 shows the elastic modulus of PEGdAs/HA semi-IPNs containing 0 (control), 10, and 20 mg/mL PLLA nanospheres. Addition of 20 mg/ml PLLA nanospheres significantly increased the elastic modulus of semi-IPNs. The incorporation of higher amounts of PLLA nanospheres (more than 25 mg/mL) resulted in breakage of sample during tensile test, suggesting the microsphere content had reached a level where it compromised the mechanical integrity of the semi-IPN network. The hydrophobic domains within 10 μm section of semi-IPNs were visualized by Sudan black B staining. Hydrophobic surface was stained black showing the hydrophobic domain distribution within the entire volume of semi-IPN control (no PLLA nanospheres, semi-IPNs) and semi-IPN/PLLA nanosphere composites (Semi-IPN composites) as shown in Figure 5.3.

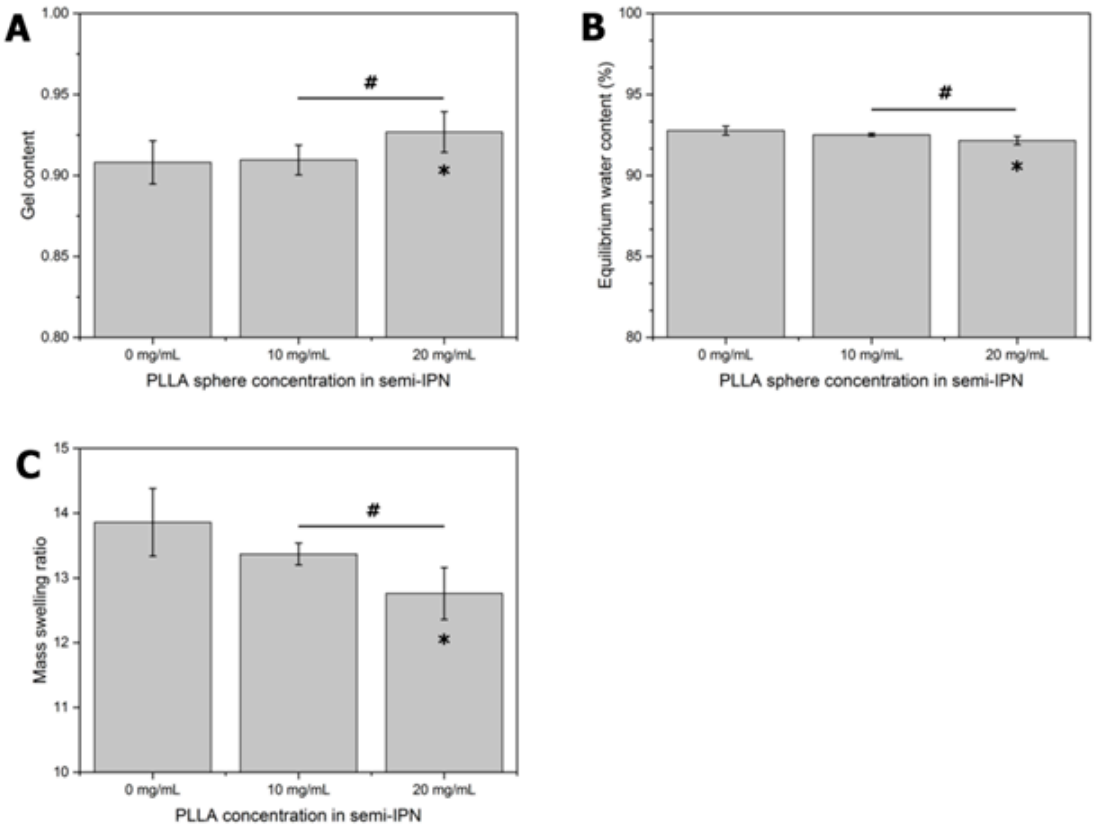

Figure 5.1 Swelling test results of 6% w/v PEGdA/0.36% w/v HA semi-IPNs containing varying amounts of PLLA nanospheres; gel content (A), equilibrium water content (B), and mass swelling ratio (C). *=$p<0.05$ relative to PEGdA/HA semi-IPNs (no nanospheres) and #=$p<0.05$ between groups.

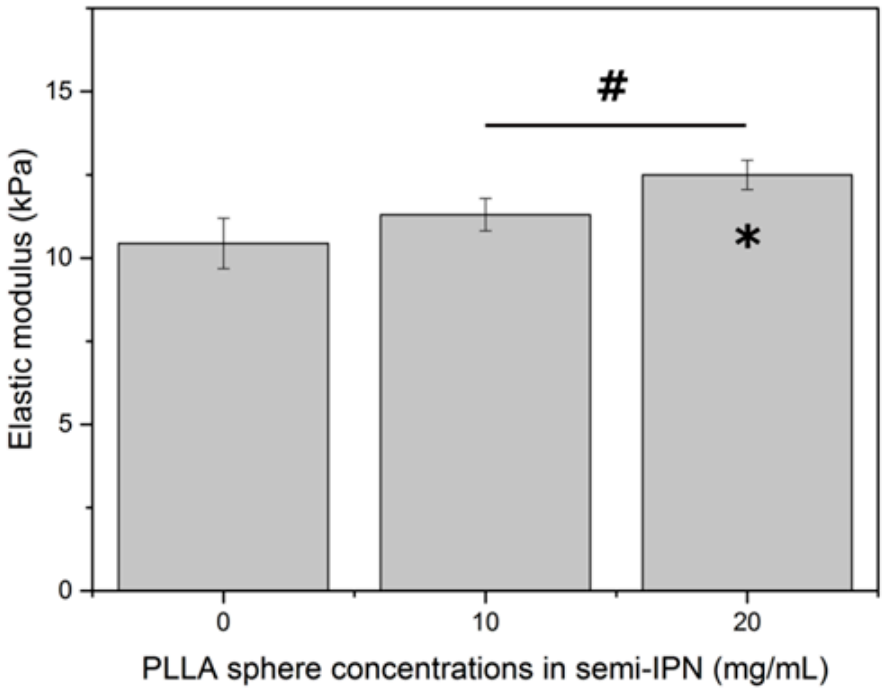

Figure 5.2 Elastic modulus of 6% w/v PEGdA/0.36% w/v HA semi-IPNs containing varying amounts of PLLA nanospheres. *=$p<0.05$ relative to PEGdA/HA semi-IPNs (no nanospheres) and #=$p<0.05$ between groups.

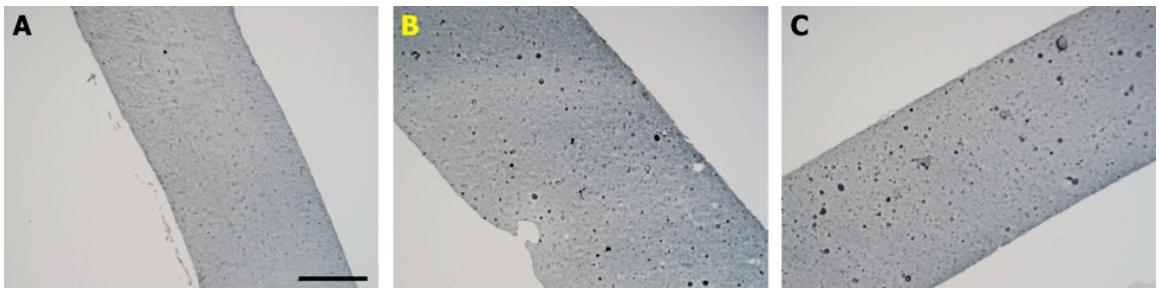

Figure 5.3 Widefield microscopy images of Sudan black B stained cryosections of 6% w/v PEGdAs / 0.36% w/v HA semi-IPNs containing 0 mg/mL (A), 10 mg/mL (B), and 20 mg/mL (C) PLLA nanospheres, scale bar = 500 μm.

5.3.3 NHDF morphology on semi-IPNs and semi-IPN composite surfaces

Both semi-IPNs (no PLLA nanospheres) and semi-IPN composites (semi-IPNs containing PLLA nanospheres) supported the survival and spreading of encapsulated NHDF. NHDF morphology within semi-IPN composites was not imaged clearly because PLLA nanospheres interfered with light penetration into the samples, resulting in increased noise level in confocal image (not shown here). The only detectable difference between groups in morphological development of NHDF was observed on sample surfaces (z=0) at 7 days in culture. NHDF on semi-IPN composites showed increased cell spreading and even dense network formation on the surface of semi-IPN composites with 20 mg/mL PLLA nanospheres (Figure 5.4).

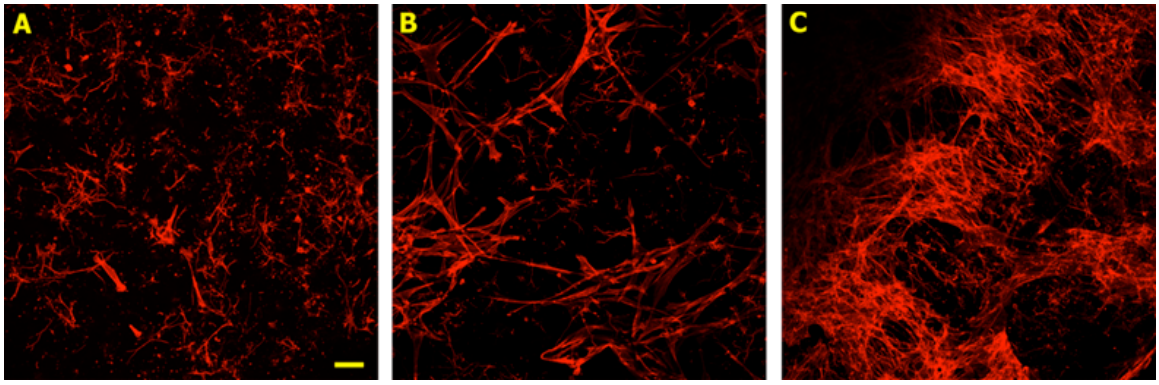

Figure 5.4 Confocal microscopy images of NHDF on the surface of 6% w/v PEGdA / 0.36% w/v HA semi-IPNs (A) and semi-IPN composites containing PLLA nanospheres at 10 mg/mL (B), and 20 mg/mL (C) concentration after 7 days in culture, scale bar = 100 μm.

5.3.4 Monitoring changes in surface mechanical property using AFM nano-indentation

The changes in elastic modulus on the surface of semi-IPNs and semi-IPN composites over entire time scale of cell culture were monitored using AFM nano-indentation technique (Figure 5.5). Elastic modulus values for acellular control semi-IPNs were in close agreement with the values measured by tensile testing (Figure 5.2). Interestingly, the surface elastic moduli values of acellular semi-IPN composites are different from tensile testing values, 11.3 ± 0.49 kPa from tensile testing vs. 5.97 ± 0.09 kPa from AFM nano-indentation for acellular semi-IPN composites with 10 mg/mL PLLA nanospheres. As for semi-IPN composites with 20 mg/mL PLLA nanospheres, AFM nano-indentation results showed higher elastic modulus value (18.01 ± 2.57 kPa) over one from tensile testing (12.5 ± 0.44 kPa). All three groups showed significant decreases in surface elastic modulus at day 7 compared to acellular groups (day 0). In case of semi-IPN composites with 20 mg/mL PLLA nanospheres, the value was an order of magnitude lower. Then, all 3 groups exhibited similar surface elastic moduli values (no significant difference) after 21 and 35 days in culture.

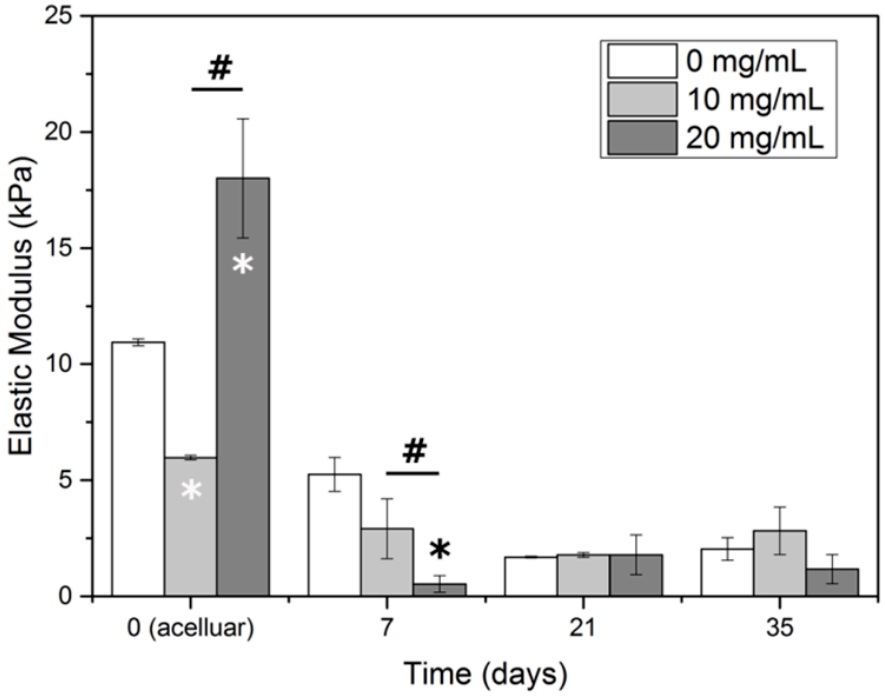

Figure 5.5 Elastic modulus of the surface of acellular and NHDF encapsulated semi-IPNs and semi-IPN composites over time obtained from AFM nano-indentation technique. *=$p<0.05$ relative to semi-IPNs (no spheres) and #=$p<0.05$ between groups.

5.3.5 Collagen deposition within NHDF encapsulated semi-IPNs and semi-IPN composites

The effect of incorporation of PLLA nanospheres in semi-IPNs on collagen deposition was visualized by histological staining and quantified by measuring total collagen content. Semi-IPN composites showed more collagen deposition over semi-IPN controls after 35 days in culture as shown in Figure 5.6. Aniline blue was used for staining collagen. No other counter stain agent was used to visualize collagen around cell (pericelluar region) as it could interfere the visualization. Within semi-IPNs and semi-IPN composites, pericellular regions are stained darker (blue), indicating collagen deposition around the cell. Also more collagen molecules were deposited on the surface of semi-IPNs and semi-IPN composites.

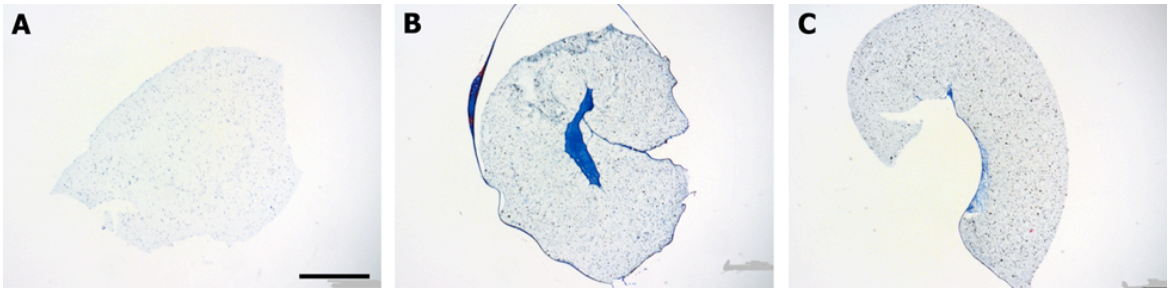

Figure 5.6 Widefield microscopy images of NHDF encapsulated semi-IPN and semi-IPN composite cryosections stained with aniline blue for collagen (stained blue) after 35 days in culture; semi-IPNs (A), semi-IPN composites with 10 mg/mL (B), and 20 mg/mL (C) PLLA nanosphere concentrations, scale bar = 500 μm.

To confirm these histological results, total collagen amounts (estimated from hydroxyproline assay results and then normalized by total DNA amounts in each sample) deposited within semi-IPNs and semi-IPN composites were compared. Due to low concentration of hydroxyproline within individual semi-IPNs and semi-IPN composite sample (close to detection threshold), a total of 4 samples were hydrolyzed together for each hydroxyproline assay (i.e. total 12 hydrogels were used for one time point in Figure 5.7). Collagen deposition in both semi-IPNs and semi-IPN composites did not show significant difference between groups at day 7 and 21. Deposited collagen amounts were significantly increased for all groups at day 21 in culture compared to day 7 groups. At day 35 in culture, semi-IPN composites exhibited significantly increased collagen deposition relative to semi-IPNs control (Figure 5.7).

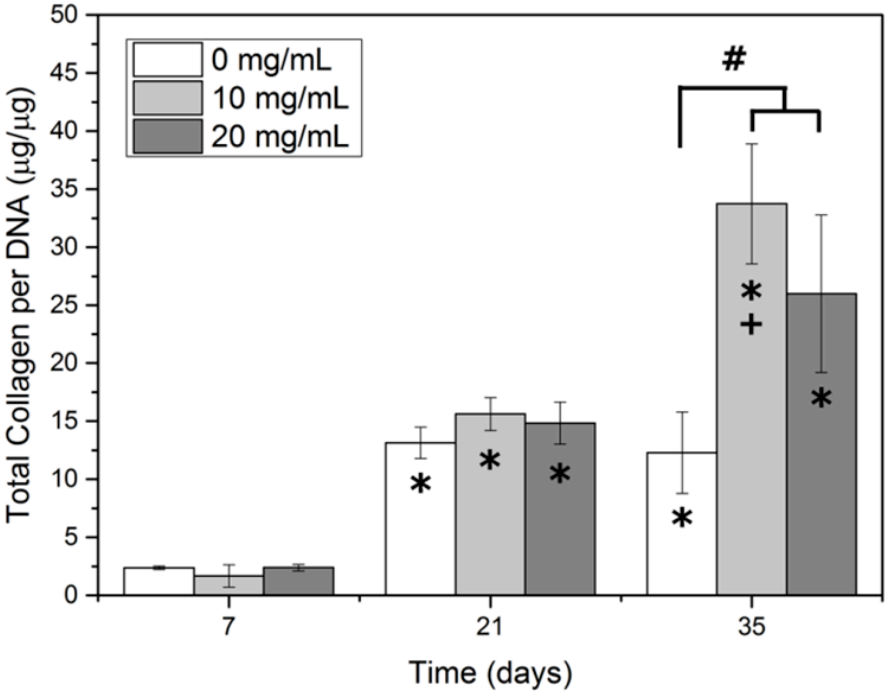

Figure 5.7 Total collagen amounts within semi-IPNs and semi-IPN composites over time obtained from hydroxyproline assay and normalized by total DNA concentration from Pico-green assay results. *=$p<0.05$ relative to total collagen measured at day 7 in each group, +=$p<0.05$ relative to total collagen measured at day 21 in each group and #=$p<0.05$ between groups.

Scanning electron microscopy images also showed ECM deposition on the surface of PLLA nanospheres (Figure 5.8 C through F) within semi-IPN composites compared to semi-IPNs (Figure 5.8A and B). Although the mean size distribution was submicron size (500 to 900 nm diameter), the diameters of PLLA nanospheres in SEM images exhibited relatively larger size diameter due to aggregated nature of hydrophobic particles inside hydrophilic hydrogel environment (Figure 5.8D and E) and deposited ECM proteins on surface of PLLA nanospheres (Figure 5.8C and F).

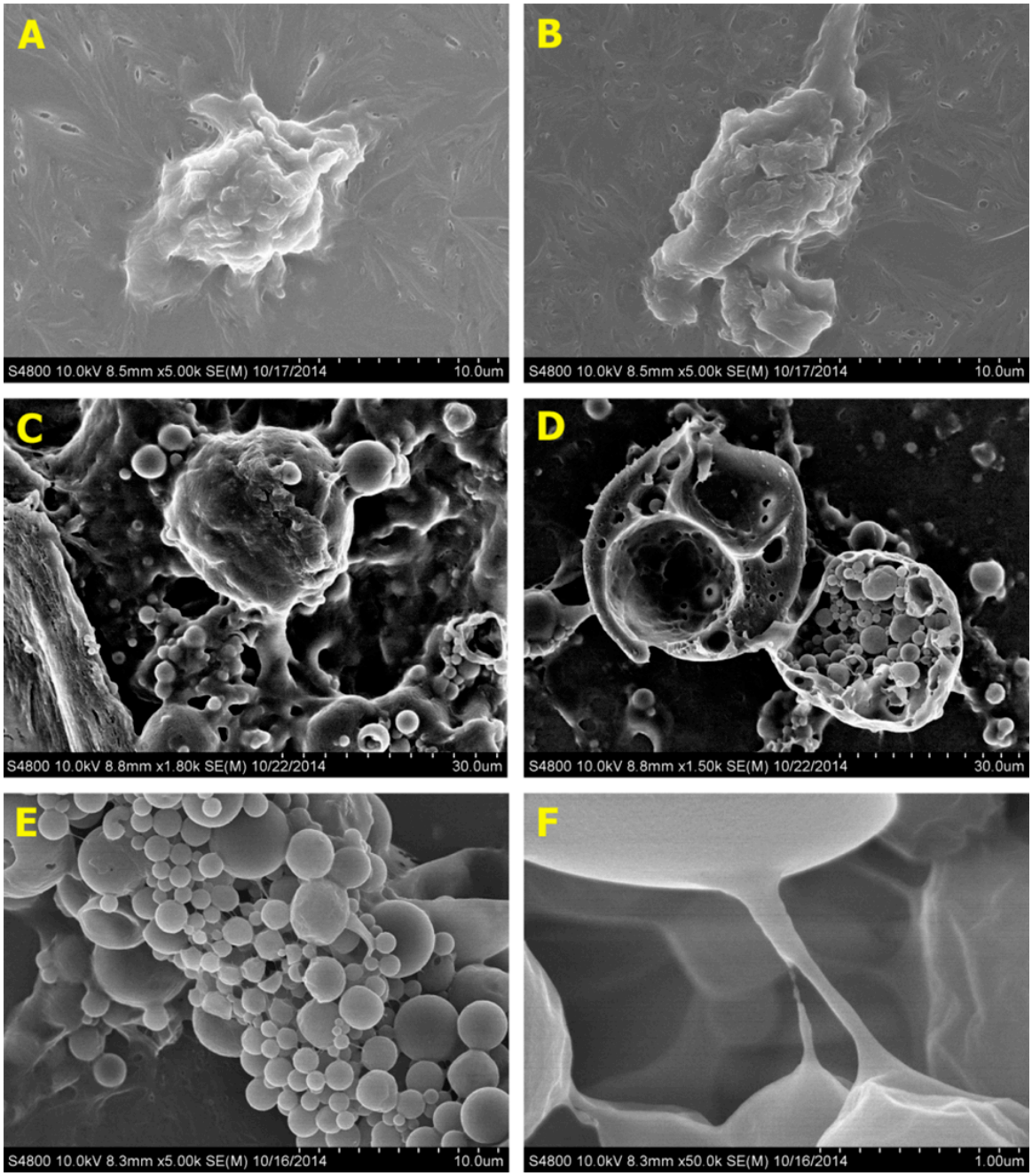

Figure 5.8 Scanning electron microscopy images of NHDF encapsulated within semi-IPNs (A and B) and PLLA nanospheres within semi-IPN composites with 10 mg/mL (C and D), and 20 mg/mL (E and F) PLLA nanosphere concentrations after 35 days in culture.

5.4 Discussion

Inside a successful cell transplantation hydrogel scaffold, encapsulated cells must produce native ECM molecules to gradually replace the original polymer network as it degrades. PEG-based hybrid hydrogel scaffolds have been widely investigated as matrices for 3D cell culture and transplantation as PEG can be easily modified with naturally derived molecules such as adhesion and MMP sensitive peptides [6,45,85]. Despite its many benefits, the original biomedical application of PEG was grafting to other surfaces such as implant or prosthetics to create anti-fouling, protein-repellent materials [162,241,242]. Therefore, PEG may not be a particularly effective material for supporting ECM binding and assembly. Many research groups have also reported diffusional loss of matrix protein produced by encapsulated cells in PEG based hydrogel scaffolds as a consequence of PEG's inability to bind these molecules [163–165,244,258]. In this study, to avoid diffusional loss of ECM molecules produced from encapsulated cells in hydrogel network, nanometer size range (500 to 950 nm diameter) hydrophobic PLLA nanospheres were incorporated within semi-IPNs to promote matrix protein deposition inside the network.

The incorporation of PLLA nanospheres affected physical properties of semi-IPNs. Our first step was to encapsulate PLLA nanospheres (along with NHDF) and confirm they were homogenously distributed (Figure 5.3 and 5.8). Interestingly, PLLA nanospheres increased elastic modulus of semi-IPNs in a dose-dependent manner up to 20 mg/mL concentration range although it damaged the network structure over 25 mg/mL concentration (breakage of sample during tensile testing) (Figure 5.2). Semi-IPN

composites with 20 mg/mL PLLA nanospheres showed significantly increased gel content and significantly decreased equilibrium water content and mass swelling ratio relative to semi-IPNs control and semi-IPN composites with 10 mg/mL PLLA nanosphere groups. This may be due to the increase in hydrophobicity of the network by encapsulated PLLA nanospheres, which could be explained by the work done by Sawhney and co-workers. They demonstrated that the addition (increase) of hydrophobic PLA or PGA groups between central PEG block and terminal acrylate groups led to micelle type conformational change. This change effectively increased the proximity of acrylate groups, resulting in more rapid polymerization [259].

After day 7 in ascorbic acid-2-phosphate supplemented culture, encapsulated NHDF showed different degree of spreading and network formation on the surface of semi-IPNs and semi-IPN composites (z at 0 μm in confocal image in Figure 5.4). Cells on semi-IPN composites showed increased cell spreading and network formation compared to semi-IPNs control, consistent with previous reports of increased cell spreading and network formation on stiffer surfaces [137,260,261]. The incorporation of PLLA nanospheres provided localized stiffer surface (18.0 ± 2.6 kPa) than semi-IPNs alone (10.9 ± 0.1 kPa) in case of semi-IPN composites with 20 mg/mL PLLA nanospheres. At day 7 in culture, the elastic modulus of semi-IPN compoistes with 20 mg/mL surface was dramatically decreased from 18.0 ± 2.6 kPa to 0.53 ± 0.36 kPa (Figure 5.5). This dramatic change reflected rapid network formation (followed by ECM deposition), and was also visualized by confocal microscopy image (Figure 5.4). AFM nano-indentation results showed biphasic behavior in elastic moduli values of semi-IPN

composites with 20 mg/mL PLLA nanosphere surface. Between day 7 and 21, all surfaces of semi-IPNs and semi-IPN composites groups were gradually covered by cellular network and deposited matrix protein and elastic moduli values from AFM nano-indentation reached the plateau. After 21 days in culture, all surfaces formed dense ECM/cellular network (Figure 5.5). The final elastic modulus values ranged around 2 kPa (no significant difference amongst groups at day 21 and 35 and between days in each group), which suggested the surfaces of semi-IPNs and semi-IPN composites were covered by matrix and densely packed cellular network, similar to the value of adipose tissue elastic modulus and human dermis range [59,262,263].

Like other ECM proteins, collagens are synthesized intracellularly and excreted into pericellular regions, and later diffuse to extracellular region *in vivo* [264]. In highly crosslinked hydrogel network system, diffusion of secreted collagen molecules may be limited to the pericellular region as hydrogel mesh size is smaller than collagen (~67 nm size for hydrated collagen fibril). Mesh size of our semi-IPNs was estimated ca. 10 nm size, comparable to other studies [187,265,266]. At initial stage of cell culture, collagens are deposited mainly within the pericellular region as hydrogel network structure remains intact. As the hydrogel network degrades, free collagens diffuse to matrix region [67,101,143,246,247,267]. However, more ECM protein deposition within semi-IPNs and less diffusional loss would be expected. HA in semi-IPNs was degraded relatively faster than PEGdA backbone by Hase activity and cells encapsulated within semi-IPNs spread as early as day 3 in culture as shown in Chapter 3. Hydrophobic surfaces of PLLA nanosphres could provide sites for ECM protein adsorption and fibril nucleation outside

the pericellular region. No significant difference in collagen deposition between semi-IPNs and semi-IPN composites up to day 21 in culture (Figure 5.7), suggesting produced collagens were deposited mainly in pericellular region also shown as darker (blue) spots within semi-IPNs and semi-IPN composites in Figure 5.6 even though HA enriched zone was enzymatically degraded as early as day 3 in culture. Collagen deposition was observed throughout the entire volume of semi-IPNs and semi-IPN composites at the end of culture at day 35 (Figure 5.6). Especially, more collagen was deposited on the surface of semi-IPNs and semi-IPN composites. At day 35, collagen deposition was significantly increased in semi-IPN composites relative to semi-IPNs control and collagen deposited within semi-IPNs control did not significantly increase after 21 days, indicating that collagen deposition mainly occurred on the surface of PLLA nanospheres, not on pericellular region after 21 days in culture. SEM images also confirmed matrix protein deposition on PLLA nanospheres after 35 days in culture (Figure 5.8C through F). Although mean size distribution of most PLLA nanosphere population ranges from 500 to 900 nm diameter, larger size PLLA partcles were spotted due to local PLLA nanosphere aggregation by hydrophobic interaction (Figure 5.8D and E) and ECM protein deposition on the surface of PLLA nanospheres (Figure 5.8D and F). Increased collagen deposition within semi-IPN composites is mainly attributed to direct accumulation of cell-secreted collagen on hydrophobic PLLA nanosphere surface. These results suggest that the incorporation of hydrophobic PLLA nanospheres within semi-IPNs support matrix protein deposition at the later stage of 3D cell culture.

5.5 Conclusions

These studies demonstrate that through the incorporation of PLLA nanospheres within the network, novel semi-IPN composites can provide localized hydrophobic and stiffer surfaces that support enhanced matrix protein adsorption and promote rapid cellular network formation relative to semi-IPNs. Newly synthesized matrix proteins were adsorbed on hydrophobic surfaces of encapsulated PLLA nanospheres after saturated deposition in the pericellular region. Additionally, the incorporation of submicron-size hydrophobic polymer spheres within semi-IPNs results in less swelled hydrogel network with significantly increased overall mechanical properties. The overall results suggest that novel semi-IPN composites system can potentially benefit wound healing applications with increased matrix molecule deposition.

CHAPTER SIX

CONCLUSIONS AND FUTURE RESEARCH SUGGESTIONS

6.1 Conclusions

The ultimate goal of scaffold-based cell transplantation is to regenerate healthy tissue at wound sites, which requires resorption/degradation of the scaffold accompanied by new tissue formation through cell division, differentiation and matrix synthesis. Toward this end, the overall goal of this dissertation study was to develop polyethylene glycol diacrylate (PEGdA) / hyaluronic acid (HA) based semi-interpenetrating polymer networks (semi-IPNs) capable of supporting 3D cell spreading, migration, differentiation, and extracellular matrix (ECM) deposition for cell therapy applications. These studies build upon previous work reporting the synthesis of three PEGdA macromers with different hydrolytic degradation kinetics [188] and the ability of PEG-bis-AP with the addition of native HA to form semi-IPNs that support encapsulated fibroblast spreading [187].

In chapter 3, it was hypothesized that the incorporation of native HA creates network defects by polymerization-induced phase separation that provides space for initial Hase-mediated cell spreading and that controlled long term cellular remodeling can be achieved by mixing of PEGdA macromers with various hydrolytic degradation rates. First, increased gel turbidity was observed in semi-IPNs, but not in copolymerized hydrogels containing methacrylated HA that did not support cell spreading, which suggests an underlying mechanism of polymerization-induced phase separation resulting

in HA-enriched defects within the network structure. These interconnected micro-domains provide the space for initial cell spreading via enzymatic degradation. Thus, PEGdA/HA semi-IPNs support two degradation mechanisms-enzymatic degradation that is relatively fast and allows cell to assume a physiological morphology that is essential to the function of most mesenchymally-derived cells, as well as more gradual hydrolytic degradation to allow sustained remodeling. Through systematic optimization of network composition, fibroblast spreading exhibited a biphasic response to HA concentration, required a minimum HA molecular weight, decreased with increasing PEGdA concentration, and was independent of hydrolytic degradation at early time points. PEGdA/HA semi-IPNs were also able to support cell spreading at relatively high levels of mechanical properties (~10 kPa elastic modulus) compared to alternative hybrid hydrogels. Optimized semi-IPN formulations using the blend of three PEGdA macromers with varying susceptibility supported long-term survival of encapsulated fibroblasts and sustained migration in a gel-within-gel encapsulation model. These results demonstrate that PEGdA/HA semi-IPNs provide dynamic microenvironments that can support 3D cell survival, spreading, and migration for a variety of cell transplant and three dimensional in vitro culture applications.

In Chapter 4, it was hypothesized that the semi-IPN with optimal mechanical properties for osteogenic differentiation could support prolonged osteogenic differentiation of mesenchymal stem cells. Selected base composition semi-IPNs fell into optimal range for osteogenic differentiation of hMSC in 3D culture condition (10 to 30 kPa) [8]. Semi-IPNs with PEGdA blends successfully supported osteogenic

differentiation of encapsulated hMSCs. hMSCs initially spread in HA-enriched zones which were degraded faster by Hase and resulting spindle morphology would benefit osteogenic differentiation because this is closer to hMSC morphology undergoing osteogenic differentiation *in vivo*. Ostetogenic differentiation of encapsulated hMSCs showed faster osteoblast maturation and similar tendency of mineralization relative to other 2D monolayer studies [220]. Physiological calcium deposition could be observed macroscopically as early as day 14. Hydrogels kept relatively comparable mechanical integrity and its initial volume up to day 35, suggesting that hydrogel network was replaced by newly generated calcified tissue with collagen, also quantitatively confirmed by AA spectrometry. Acellular semi-IPN control result showed there was autologous calcium deposition and culture without dexamethasone also confirmed the dependency of osteogenic differentiation of hMSCs on dexamethasone. These results demonstrate that PEGdA/HA semi-IPNs can support long-term osteogenic differentiation of hMSCs and can be used as scaffolds for hard tissue (orthopaedic) engineering applications.

In Chapter 5, it was hypothesized that hydrogels have limited capacity for protein adsorption due to their hydrophilic nature. In order to overcome this, biodegradable poly-L-lactic acid (PLLA) nanospheres were incorporated within the networksto provide hydrophobic surfaces for protein adsorption. Compared to control group (no microspheres), higher degree of collagen deposition and more cellular network formation inside semi-IPNs were clearly observed at day 35 in histological staining. Additionally, the incorporation of PLLA nanospheres increased overall elastic modulus value and gel content of semi-IPNs, and decreased equibrium water content and mass swelling ratio of

semi-IPNs, suggesting that encapsulated hydrophobic PLLA nanospheres enhanced polymerization process. Locally increased surface stiffness by PLLA microspheres accommodated increased cellular spreading and accelerated network formation. These results demonstrate that semi-IPN composites containing biodegradable hydrophobic nanospheres provide dynamic microenvironments that can further accelerate ECM remodeling relative to pure hydrogel scaffolds.

Overall, these studies demonstrated that PEGdA/HA semi-IPN system successfully supported long-term cellular remodeling and its bioactivity could be further enhanced via the incorporation of hydrophobic nanospheres. Both semi-IPNs and semi-IPN composites could be used as cell transplant tissue engineering scaffold and 3D *in vitro* culture system for both soft and hard tissue applications.

6.2 Future Research Suggestions

As a next step, successful *in vitro* culture results should be evaluated *in vivo*. Cells encapsulated within semi-IPNs can be transplanted to verify degradation profile and tissue reconstruction capability *in vivo*. And following studies are suggested for each specific aims.

Aim 1: To further optimize semi-IPN composition for different target elastic moduli values

Although semi-IPNs are fairly well optimized, it can be further tested for higher MW of HA (more than 1.5 MDa) or higher PEGdA concentration with higher PEGdA/HA ratios. We have already tested 6% PEGdA/HA ratios and found 6% optimal.

However, at higher PEGdA concentration over 8% w/v, the ratio of PEGdA/HA higher than 6% has not been tested. Cells react differently to elastic modulus of scaffold. If optimal composition for different PEGdA concentration (i.e. different elastic modulus value) can be identified for corresponding target mechanical properties, the application can be extended.

Aim 2: To expand semi-IPN application toward other stem cell differentiation lineage and test the conjugation of bioactive molecule to enhance its functionality

Similar semi-IPN compositions can be used for hMSC differentiation toward chondrogenic and adipogenic differentiation *in vitro*. These two differentiation conditions can easily be applied as hMSCs are capable of differentiating toward these lineages. Ongoing studies are examining covalent conjugation of bioactive molecules such as dexamethasone to the HA component of these networks for sequestration and cell-mediated release during network remodeling. In addition, conjugating other drugs with dexamethasone would create bilayer scaffolds that can target osteochondral defects with two different zones, one for bone and the other for cartilage.

Aim 3: To further investigate the effect of incorporation of PLLA nanospheres on surface roughness and gene expression, and to further enhance bioactivity by loading bioactive growth factors within PLLA nanospheres as delivery vehicle along with cell transplant scaffold

3.1 Surface roughness analysis

Material surface roughness affects cell adhesion and other cellular activities [268,269]. Although the difference observed in network formation rate on semi-IPNs and semi-IPN composites was attributed to differences in surface stiffness, it is also possible that changes in surface roughness may have contributed. Therefore, surface roughness measurement (surface profile) should be done to identify the effect of PLLA nanospheres on surface roughness.

3.2 Matrix analysis

Although changes in collagen content have been attributed to increased adsorption to the surface of hydrophobic nanospheres resulting in improved retention within the network, it is also possible that the changes in mechanical properties between semi-IPNs and semi-IPN composites may also affect collagen synthesis. Therefore, it would be beneficial to compare type I collagen transcriptional activity between cells encapsulated within composite and control semi-IPNs to determine if this mechanism may also be contributing to the observed results.

3.3 Use of nanoparticle to deliver drugs/growth factors

In this dissertation study, only non-porous PLLA spheres were used for semi-IPN composites in order to investigate the effect of inclusion of hydrophobic surface. Double emulsion technique can be applied to include various growth factors such as TGF-β1, vascular endothelial growth factor (VEGF), and fibroblast growth factor (FGF) in accordance with target application for enhanced bioactivity of semi-IPN composites.

REFERENCES

[1] Robey TE, Saiget MK, Reinecke H, Murry CE. Systems approaches to preventing transplanted cell death in cardiac repair. J Mol Cell Cardiol 2008;45:567–81. doi:10.1016/j.yjmcc.2008.03.009.

[2] T. Brown P, M. Handorf A, Bae Jeon W, Li W-J. Stem Cell-based Tissue Engineering Approaches for Musculoskeletal Regeneration. Curr Pharm Des 2013;19:3429–45. doi:10.2174/13816128113199990350.

[3] Freyman T, Polin G, Osman H, Crary J, Lu M, Cheng L, et al. A quantitative, randomized study evaluating three methods of mesenchymal stem cell delivery following myocardial infarction. Eur Heart J 2006;27:1114–22. doi:10.1093/eurheartj/ehi818.

[4] Gaetani R, Rizzitelli G, Chimenti I, Barile L, Forte E, Ionta V, et al. Cardiospheres and tissue engineering for myocardial regeneration: potential for clinical application. J Cell Mol Med 2010;14:1071–7. doi:10.1111/j.1582-4934.2010.01078.x.

[5] Laflamme M a, Chen KY, Naumova A V, Muskheli V, Fugate J a, Dupras SK, et al. Cardiomyocytes derived from human embryonic stem cells in pro-survival factors enhance function of infarcted rat hearts. Nat Biotechnol 2007;25:1015–24. doi:10.1038/nbt1327.

[6] Lutolf MP, Hubbell J a. Synthetic biomaterials as instructive extracellular microenvironments for morphogenesis in tissue engineering. Nat Biotechnol 2005;23:47–55. doi:10.1038/nbt1055.

[7] Kang A, Park J, Ju J, Jeong GS, Lee S-H. Cell encapsulation via microtechnologies. Biomaterials 2014;35:2651–63. doi:10.1016/j.biomaterials.2013.12.073.

[8] Huebsch N, Arany PR, Mao AS, Shvartsman D, Ali O a, Bencherif S a, et al. Harnessing traction-mediated manipulation of the cell/matrix interface to control stem-cell fate. Nat Mater 2010;9:518–26. doi:10.1038/nmat2732.

[9] Khetan S, Guvendiren M, Legant WR, Cohen DM, Chen CS, Burdick J a. Degradation-mediated cellular traction directs stem cell fate in covalently crosslinked three-dimensional hydrogels. Nat Mater 2013;12:458–65. doi:10.1038/nmat3586.

[10] Cukierman E, Pankov R, Stevens D, Yamada K. Taking cell-matrix adhesions to the third dimension. Science (80-) 2001;294:1708–12.

[11] Tibbitt MW, Anseth KS. Hydrogels as extracellular matrix mimics for 3D cell culture. Biotechnol Bioeng 2009;103:655–63. doi:10.1002/bit.22361.

[12] Gelain F, Horii A, Zhang S. Designer self-assembling peptide scaffolds for 3-d tissue cell cultures and regenerative medicine. Macromol Biosci 2007;7:544–51. doi:10.1002/mabi.200700033.

[13] Ashe HL, Briscoe J. The interpretation of morphogen gradients. Development 2006;133:385–94. doi:10.1242/dev.02238.

[14] Petersen O. Interaction with basement membrane serves to rapidly distinguish growth and differentiation pattern of normal and malignant human breast epithelial cells. Proc Natl Acad Sci U S A 1992;89:9064–8.

[15] Tanaka H, Murphy CL, Murphy C, Kimura M, Kawai S, Polak JM. Chondrogenic differentiation of murine embryonic stem cells: effects of culture conditions and dexamethasone. J Cell Biochem 2004;93:454–62. doi:10.1002/jcb.20171.

[16] Birgersdotter A, Sandberg R, Ernberg I. Gene expression perturbation in vitro--a growing case for three-dimensional (3D) culture systems. Semin Cancer Biol 2005;15:405–12. doi:10.1016/j.semcancer.2005.06.009.

[17] Tirrell DA, Ph D, Mccollum R, Corcoran WH. 2012 NSF BIOMATERIALS WORKSHOP Biomaterials : Important Areas for Future Investment 2012.

[18] Mouw JK, Ou G, Weaver VM. Extracellular matrix assembly: a multiscale deconstruction. Nat Rev Mol Cell Biol 2014. doi:10.1038/nrm3902.

[19] Alberts B, Johnson A, Lewis J, Raff M, Roberts K, Walter P. Molecular Biology of The Cell. 5th ed. New York: Garland Science; 2008.

[20] Frantz C, Stewart KM, Weaver VM. The extracellular matrix at a glance. J Cell Sci 2010;123:4195–200. doi:10.1242/jcs.023820.

[21] Rozario T, DeSimone DW. The extracellular matrix in development and morphogenesis: a dynamic view. Dev Biol 2010;341:126–40. doi:10.1016/j.ydbio.2009.10.026.

[22] Schaefer L, Schaefer RM. Proteoglycans: from structural compounds to signaling molecules. Cell Tissue Res 2010;339:237–46. doi:10.1007/s00441-009-0821-y.

[23] Iozzo R, Murdoch A. Proteoglycans of the extracellular environment: clues from the gene and protein side offer novel perspectives in molecular diversity and function. FASEB J 1996;10:598–614.

[24] Sasisekharan R, Shriver Z, Venkataraman G, Narayanasami U. Roles of heparan-sulphate glycosaminoglycans in cancer. Nat Rev Cancer 2002;2:521–8. doi:10.1038/nrc842.

[25] Patino MG, Neiders ME, Andreana S, Noble B, Cohen RE. Collagen as an implantable material in medicine and dentistry. J Oral Implantol 2002;28:220–5. doi:10.1563/1548-1336(2002)028<0220:CAAIMI>2.3.CO;2.

[26] Gordon MK, Hahn R a. Collagens. Cell Tissue Res 2010;339:247–57. doi:10.1007/s00441-009-0844-4.

[27] Myllyharju J, Kivirikko KI. Collagens, modifying enzymes and their mutations in humans, flies and worms. Trends Genet 2004;20:33–43. doi:10.1016/j.tig.2003.11.004.

[28] Patterson J, Hubbell J a. Enhanced proteolytic degradation of molecularly engineered PEG hydrogels in response to MMP-1 and MMP-2. Biomaterials 2010;31:7836–45. doi:10.1016/j.biomaterials.2010.06.061.

[29] Smith ML, Gourdon D, Little WC, Kubow KE, Eguiluz RA, Luna-Morris S, et al. Force-induced unfolding of fibronectin in the extracellular matrix of living cells. PLoS Biol 2007;5:e268. doi:10.1371/journal.pbio.0050268.

[30] Daley WP, Peters SB, Larsen M. Extracellular matrix dynamics in development and regenerative medicine. J Cell Sci 2008;121:255–64. doi:10.1242/jcs.006064.

[31] Tsang KY, Cheung MCH, Chan D, Cheah KSE. The developmental roles of the extracellular matrix: beyond structure to regulation. Cell Tissue Res 2010;339:93–110. doi:10.1007/s00441-009-0893-8.

[32] Hynes RO. The extracellular matrix: not just pretty fibrils. Science 2009;326:1216–9. doi:10.1126/science.1176009.

[33] Vu TH. Matrix metalloproteinases: effectors of development and normal physiology. Genes Dev 2000;14:2123–33. doi:10.1101/gad.815400.

[34] Somerville RPT, Oblander SA, Apte SS. Matrix metalloproteinases: old dogs with new tricks. Genome Biol 2003;4:216. doi:10.1186/gb-2003-4-6-216.

[35] Singer AJ, Clark RA. Cutaneous wound healing. N Engl J Med 1999;341:738–46. doi:10.1056/NEJM199909023411006.

[36] Mott JD, Werb Z. Regulation of matrix biology by matrix metalloproteinases. Curr Opin Cell Biol 2004;16:558–64. doi:10.1016/j.ceb.2004.07.010.

[37] Lucero H a, Kagan HM. Lysyl oxidase: an oxidative enzyme and effector of cell function. Cell Mol Life Sci 2006;63:2304–16. doi:10.1007/s00018-006-6149-9.

[38] Sands RW, Mooney DJ. Polymers to direct cell fate by controlling the microenvironment. Curr Opin Biotechnol 2007;18:448–53. doi:10.1016/j.copbio.2007.10.004.

[39] Chen RR, Mooney DJ. Polymeric Growth Factor Delivery Strategies for Tissue Engineering. Pharm Res 2003;20:1103–12.

[40] Levi E, Fridmantt R, Miao H, Ma Y, Yayon A, Vlodavsky I. Matrix metalloproteinase 2 releases active soluble ectodomain of fibroblast growth factor receptor 1. Proc Natl Acad Sci U S A 1996;93:7069–74.

[41] Schultz GS, Wysocki A. Interactions between extracellular matrix and growth factors in wound healing. Wound Repair Regen 2009;17:153–62. doi:10.1111/j.1524-475X.2009.00466.x.

[42] Velnar T, Bailey T, Smrkolj V. The Wound Healing Process: An Overview of the Cellular and Molecular Mechanisms. J Int Med Res 2009;37:1528–42. doi:10.1177/147323000903700531.

[43] Schäfer M, Werner S. Cancer as an overhealing wound: an old hypothesis revisited. Nat Rev Mol Cell Biol 2008;9:628–38. doi:10.1038/nrm2455.

[44] Drury JL, Mooney DJ. Hydrogels for tissue engineering: scaffold design variables and applications. Biomaterials 2003;24:4337–51. doi:10.1016/S0142-9612(03)00340-5.

[45] Zhu J. Bioactive modification of poly(ethylene glycol) hydrogels for tissue engineering. Biomaterials 2010;31:4639–56. doi:10.1016/j.biomaterials.2010.02.044.

[46] Lee CH, Singla A, Lee Y. Biomedical applications of collagen. Int J Pharm 2001;221:1–22. doi:10.1016/S0378-5173(01)00691-3.

[47] Lee C., Grodzinsky a. ., Spector M. The effects of cross-linking of collagen-glycosaminoglycan scaffolds on compressive stiffness, chondrocyte-mediated

contraction, proliferation and biosynthesis. Biomaterials 2001;22:3145–54. doi:10.1016/S0142-9612(01)00067-9.

[48] Park S-N, Park J-C, Kim HO, Song MJ, Suh H. Characterization of porous collagen/hyaluronic acid scaffold modified by 1-ethyl-3-(3-dimethylaminopropyl)carbodiimide cross-linking. Biomaterials 2002;23:1205–12. doi:10.1016/S0142-9612(01)00235-6.

[49] Schoof H, Apel J, Heschel I, Rau G. Control of pore structure and size in freeze-dried collagen sponges. J Biomed Mater Res 2001;58:352–7. doi:10.1002/jbm.1028.

[50] Tan W, Krishnaraj R, Desai TA. Evaluation of nanostructured composite collagen--chitosan matrices for tissue engineering. Tissue Eng 2001;7:203–10. doi:10.1089/107632701300062831.

[51] HUANG L, NAGAPUDI K. Engineered collagen–PEO nano bers and fabrics. J Biomater Sci Polym Ed 2001;12:979–93.

[52] Patterson J, Martino MM, Hubbell J a. Biomimetic materials in tissue engineering. Mater Today 2010;13:14–22. doi:10.1016/S1369-7021(10)70013-4.

[53] Fisher OZ, Khademhosseini A, Langer R, Peppas N a. Bioinspired materials for controlling stem cell fate. Acc Chem Res 2010;43:419–28. doi:10.1021/ar900226q.

[54] Lutolf MP. Integration column: artificial ECM: expanding the cell biology toolbox in 3D. Integr Biol (Camb) 2009;1:235–41. doi:10.1039/b902243k.

[55] Nuttelman CR, Benoit DSW, Tripodi MC, Anseth KS. The effect of ethylene glycol methacrylate phosphate in PEG hydrogels on mineralization and viability of encapsulated hMSCs. Biomaterials 2006;27:1377–86. doi:10.1016/j.biomaterials.2005.08.014.

[56] Cushing MC, Anseth KS. Materials science. Hydrogel cell cultures. Science 2007;316:1133–4. doi:10.1126/science.1140171.

[57] Lutolf MP. Biomaterials: Spotlight on hydrogels. Nat Mater 2009;8:451–3. doi:10.1038/nmat2458.

[58] Kopecek J. Hydrogel biomaterials: a smart future? Biomaterials 2007;28:5185–92. doi:10.1016/j.biomaterials.2007.07.044.

[59] Nemir S, West JL. Synthetic materials in the study of cell response to substrate rigidity. Ann Biomed Eng 2010;38:2–20. doi:10.1007/s10439-009-9811-1.

[60] Kharkar PM, Kiick KL, Kloxin AM. Designing degradable hydrogels for orthogonal control of cell microenvironments. Chem Soc Rev 2013;42:7335–72. doi:10.1039/c3cs60040h.

[61] Lowe AB. Thiol-ene "click" reactions and recent applications in polymer and materials synthesis. Polym Chem 2010;1:17. doi:10.1039/b9py00216b.

[62] Liu V, Bhatia S. Three-dimensional photopatterning of hydrogels containing living cells. Biomed Microdevices 2002;4:257–66.

[63] Guyton AC, Hall JE. Textbook of Medical Physiology. 11th ed. Philadelphia, PA: Elsevier Saunders; 2005.

[64] Lu S, Ramirez WF, Anseth KS. Photopolymerized, multilaminated matrix devices with optimized nonuniform initial concentration profiles to control drug release. J Pharm Sci 2000;89:45–51. doi:10.1002/(SICI)1520-6017(200001)89:1<45::AID-JPS5>3.0.CO;2-8.

[65] Tanaka H, Matsumura M, Veliky IA. Diffusion characteristics of substrates in Ca-alginate gel beads. Biotechnol Bioeng 1984;26:53–8. doi:10.1002/bit.260260111.

[66] Li RH, Altreuter DH, Gentile FT. Transport characterization of hydrogel matrices for cell encapsulation. Biotechnol Bioeng 1996;50:365–73. doi:10.1002/(SICI)1097-0290(19960520)50:4<365::AID-BIT3>3.0.CO;2-J.

[67] Lu S, Anseth KS. Release Behavior of High Molecular Weight Solutes from Poly(ethylene glycol)-Based Degradable Networks. Macromolecules 2000;33:2509–15. doi:10.1021/ma9915024.

[68] Elisseeff J, Anseth K. Transdermal photopolymerization for minimally invasive implantation. Proc Natl Acad Sci U S A 1999;96:3104–7.

[69] Paige KT, Cima LG, Yaremchuk MJ, Vacanti JP. Injectable Cartilage. Plast Reconstr Surg 1995;96:1390–8.

[70] He S, J. Yaszemski M, Yasko AW, Engel PS, Mikos AG. Injectable biodegradable polymer composites based on poly(propylene fumarate) crosslinked with poly(ethylene glycol)-dimethacrylate. Biomaterials 2000;21:2389–94. doi:10.1016/S0142-9612(00)00106-X.

[71] Jeong B, Bae Y, Lee D, Kim S. Biodegradable block copolymers as injectable drug-delivery systems. Nature 1997;388:860–2.

[72] Cruise GM, Scharp DS, Hubbell J a. Characterization of permeability and network structure of interfacially photopolymerized poly(ethylene glycol) diacrylate hydrogels. Biomaterials 1998;19:1287–94. doi:10.1016/S0142-9612(98)00025-8.

[73] Mann BK, Gobin a S, Tsai a T, Schmedlen RH, West JL. Smooth muscle cell growth in photopolymerized hydrogels with cell adhesive and proteolytically degradable domains: synthetic ECM analogs for tissue engineering. Biomaterials 2001;22:3045–51.

[74] West JL, Hubbell JA. Polymeric Biomaterials with Degradation Sites for Proteases Involved in Cell Migration. Macromolecules 1999;32:241–4. doi:10.1021/ma981296k.

[75] Huh KM, Bae YH. Synthesis and characterization of poly(ethylene glycol)/poly(l-lactic acid) alternating multiblock copolymers. Polymer (Guildf) 1999;40:6147–55. doi:10.1016/S0032-3861(98)00822-2.

[76] Hubbell J a. Synthetic biodegradable polymers for tissue engineering and drug delivery. Curr Opin Solid State Mater Sci 1998;3:246–51. doi:10.1016/S1359-0286(98)80098-3.

[77] Beamish J a, Zhu J, Kottke-Marchant K, Marchant RE. The effects of monoacrylated poly(ethylene glycol) on the properties of poly(ethylene glycol) diacrylate hydrogels used for tissue engineering. J Biomed Mater Res A 2010;92:441–50. doi:10.1002/jbm.a.32353.

[78] Hahn MS, McHale MK, Wang E, Schmedlen RH, West JL. Physiologic pulsatile flow bioreactor conditioning of poly(ethylene glycol)-based tissue engineered vascular grafts. Ann Biomed Eng 2007;35:190–200. doi:10.1007/s10439-006-9099-3.

[79] Buxton AN, Zhu J, Marchant R, West JL, Yoo JU, Johnstone B. Design and characterization of poly(ethylene glycol) photopolymerizable semi-interpenetrating networks for chondrogenesis of human mesenchymal stem cells. Tissue Eng 2007;13:2549–60. doi:10.1089/ten.2007.0075.

[80] Metters A, Hubbell J. Network formation and degradation behavior of hydrogels formed by Michael-type addition reactions. Biomacromolecules 2005;6:290–301. doi:10.1021/bm049607o.

[81] Park Y, Lutolf MP, Hubbell JA, Hunziker EB, Wong M. Bovine primary chondrocyte culture in synthetic matrix metalloproteinase-sensitive poly(ethylene glycol)-based hydrogels as a scaffold for cartilage repair. Tissue Eng 2004;10:515–22. doi:10.1089/107632704323061870.

[82] Polizzotti BD, Fairbanks BD, Anseth KS. Three-dimensional biochemical patterning of click-based composite hydrogels via thiolene photopolymerization. Biomacromolecules 2008;9:1084–7. doi:10.1021/bm7012636.

[83] Malkoch M, Vestberg R, Gupta N, Mespouille L, Dubois P, Mason AF, et al. Synthesis of well-defined hydrogel networks using Click chemistry. Chem Commun 2006:2774. doi:10.1039/b603438a.

[84] Odian G. Principles of Polymerization. 4th ed. Hoboken, NJ: Wiley-Interscience; 2004.

[85] Lin C-C, Anseth KS. PEG hydrogels for the controlled release of biomolecules in regenerative medicine. Pharm Res 2009;26:631–43. doi:10.1007/s11095-008-9801-2.

[86] Ifkovits JL, Burdick J a. Review: photopolymerizable and degradable biomaterials for tissue engineering applications. Tissue Eng 2007;13:2369–85. doi:10.1089/ten.2007.0093.

[87] Vermonden T, Censi R, Hennink WE. Hydrogels for protein delivery. Chem Rev 2012;112:2853–88. doi:10.1021/cr200157d.

[88] Rizzi SC, Hubbell J a, Ehrbar M, Halstenberg S, Raeber GP, Schmoekel HG, et al. Recombinant protein-co-PEG networks as cell-adhesive and proteolytically degradable hydrogel matrixes. Part I: Development and physicochemical characteristics. Biomacromolecules 2005;6:3019–29. doi:10.1021/bm049614c.

[89] Lutolf MP, Raeber GP, Zisch a. H, Tirelli N, Hubbell J a. Cell-Responsive Synthetic Hydrogels. Adv Mater 2003;15:888–92. doi:10.1002/adma.200304621.

[90] Mooney DJ, Atala A, editors. Synthetic Biodegradable Polymer Scaffolds. Boston, MA: Birkhauser; 1997.

[91] Rowley J a., Madlambayan G, Mooney DJ. Alginate hydrogels as synthetic extracellular matrix materials. Biomaterials 1999;20:45–53. doi:10.1016/S0142-9612(98)00107-0.

[92] Haubner R, Gratias R, Diefenbach B, Goodman SL, Jonczyk A, Kessler H. Structural and Functional Aspects of RGD-Containing Cyclic Pentapeptides as Highly Potent and Selective Integrin α V β 3 Antagonists. J Am Chem Soc 1996;118:7461–72. doi:10.1021/ja9603721.

[93] Haubner R, Schmitt W, Hölzemann G, Goodman SL, Jonczyk A, Kessler H. Cyclic RGD Peptides Containing β-Turn Mimetics. J Am Chem Soc 1996;118:7881–91. doi:10.1021/ja9608757.

[94] Kaufmann D, Fiedler A, Junger A, Auernheimer J, Kessler H, Weberskirch R. Chemical conjugation of linear and cyclic RGD moieties to a recombinant elastin-mimetic polypeptide--a versatile approach towards bioactive protein hydrogels. Macromol Biosci 2008;8:577–88. doi:10.1002/mabi.200700234.

[95] Zhu J, Tang C, Kottke-Marchant K, Marchant RE. Design and synthesis of biomimetic hydrogel scaffolds with controlled organization of cyclic RGD peptides. Bioconjug Chem 2009;20:333–9. doi:10.1021/bc800441v.

[96] Raeber GP, Lutolf MP, Hubbell J a. Molecularly engineered PEG hydrogels: a novel model system for proteolytically mediated cell migration. Biophys J 2005;89:1374–88. doi:10.1529/biophysj.104.050682.

[97] Moon JJ, Saik JE, Poché R a, Leslie-Barbick JE, Lee S-H, Smith A a, et al. Biomimetic hydrogels with pro-angiogenic properties. Biomaterials 2010;31:3840–7. doi:10.1016/j.biomaterials.2010.01.104.

[98] Papavasiliou G, Cheng M-H, Brey EM. Strategies for vascularization of polymer scaffolds. J Investig Med 2010;58:838–44.

[99] Metters A. Fundamental studies of a novel, biodegradable PEG-b-PLA hydrogel. Polymer (Guildf) 2000;41:3993–4004. doi:10.1016/S0032-3861(99)00629-1.

[100] Nuttleman CR, Kloxin AM, Anseth KS. Tissue Engineering. vol. 585. Boston, MA: Springer US; 2007. doi:10.1007/978-0-387-34133-0.

[101] Bryant SJ, Durand KL, Anseth KS. Manipulations in hydrogel chemistry control photoencapsulated chondrocyte behavior and their extracellular matrix production. J Biomed Mater Res A 2003;67:1430–6. doi:10.1002/jbm.a.20003.

[102] Tsuji H. Autocatalytic hydrolysis of amorphous-made polylactides: effects of l-lactide content, tacticity, and enantiomeric polymer blending. Polymer (Guildf) 2002;43:1789–96. doi:10.1016/S0032-3861(01)00752-2.

[103] Saito N, Okada T, Horiuchi H, Murakami N, Takahashi J, Nawata M, et al. A biodegradable polymer as a cytokine delivery system for inducing bone formation. Nat Biotechnol 2001;19:332–5. doi:10.1038/86715.

[104] Park JB, Lakes RS. Biomaterials An Introduction. 3rd ed. New York, NY: 2007.

[105] Seliktar D, Zisch AH, Lutolf MP, Wrana JL, Hubbell JA. MMP-2 sensitive, VEGF-bearing bioactive hydrogels for promotion of vascular healing. J Biomed Mater Res A 2004;68:704–16. doi:10.1002/jbm.a.20091.

[106] Lee S-H, Moon JJ, Miller JS, West JL. Poly(ethylene glycol) hydrogels conjugated with a collagenase-sensitive fluorogenic substrate to visualize collagenase activity during three-dimensional cell migration. Biomaterials 2007;28:3163–70. doi:10.1016/j.biomaterials.2007.03.004.

[107] Gobin AS, West JL. Cell migration through defined, synthetic ECM analogs. FASEB J 2002;16:751–3. doi:10.1096/fj.01-0759fje.

[108] Lutolf MP, Weber FE, Schmoekel HG, Schense JC, Kohler T, Müller R, et al. Repair of bone defects using synthetic mimetics of collagenous extracellular matrices. Nat Biotechnol 2003;21:513–8. doi:10.1038/nbt818.

[109] Turk BE, Huang LL, Piro ET, Cantley LC. Determination of protease cleavage site motifs using mixture-based oriented peptide libraries. Nat Biotechnol 2001;19:661–7. doi:10.1038/90273.

[110] Patterson J, Hubbell J a. SPARC-derived protease substrates to enhance the plasmin sensitivity of molecularly engineered PEG hydrogels. Biomaterials 2011;32:1301–10. doi:10.1016/j.biomaterials.2010.10.016.

[111] Miller JS, Shen CJ, Legant WR, Baranski JD, Blakely BL, Chen CS. Bioactive hydrogels made from step-growth derived PEG-peptide macromers. Biomaterials 2010;31:3736–43. doi:10.1016/j.biomaterials.2010.01.058.

[112] Sokic S, Papavasiliou G. Controlled Proteolytic Cleavage Site Presentation in Biomimetic PEGDA Hydrogels Enhances Neovascularization In Vitro. Tissue Eng Part A 2012;18:2477–86. doi:10.1089/ten.tea.2012.0173.

[113] Kim BS, Nikolovski J, Bonadio J, Mooney DJ. Cyclic mechanical strain regulates the development of engineered smooth muscle tissue. Nat Biotechnol 1999;17:979–83. doi:10.1038/13671.

[114] Butler DL, Goldstein SA, Guilak F. Functional Tissue Engineering: The Role of Biomechanics. J Biomech Eng 2000;122:570. doi:10.1115/1.1318906.

[115] Cowin SC. How Is a Tissue Built?1. J Biomech Eng 2000;122:553. doi:10.1115/1.1324665.

[116] Sikavitsas VI, Temenoff JS, Mikos AG. Biomaterials and bone mechanotransduction. Biomaterials 2001;22:2581–93. doi:10.1016/S0142-9612(01)00002-3.

[117] Burridge K, Chrzanowska-Wodnicka M. Focal adhesions, contractility, and signaling. Annu Rev Cell Dev Biol 1996;12:463–518. doi:10.1146/annurev.cellbio.12.1.463.

[118] Mège R-M, Gavard J, Lambert M. Regulation of cell-cell junctions by the cytoskeleton. Curr Opin Cell Biol 2006;18:541–8. doi:10.1016/j.ceb.2006.08.004.

[119] Barbee KA, Davies PF, Lal R. Shear stress-induced reorganization of the surface topography of living endothelial cells imaged by atomic force microscopy. Circ Res 1994;74:163–71. doi:10.1161/01.RES.74.1.163.

[120] Rho J, Ashman R, Turner C. Young's modulus of trabecular and cortical bone material: ultrasonic and microtensile measurements. J Biomech 1993;26:111–9.

[121] Discher DE, Janmey P, Wang Y. Tissue cells feel and respond to the stiffness of their substrate. Science 2005;310:1139–43. doi:10.1126/science.1116995.

[122] Jaalouk DE, Lammerding J. Mechanotransduction gone awry. Nat Rev Mol Cell Biol 2009;10:63–73. doi:10.1038/nrm2597.

[123] Martinac B. Mechanosensitive ion channels: molecules of mechanotransduction. J Cell Sci 2004;117:2449–60. doi:10.1242/jcs.01232.

[124] Berbari NF, O'Connor AK, Haycraft CJ, Yoder BK. The primary cilium as a complex signaling center. Curr Biol 2009;19:R526–35. doi:10.1016/j.cub.2009.05.025.

[125] Galbraith CG, Yamada KM, Sheetz MP. The relationship between force and focal complex development. J Cell Biol 2002;159:695–705. doi:10.1083/jcb.200204153.

[126] Makino A, Prossnitz ER, Bünemann M, Wang JM, Yao W, Schmid-Schönbein GW. G protein-coupled receptors serve as mechanosensors for fluid shear stress in neutrophils. Am J Physiol Cell Physiol 2006;290:C1633–9. doi:10.1152/ajpcell.00576.2005.

[127] Osawa M, Masuda M, Kusano K, Fujiwara K. Evidence for a role of platelet endothelial cell adhesion molecule-1 in endothelial cell mechanosignal transduction: is it a mechanoresponsive molecule? J Cell Biol 2002;158:773–85. doi:10.1083/jcb.200205049.

[128] Wang N, Butler J, Ingber D. Mechanotransduction across the cell surface and through the cytoskeleton. Science (80-) 1993;260:1124–7. doi:10.1126/science.7684161.

[129] Hynes RO. IntegrinsBidirectional, Allosteric Signaling Machines. Cell 2002;110:673–87. doi:10.1016/S0092-8674(02)00971-6.

[130] Plow EF, Haas T a, Zhang L, Loftus J, Smith JW. Ligand binding to integrins. J Biol Chem 2000;275:21785–8. doi:10.1074/jbc.R000003200.

[131] Kumar S, Maxwell IZ, Heisterkamp A, Polte TR, Lele TP, Salanga M, et al. Viscoelastic retraction of single living stress fibers and its impact on cell shape, cytoskeletal organization, and extracellular matrix mechanics. Biophys J 2006;90:3762–73. doi:10.1529/biophysj.105.071506.

[132] Lee J. Traction forces generated by locomoting keratocytes. J Cell Biol 1994;127:1957–64. doi:10.1083/jcb.127.6.1957.

[133] Rodriguez OC, Schaefer AW, Mandato C a, Forscher P, Bement WM, Waterman-Storer CM. Conserved microtubule-actin interactions in cell movement and morphogenesis. Nat Cell Biol 2003;5:599–609. doi:10.1038/ncb0703-599.

[134] Engler A, Bacakova L, Newman C, Hategan A, Griffin M, Discher D. Substrate Compliance versus Ligand Density in Cell on Gel Responses. Biophys J 2004;86:617–28. doi:10.1016/S0006-3495(04)74140-5.

[135] Genes NG, Rowley J a, Mooney DJ, Bonassar LJ. Effect of substrate mechanics on chondrocyte adhesion to modified alginate surfaces. Arch Biochem Biophys 2004;422:161–7. doi:10.1016/j.abb.2003.11.023.

[136] Ghibaudo M, Saez A, Trichet L, Xayaphoummine A, Browaeys J, Silberzan P, et al. Traction forces and rigidity sensing regulate cell functions. Soft Matter 2008;4:1836. doi:10.1039/b804103b.

[137] Yeung T, Georges PC, Flanagan L a, Marg B, Ortiz M, Funaki M, et al. Effects of substrate stiffness on cell morphology, cytoskeletal structure, and adhesion. Cell Motil Cytoskeleton 2005;60:24–34. doi:10.1002/cm.20041.

[138] Engler AJ, Griffin M a, Sen S, Bönnemann CG, Sweeney HL, Discher DE. Myotubes differentiate optimally on substrates with tissue-like stiffness: pathological implications for soft or stiff microenvironments. J Cell Biol 2004;166:877–87. doi:10.1083/jcb.200405004.

[139] Califano JP, Reinhart-King CA. Substrate Stiffness and Cell Area Predict Cellular Traction Stresses in Single Cells and Cells in Contact. Cell Mol Bioeng 2010;3:68–75. doi:10.1007/s12195-010-0102-6.

[140] Reinhart-King C a, Dembo M, Hammer D a. Cell-cell mechanical communication through compliant substrates. Biophys J 2008;95:6044–51. doi:10.1529/biophysj.107.127662.

[141] Lo CM, Wang HB, Dembo M, Wang YL. Cell movement is guided by the rigidity of the substrate. Biophys J 2000;79:144–52. doi:10.1016/S0006-3495(00)76279-5.

[142] Engler AJ, Sen S, Sweeney HL, Discher DE. Matrix elasticity directs stem cell lineage specification. Cell 2006;126:677–89. doi:10.1016/j.cell.2006.06.044.

[143] Bryant SJ, Anseth KS. Hydrogel properties influence ECM production by chondrocytes photoencapsulated in poly(ethylene glycol) hydrogels. J Biomed Mater Res 2002;59:63–72.

[144] Bencherif S a, Srinivasan A, Horkay F, Hollinger JO, Matyjaszewski K, Washburn NR. Influence of the degree of methacrylation on hyaluronic acid hydrogels properties. Biomaterials 2008;29:1739–49. doi:10.1016/j.biomaterials.2007.11.047.

[145] Patenaude M, Hoare T. Injectable, mixed natural-synthetic polymer hydrogels with modular properties. Biomacromolecules 2012;13:369–78. doi:10.1021/bm2013982.

[146] Freeman I, Kedem A, Cohen S. The effect of sulfation of alginate hydrogels on the specific binding and controlled release of heparin-binding proteins. Biomaterials 2008;29:3260–8. doi:10.1016/j.biomaterials.2008.04.025.

[147] Yamaguchi N, Kiick KL. Polysaccharide-poly(ethylene glycol) star copolymer as a scaffold for the production of bioactive hydrogels. Biomacromolecules 2005;6:1921–30. doi:10.1021/bm050003+.

[148] Mann BK, Schmedlen RH, West JL. Tethered-TGF-β increases extracellular matrix production of vascular smooth muscle cells. Biomaterials 2001;22:439–44. doi:10.1016/S0142-9612(00)00196-4.

[149] Suzuki Y, Tanihara M, Suzuki K, Saitou A, Sufan W, Nishimura Y. Alginate hydrogel linked with synthetic oligopeptide derived from BMP-2 allows ectopic osteoinduction in vivo. J Biomed Mater Res 2000;50:405–9. doi:10.1002/(SICI)1097-4636(20000605)50:3<405::AID-JBM15>3.0.CO;2-Z.

[150] Elisseeff J, McIntosh W, Fu K, Blunk BT, Langer R. Controlled-release of IGF-I and TGF-beta1 in a photopolymerizing hydrogel for cartilage tissue engineering. J Orthop Res 2001;19:1098–104. doi:10.1016/S0736-0266(01)00054-7.

[151] Kubow KE, Klotzsch E, Smith ML, Gourdon D, Little WC, Vogel V. Crosslinking of cell-derived 3D scaffolds up-regulates the stretching and unfolding of new extracellular matrix assembled by reseeded cells. Integr Biol (Camb) 2009;1:635–48. doi:10.1039/b914996a.

[152] Legant WR, Chen CS, Vogel V. Force-induced fibronectin assembly and matrix remodeling in a 3D microtissue model of tissue morphogenesis. Integr Biol (Camb) 2012;4:1164–74. doi:10.1039/c2ib20059g.

[153] Zhou M, Ulijn R V, Gough JE. Extracellular matrix formation in self-assembled minimalistic bioactive hydrogels based on aromatic peptide amphiphiles. J Tissue Eng 2014;5:2041731414531593. doi:10.1177/2041731414531593.

[154] Hartgerink JD, Beniash E, Stupp SI. Self-assembly and mineralization of peptide-amphiphile nanofibers. Science (80-) 2001;294:1684–8. doi:10.1126/science.1063187.

[155] Ridley AJ, Schwartz MA, Burridge K, Firtel RA, Ginsberg MH, Borisy G, et al. Cell migration: integrating signals from front to back. Science (80-) 2003;302:1704–9. doi:10.1126/science.1092053.

[156] Schwartz MP, Fairbanks BD, Rogers RE, Rangarajan R, Zaman MH, Anseth KS. A synthetic strategy for mimicking the extracellular matrix provides new insight about tumor cell migration. Integr Biol (Camb) 2010;2:32–40. doi:10.1039/b912438a.

[157] Langer R, Vacanti JP. Tissue Engineering. Science (80-) 1993;260:920–6.

[158] Berthiaume F, Maguire TJ, Yarmush ML. Tissue engineering and regenerative medicine: history, progress, and challenges. Annu Rev Chem Biomol Eng 2011;2:403–30. doi:10.1146/annurev-chembioeng-061010-114257.

[159] Hubbell J. Bioactive biomaterials. Curr Opin Biotechnol 1999;10:123–9. doi:10.1016/S0958-1669(99)80021-4.

[160] Lee KY, Mooney DJ. Hydrogels for Tissue Engineering. Chem Rev 2001;101:1869–80. doi:10.1021/cr000108x.

[161] Chung EH, Gilbert M, Virdi AS, Sena K, Sumner DR, Healy KE. Biomimetic artificial ECMs stimulate bone regeneration. J Biomed Mater Res A 2006;79:815–26. doi:10.1002/jbm.a.30809.

[162] Alcantar NA, Aydil ES, Israelachvili JN. Polyethylene glycol-coated biocompatible surfaces. J Biomed Mater Res 2000;51:343–51. doi:10.1002/1097-4636(20000905)51:3<343::AID-JBM7>3.0.CO;2-D.

[163] Hansen JK, Thibeault SL, Walsh JF, Shu XZ, Prestwich GD. In vivo engineering of the vocal fold extracellular matrix with injectable hyaluronic acid hydrogels: early effects on tissue repair and biomechanics in a rabbit model. Ann Otol Rhinol Laryngol 2005;114:662–70.

[164] Connors RC, Muir JJ, Liu Y, Reiss GR, Kouretas PC, Whitten MG, et al. Postoperative pericardial adhesion prevention using Carbylan-SX in a rabbit model. J Surg Res 2007;140:237–42. doi:10.1016/j.jss.2007.03.014.

[165] Coburn J, Gibson M, Bandalini P. Biomimetics of the extracellular matrix: an integrated three-dimensional fiber-hydrogel composite for cartilage tissue engineering. Smart Struct Syst 2011;7:213–22.

[166] Nicodemus GD, Bryant SJ. Cell encapsulation in biodegradable hydrogels for tissue engineering applications. Tissue Eng Part B Rev 2008;14:149–65. doi:10.1089/ten.teb.2007.0332.

[167] Slaughter B V, Khurshid SS, Fisher OZ, Khademhosseini A, Peppas N a. Hydrogels in regenerative medicine. Adv Mater 2009;21:3307–29. doi:10.1002/adma.200802106.

[168] Jia X, Kiick KL. Hybrid multicomponent hydrogels for tissue engineering. Macromol Biosci 2009;9:140–56. doi:10.1002/mabi.200800284.

[169] Hern DL, Hubbell J a. Incorporation of adhesion peptides into nonadhesive hydrogels useful for tissue resurfacing. J Biomed Mater Res 1998;39:266–76.

[170] Anderson SB, Lin C-C, Kuntzler D V, Anseth KS. The performance of human mesenchymal stem cells encapsulated in cell-degradable polymer-peptide hydrogels. Biomaterials 2011;32:3564–74. doi:10.1016/j.biomaterials.2011.01.064.

[171] Ehrbar M, Rizzi SC, Hlushchuk R, Djonov V, Zisch AH, Hubbell J a, et al. Enzymatic formation of modular cell-instructive fibrin analogs for tissue engineering. Biomaterials 2007;28:3856–66. doi:10.1016/j.biomaterials.2007.03.027.

[172] Phelps EA, Landázuri N, Thulé PM, Taylor WR, García AJ. Bioartificial matrices for therapeutic vascularization. Proc Natl Acad Sci U S A 2010;107:3323–8. doi:10.1073/pnas.0905447107.

[173] Leslie-Barbick JE, Saik JE, Gould DJ, Dickinson ME, West JL. The promotion of microvasculature formation in poly(ethylene glycol) diacrylate hydrogels by an immobilized VEGF-mimetic peptide. Biomaterials 2011;32:5782–9. doi:10.1016/j.biomaterials.2011.04.060.

[174] Mariner PD, Wudel JM, Miller DE, Genova EE, Streubel S-O, Anseth KS. Synthetic hydrogel scaffold is an effective vehicle for delivery of INFUSE (rhBMP2) to critical-sized calvaria bone defects in rats. J Orthop Res 2013;31:401–6. doi:10.1002/jor.22243.

[175] Jo YS, Rizzi SC, Ehrbar M, Weber FE, Hubbell J a, Lutolf MP. Biomimetic PEG hydrogels crosslinked with minimal plasmin-sensitive tri-amino acid peptides. J Biomed Mater Res A 2010;93:870–7. doi:10.1002/jbm.a.32580.

[176] Bott K, Upton Z, Schrobback K, Ehrbar M, Hubbell JA, Lutolf MP, et al. The effect of matrix characteristics on fibroblast proliferation in 3D gels. Biomaterials 2010;31:8454–64. doi:10.1016/j.biomaterials.2010.07.046.

[177] Loessner D, Stok KS, Lutolf MP, Hutmacher DW, Clements J a, Rizzi SC. Bioengineered 3D platform to explore cell-ECM interactions and drug resistance of epithelial ovarian cancer cells. Biomaterials 2010;31:8494–506. doi:10.1016/j.biomaterials.2010.07.064.

[178] Ehrbar M, Sala a, Lienemann P, Ranga a, Mosiewicz K, Bittermann a, et al. Elucidating the role of matrix stiffness in 3D cell migration and remodeling. Biophys J 2011;100:284–93. doi:10.1016/j.bpj.2010.11.082.

[179] Sokic S, Papavasiliou G. FGF-1 and proteolytically mediated cleavage site presentation influence three-dimensional fibroblast invasion in biomimetic PEGDA hydrogels. Acta Biomater 2012;8:2213–22. doi:10.1016/j.actbio.2012.03.017.

[180] Ghosh K, Ren X, Shu X. Fibronectin functional domains coupled to hyaluronan stimulate adult human dermal fibroblast responses critical for wound healing. Tissue Eng Part A 2006;12:601–13.

[181] Almany L, Seliktar D. Biosynthetic hydrogel scaffolds made from fibrinogen and polyethylene glycol for 3D cell cultures. Biomaterials 2005;26:2467–77. doi:10.1016/j.biomaterials.2004.06.047.

[182] Peled E, Boss J, Bejar J, Zinman C, Seliktar D. A novel poly(ethylene glycol)-fibrinogen hydrogel for tibial segmental defect repair in a rat model. J Biomed Mater Res A 2007;80:874–84. doi:10.1002/jbm.a.30928.

[183] Sarig-Nadir O, Seliktar D. Compositional alterations of fibrin-based materials for regulating in vitro neural outgrowth. Tissue Eng Part A 2008;14:401–11. doi:10.1089/tea.2007.0029.

[184] Zhang G, Wang X, Wang Z, Zhang J, Suggs L. A PEGylated fibrin patch for mesenchymal stem cell delivery. Tissue Eng 2006;12:9–19. doi:10.1089/ten.2006.12.9.

[185] Zhang G, Drinnan CT, Geuss LR, Suggs LJ. Vascular differentiation of bone marrow stem cells is directed by a tunable three-dimensional matrix. Acta Biomater 2010;6:3395–403. doi:10.1016/j.actbio.2010.03.019.

[186] Zheng Shu X, Liu Y, Palumbo FS, Luo Y, Prestwich GD. In situ crosslinkable hyaluronan hydrogels for tissue engineering. Biomaterials 2004;25:1339–48. doi:10.1016/j.biomaterials.2003.08.014.

[187] Kutty JK, Cho E, Soo Lee J, Vyavahare NR, Webb K. The effect of hyaluronic acid incorporation on fibroblast spreading and proliferation within PEG-diacrylate based semi-interpenetrating networks. Biomaterials 2007;28:4928–38. doi:10.1016/j.biomaterials.2007.08.007.

[188] Cho E, Kutty JK, Datar K, Lee JS, Vyavahare NR, Webb K. A novel synthetic route for the preparation of hydrolytically degradable synthetic hydrogels. J Biomed Mater Res A 2009;90:1073–82. doi:10.1002/jbm.a.32172.

[189] Kutty JK, Webb K. Mechanomimetic hydrogels for vocal fold lamina propria regeneration. J Biomater Sci Polym Ed 2009;20:737–56. doi:10.1163/156856209X426763.

[190] Gao L, McBeath R, Chen CS. Stem cell shape regulates a chondrogenic versus myogenic fate through Rac1 and N-cadherin. Stem Cells 2010;28:564–72. doi:10.1002/stem.308.

[191] McBeath R, Pirone DM, Nelson CM, Bhadriraju K, Chen CS. Cell shape, cytoskeletal tension, and RhoA regulate stem cell lineage commitment. Dev Cell 2004;6:483–95.

[192] Chen CS. Geometric Control of Cell Life and Death. Science (80-) 1997;276:1425–8. doi:10.1126/science.276.5317.1425.

[193] Kuo JW. Practical Aspects of Hyaluronan Based Medical Products. CRC Press; 2005.

[194] Dick HB, Schwenn O. Viscoelastics in Ophthalmic Surgery. Berlin, Heidelberg: Springer Berlin Heidelberg; 2000. doi:10.1007/978-3-642-59779-4.

[195] Ouasti S, Donno R, Cellesi F, Sherratt MJ, Terenghi G, Tirelli N. Network connectivity, mechanical properties and cell adhesion for hyaluronic acid/PEG hydrogels. Biomaterials 2011;32:6456–70. doi:10.1016/j.biomaterials.2011.05.044.

[196] Cowman MK, Matsuoka S. Experimental approaches to hyaluronan structure. Carbohydr Res 2005;340:791–809. doi:10.1016/j.carres.2005.01.022.

[197] Rizzi SC, Ehrbar M, Halstenberg S, Raeber GP, Schmoekel HG, Hagenmüller H, et al. Recombinant protein-co-PEG networks as cell-adhesive and proteolytically degradable hydrogel matrixes. Part II: biofunctional characteristics. Biomacromolecules 2006;7:3019–29. doi:10.1021/bm060504a.

[198] Yang PJ, Levenston ME, Temenoff JS. Modulation of mesenchymal stem cell shape in enzyme-sensitive hydrogels is decoupled from upregulation of fibroblast markers under cyclic tension. Tissue Eng Part A 2012;18:2365–75. doi:10.1089/ten.TEA.2011.0727.

[199] Quick DJ, Anseth KS. DNA delivery from photocrosslinked PEG hydrogels: encapsulation efficiency, release profiles, and DNA quality. J Control Release 2004;96:341–51. doi:10.1016/j.jconrel.2004.01.021.

[200] Togawa D, Bauer T, Lieberman I. Lumbar intervertebral body fusion cages: histological evaluation of clinically failed cages retrieved from humans. J Bone Joint Surg Am 2004;86-A:70–9.

[201] Burg KJ., Porter S, Kellam JF. Biomaterial developments for bone tissue engineering. Biomaterials 2000;21:2347–59. doi:10.1016/S0142-9612(00)00102-2.

[202] Hing KA. Bone repair in the twenty-first century: biology, chemistry or engineering? Philos Trans A Math Phys Eng Sci 2004;362:2821–50. doi:10.1098/rsta.2004.1466.

[203] Meeder P-J, Eggers C. 2. Techniques for obtaining autogenous bone graft. Injury 1994;25:SA5–16. doi:10.1016/0020-1383(94)90255-0.

[204] Meeder P-J, Eggers C. 1. The history of autogenous bone grafting. Injury 1994;25:SA2–4. doi:10.1016/0020-1383(94)90254-2.

[205] Salgado AJ, Coutinho OP, Reis RL. Bone tissue engineering: state of the art and future trends. Macromol Biosci 2004;4:743–65. doi:10.1002/mabi.200400026.

[206] Reddi AH. Morphogenesis and tissue engineering of bone and cartilage: inductive signals, stem cells, and biomimetic biomaterials. Tissue Eng 2000;6:351–9. doi:10.1089/107632700418074.

[207] Wilson CE, de Bruijn JD, van Blitterswijk CA, Verbout AJ, Dhert WJA. Design and fabrication of standardized hydroxyapatite scaffolds with a defined macro-architecture by rapid prototyping for bone-tissue-engineering research. J Biomed Mater Res A 2004;68:123–32. doi:10.1002/jbm.a.20015.

[208] Burdick J a, Frankel D, Dernell WS, Anseth KS. An initial investigation of photocurable three-dimensional lactic acid based scaffolds in a critical-sized cranial defect. Biomaterials 2003;24:1613–20. doi:10.1016/S0142-9612(02)00538-0.

[209] Merkx M a. W, Maltha JC, Freihofer H-PM, Kuijpers-Jagtman AM. Incorporation of three types of bone block implants in the facial skeleton. Biomaterials 1999;20:639–45. doi:10.1016/S0142-9612(98)00219-1.

[210] Lee KY, Alsberg E, Mooney DJ. Degradable and injectable poly(aldehyde guluronate) hydrogels for bone tissue engineering. J Biomed Mater Res 2001;56:228–33.

[211] Burdick J a., Anseth KS. Photoencapsulation of osteoblasts in injectable RGD-modified PEG hydrogels for bone tissue engineering. Biomaterials 2002;23:4315–23. doi:10.1016/S0142-9612(02)00176-X.

[212] Trojani C, Balaguer T, Boukhechba F, Carle G-F, Boileau P, Rochet N. [Cellular strategies in bone tissue engineering: a review]. Rev Chir Orthop Reparatrice Appar Mot 2008;94:1–11. doi:10.1016/j.rco.2007.11.001.

[213] Shih Y-R V, Tseng K-F, Lai H-Y, Lin C-H, Lee OK. Matrix stiffness regulation of integrin-mediated mechanotransduction during osteogenic differentiation of human mesenchymal stem cells. J Bone Miner Res 2011;26:730–8. doi:10.1002/jbmr.278.

[214] Hsiong SX, Carampin P, Kong H-J, Lee K-Y, Mooney DJ. Differentiation stage alters matrix control of stem cells. J Biomed Mater Res A 2008;85:145–56. doi:10.1002/jbm.a.31521.

[215] Rowlands AS, George P a, Cooper-White JJ. Directing osteogenic and myogenic differentiation of MSCs: interplay of stiffness and adhesive ligand presentation. Am J Physiol Cell Physiol 2008;295:C1037–44. doi:10.1152/ajpcell.67.2008.

[216] Jha AK, Jackson WM, Healy KE. Controlling osteogenic stem cell differentiation via soft bioinspired hydrogels. PLoS One 2014;9:e98640. doi:10.1371/journal.pone.0098640.

[217] Hudalla G a, Eng TS, Murphy WL. An approach to modulate degradation and mesenchymal stem cell behavior in poly(ethylene glycol) networks. Biomacromolecules 2008;9:842–9. doi:10.1021/bm701179s.

[218] Benoit DSW, Durney AR, Anseth KS. Manipulations in hydrogel degradation behavior enhance osteoblast function and mineralized tissue formation. Tissue Eng 2006;12:1663–73. doi:10.1089/ten.2006.12.1663.

[219] Hernández RM a, Orive G, Murua A, Pedraz JL. Microcapsules and microcarriers for in situ cell delivery. Adv Drug Deliv Rev 2010;62:711–30. doi:10.1016/j.addr.2010.02.004.

[220] Stein G, Lian J, Owen T. Relationship of cell growth to the regulation of tissue-specific gene expression during osteoblast differentiation. FASEB J 1990;4:3111–23.

[221] Livak KJ, Schmittgen TD. Analysis of relative gene expression data using real-time quantitative PCR and the 2(-Delta Delta C(T)) Method. Methods 2001;25:402–8. doi:10.1006/meth.2001.1262.

[222] Temenoff JS, Park H, Jabbari E, Sheffield TL, LeBaron RG, Ambrose CG, et al. In vitro osteogenic differentiation of marrow stromal cells encapsulated in biodegradable hydrogels. J Biomed Mater Res A 2004;70:235–44. doi:10.1002/jbm.a.30064.

[223] Anselme K. Osteoblast adhesion on biomaterials. Biomaterials 2000;21:667–81. doi:10.1016/S0142-9612(99)00242-2.

[224] Li W-J, Tuli R, Huang X, Laquerriere P, Tuan RS. Multilineage differentiation of human mesenchymal stem cells in a three-dimensional nanofibrous scaffold. Biomaterials 2005;26:5158–66. doi:10.1016/j.biomaterials.2005.01.002.

[225] Hwang NS, Varghese S, Li H, Elisseeff J. Regulation of osteogenic and chondrogenic differentiation of mesenchymal stem cells in PEG-ECM hydrogels. Cell Tissue Res 2011;344:499–509. doi:10.1007/s00441-011-1153-2.

[226] Born A-K, Rottmar M, Lischer S, Pleskova M, Bruinink A. CORRELATING CELL ARCHITECTURE WITH OSTEOGENESIS : FIRST STEPS TOWARDS LIVE SINGLE CELL MONITORING. Eur Cells Mater 2009;18:49–62.

[227] Pek YS, Wan AC a, Ying JY. The effect of matrix stiffness on mesenchymal stem cell differentiation in a 3D thixotropic gel. Biomaterials 2010;31:385–91. doi:10.1016/j.biomaterials.2009.09.057.

[228] Nishio Y, Dong Y, Paris M, O'Keefe RJ, Schwarz EM, Drissi H. Runx2-mediated regulation of the zinc finger Osterix/Sp7 gene. Gene 2006;372:62–70. doi:10.1016/j.gene.2005.12.022.

[229] Nakashima K, Zhou X, Kunkel G, Zhang Z, Deng JM, Behringer RR, et al. The Novel Zinc Finger-Containing Transcription Factor Osterix Is Required for Osteoblast Differentiation and Bone Formation. Cell 2002;108:17–29. doi:10.1016/S0092-8674(01)00622-5.

[230] Tye CE, Hunter GK, Goldberg H a. Identification of the type I collagen-binding domain of bone sialoprotein and characterization of the mechanism of interaction. J Biol Chem 2005;280:13487–92. doi:10.1074/jbc.M408923200.

[231] Hutchens S a, Benson RS, Evans BR, O'Neill HM, Rawn CJ. Biomimetic synthesis of calcium-deficient hydroxyapatite in a natural hydrogel. Biomaterials 2006;27:4661–70. doi:10.1016/j.biomaterials.2006.04.032.

[232] Liu G, Zhao D, Tomsia AP, Minor AM, Song X, Saiz E. Three-dimensional biomimetic mineralization of dense hydrogel templates. J Am Chem Soc 2009;131:9937–9. doi:10.1021/ja903817z.

[233] Qu H, Xia Z, Knecht D a, Wei M. Synthesis of Dense Collagen/Apatite Composites Using a Biomimetic Method. J Am Ceram Soc 2008;91:3211–5. doi:10.1111/j.1551-2916.2008.02634.x.

[234] Song J, Saiz E, Bertozzi CR. A new approach to mineralization of biocompatible hydrogel scaffolds: an efficient process toward 3-dimensional bonelike composites. J Am Chem Soc 2003;125:1236–43. doi:10.1021/ja028559h.

[235] Trebaul a, Chan EK, Midwood KS. Regulation of fibroblast migration by tenascin-C. Biochem Soc Trans 2007;35:695–7. doi:10.1042/BST0350695.

[236] Gailit J, Clarke C, Newman D, Tonnesen MG, Mosesson MW, Clark RA. Human fibroblasts bind directly to fibrinogen at RGD sites through integrin alpha(v)beta3. Exp Cell Res 1997;232:118–26. doi:10.1006/excr.1997.3512.

[237] Singh P, Carraher C, Schwarzbauer JE. Assembly of fibronectin extracellular matrix. Annu Rev Cell Dev Biol 2010;26:397–419. doi:10.1146/annurev-cellbio-100109-104020.

[238] Hocking DC. A novel role for the integrin-binding III-10 module in fibronectin matrix assembly. J Cell Biol 1996;133:431–44. doi:10.1083/jcb.133.2.431.

[239] Hocking DC. Stimulation of Integrin-mediated Cell Contractility by Fibronectin Polymerization. J Biol Chem 2000;275:10673–82. doi:10.1074/jbc.275.14.10673.

[240] Kadler KE, Hill A, Canty-Laird EG. Collagen fibrillogenesis: fibronectin, integrins, and minor collagens as organizers and nucleators. Curr Opin Cell Biol 2008;20:495–501. doi:10.1016/j.ceb.2008.06.008.

[241] Gombotz WR, Wang GH, Horbett TA, Hoffman AS. Protein adsorption to poly(ethylene oxide) surfaces. J Biomed Mater Res 1991;25:1547–62. doi:10.1002/jbm.820251211.

[242] LEE J, LEE H, ANDRADE J. Blood compatibility of polyethylene oxide surfaces. Prog Polym Sci 1995;20:1043–79. doi:10.1016/0079-6700(95)00011-4.

[243] Kadler E, Prockops J. Assembly of Collagen Fibrils de Nouo by Cleavage of the Type I PC- Collagen with Procollagen C-Proteinase. J Biol Chem 1987;260:15696–701.

[244] Du H, Chandaroy P, Hui SW. Grafted poly-(ethylene glycol) on lipid surfaces inhibits protein adsorption and cell adhesion. Biochim Biophys Acta - Biomembr 1997;1326:236–48. doi:10.1016/S0005-2736(97)00027-8.

[245] Benoit DSW, Anseth KS. Heparin functionalized PEG gels that modulate protein adsorption for hMSC adhesion and differentiation. Acta Biomater 2005;1:461–70. doi:10.1016/j.actbio.2005.03.002.

[246] Bryant SJ, Anseth KS. Controlling the spatial distribution of ECM components in degradable PEG hydrogels for tissue engineering cartilage. J Biomed Mater Res A 2003;64:70–9. doi:10.1002/jbm.a.10319.

[247] Erickson IE, Kestle SR, Zellars KH, Farrell MJ, Kim M, Burdick J a, et al. High mesenchymal stem cell seeding densities in hyaluronic acid hydrogels produce engineered cartilage with native tissue properties. Acta Biomater 2012;8:3027–34. doi:10.1016/j.actbio.2012.04.033.

[248] Hempel U, Hintze V, Möller S, Schnabelrauch M, Scharnweber D, Dieter P. Artificial extracellular matrices composed of collagen I and sulfated hyaluronan with adsorbed transforming growth factor β1 promote collagen synthesis of human mesenchymal stromal cells. Acta Biomater 2012;8:659–66. doi:10.1016/j.actbio.2011.10.026.

[249] Lee HJ, Lee J-S, Chansakul T, Yu C, Elisseeff JH, Yu SM. Collagen mimetic peptide-conjugated photopolymerizable PEG hydrogel. Biomaterials 2006;27:5268–76. doi:10.1016/j.biomaterials.2006.06.001.

[250] Solorio LD, Vieregge EL, Dhami CD, Alsberg E. High-density cell systems incorporating polymer microspheres as microenvironmental regulators in engineered cartilage tissues. Tissue Eng Part B Rev 2013;19:209–20. doi:10.1089/ten.TEB.2012.0252.

[251] Mercier NR, Costantino HR, Tracy M a, Bonassar LJ. Poly(lactide-co-glycolide) microspheres as a moldable scaffold for cartilage tissue engineering. Biomaterials 2005;26:1945–52. doi:10.1016/j.biomaterials.2004.06.030.

[252] Tous E, Weber HM, Lee MH, Koomalsingh KJ, Shuto T, Kondo N, et al. Tunable hydrogel-microsphere composites that modulate local inflammation and collagen bulking. Acta Biomater 2012;8:3218–27. doi:10.1016/j.actbio.2012.05.027.

[253] Bilati U, Allémann E, Doelker E. Poly(D,L-lactide-co-glycolide) protein-loaded nanoparticles prepared by the double emulsion method--processing and formulation issues for enhanced entrapment efficiency. J Microencapsul 2005;22:205–14. doi:10.1080/02652040400026442.

[254] Drira Z, Yadavalli VK. Nanomechanical measurements of polyethylene glycol hydrogels using atomic force microscopy. J Mech Behav Biomed Mater 2013;18:20–8. doi:10.1016/j.jmbbm.2012.09.015.

[255] García R. Dynamic atomic force microscopy methods. Surf Sci Rep 2002;47:197–301. doi:10.1016/S0167-5729(02)00077-8.

[256] Neuman RE, Logan MA. The determination of hydroxyproline. J Biol Chem 1950;184:299–306.

[257] Woessner JJ. The determination of hydroxyproline in tissue and protein samples containing small proportions of this imino acid. Arch Biochem Biophys 1961;93:440–7.

[258] Mazzitelli S, Pagano C, Giusepponi D, Nastruzzi C, Perioli L. Hydrogel blends with adjustable properties as patches for transdermal delivery. Int J Pharm 2013;454:47–57. doi:10.1016/j.ijpharm.2013.06.081.

[259] Sawhney AS, Pathak CP, Hubbell JA. Bioerodible hydrogels based on photopolymerized poly(ethylene glycol)-co-poly(.alpha.-hydroxy acid) diacrylate macromers. Macromolecules 1993;26:581–7. doi:10.1021/ma00056a005.

[260] Byfield FJ, Reen RK, Shentu T-P, Levitan I, Gooch KJ. Endothelial actin and cell stiffness is modulated by substrate stiffness in 2D and 3D. J Biomech 2009;42:1114–9. doi:10.1016/j.jbiomech.2009.02.012.

[261] Califano JP, Reinhart-King CA. A Balance of Substrate Mechanics and Matrix Chemistry Regulates Endothelial Cell Network Assembly. Cell Mol Bioeng 2008;1:122–32. doi:10.1007/s12195-008-0022-x.

[262] Achterberg VF, Buscemi L, Diekmann H, Smith-Clerc J, Schwengler H, Meister J-J, et al. The nano-scale mechanical properties of the extracellular matrix regulate dermal fibroblast function. J Invest Dermatol 2014;134:1862–72. doi:10.1038/jid.2014.90.

[263] Samani A, Plewes D. A method to measure the hyperelastic parameters of ex vivo breast tissue samples. Phys Med Biol 2004;49:4395–405. doi:10.1088/0031-9155/49/18/014.

[264] Poole C. Review. Articular cartilage chondrons: form, function and failure. J Anat 1997;191:1–13.

[265] Orgel JPRO, San Antonio JD, Antipova O. Molecular and structural mapping of collagen fibril interactions. Connect Tissue Res 2011;52:2–17. doi:10.3109/03008207.2010.511353.

[266] McGuinness K, Khan IJ, Nanda V. Morphological Diversity and Polymorphism of Self-Assembling Collagen Peptides Controlled by Length of Hydrophobic Domains. ACS Nano 2014. doi:10.1021/nn505369d.

[267] Shah DN, Recktenwall-Work SM, Anseth KS. The effect of bioactive hydrogels on the secretion of extracellular matrix molecules by valvular interstitial cells. Biomaterials 2008;29:2060–72. doi:10.1016/j.biomaterials.2008.01.001.

[268] Khan SP, Auner GG, Newaz GM. Influence of nanoscale surface roughness on neural cell attachment on silicon. Nanomedicine 2005;1:125–9. doi:10.1016/j.nano.2005.03.007.

[269] Huang H-H, Ho C-T, Lee T-H, Lee T-L, Liao K-K, Chen F-L. Effect of surface roughness of ground titanium on initial cell adhesion. Biomol Eng 2004;21:93–7. doi:10.1016/j.bioeng.2004.05.001.